2008

THE LYS-EGFP-KI MOUSE MODEL REVEALS PREVIOUSLY UNIDENTIFIED POPULATIONS OF HEMATOGENOUS AND MICROGLIAL MACROPHAGES FOLLOWING SPINAL CORD INJURY

SAKINA G. THAWER
Western University

THE *LYS*-EGFP-*KI* MOUSE MODEL REVEALS PREVIOUSLY UNIDENTIFIED POPULATIONS OF HEMATOGENOUS AND MICROGLIAL MACROPHAGES FOLLOWING SPINAL CORD INJURY

(Spine title: Diverse Macrophage Populations in the Injured Spinal Cord)

(Thesis format: Monograph)

BY

SAKINA G. THAWER

GRADUATE PROGRAM IN MICROBIOLOGY AND IMMUNOLOGY

SUBMITTED IN PARTIAL FULFILLMENT OF THE REQUIREMENTS FOR THE DEGREE OF MASTER OF SCIENCE

SCHOOL OF GRADUATE AND POSTDOCTORAL STUDIES
THE UNIVERSITY OF WESTERN ONTARIO
LONDON, ONTARIO, CANADA

AUGUST, 2008

THE UNIVERSITY OF WESTERN ONTARIO
SCHOOL OF GRADUATE AND POSTDOCTORAL STUDIES

CERTIFICATE OF EXAMINATION

Supervisor	Examiners
Dr. Gregory Dekaban	Dr. Ewa Cairns
Supervisory Committee	Dr. Stephen Karlik
Dr. Arthur Brown	Dr. Vincent Morris
Dr. Bosco Chan	

The thesis by

Sakina G. Thawer

entitled:

The *Lys*-EGFP-*ki* mouse model reveals previously unidentified populations of hematogenous and microglial macrophages following Spinal Cord Injury

is accepted in partial fulfillment of the
requirements for the degree of Master of Science

Date_____

_____
Chair of the Thesis Examination Board

ABSTRACT

Administration of a monoclonal antibody to the CD11d/CD18 integrin results in significant functional recovery in rodent models of spinal cord injury (SCI). This treatment selectively delays the influx of monocyte-derived hematogenous macrophages (hMØ), suggesting that hMØ exhibit neurodegenerative or neuroprotective effects depending upon the temporal microenvironment of the SCI lesion. hMØ and microglial macrophages (mMØ) are indistinguishable; hence, their roles in response to SCI remain unclear. Using SCI *lys*-EGFP-*ki* mice that enable distinction of $EGFP^+$ hMØ from $EGFP^-$ mMØ, we demonstrate that both populations peak in the lesion at 7d post-SCI. The 'classical inflammatory' monocytes/hMØ and 'non-classical resident' monocytes/hMØ respond to the acute (1d, 3d, 7d) and chronic (14d, 6wks) stages of SCI, respectively. We report the depletion of a possibly novel blood subset in response to SCI that expresses monocyte and dendritic cell markers. Our study provides new insights for the mechanism of dichotomous response of hMØ to SCI.

KEYWORDS

CD11d/CD18 integrin; Classical inflammatory monocytes; Flow Cytometry; Inflammation; Intermediate monocytes; *Lys*-EGFP-*ki* Mouse; M1/M2 Macrophage Polarization; Macrophage; Microglia; Non-classical monocytes; Spinal Cord Injury.

For My Family

ACKNOWLEDGEMENTS

I would like to express gratitude to my supervisor, Dr. Greg Dekaban, for providing me the opportunity to conduct innovative research in his laboratory, and for his constant support and guidance throughout this project. I would also like to acknowledge members of my Advisory committee, Dr. Arthur Brown and Dr. Bosco Chan for sharing their knowledge, and their assistance with this thesis. I have to thank Dr. Peta O'Connell for her insight on flow cytometry, Dr. Kristin Chadwick for her help and support with cell sorting, and Dr. Lynne Weaver for her guidance with statistical analysis. I would also like to thank Anna Pniak, Carmen Simedrea, and Yuhua Chen for their assistance with animal surgeries. Also, I would like to appreciate the assistance of the following people with technical assistance and/or animal care: Katherine Bielas, Elena Iosef, Dr. Nicole Geremia, Man (Kathy) He, and Stacey Xu. I must thank members of the Dekaban Laboratory, both past and present, for their technical and/or moral support with my project: Christy Willert, Dr. Jin Su, Kemi Adeyanju, Monty McKillop, Mia Merrill, Dr. Terlika Sharma, and Sonali de Chickera. Finally, I would like to acknowledge my parents, Gulamraza and Tahera, and my brothers and sisters, Fatema, Aliasgher, Shane Mohammed, Ali, Narjis Khatoon, Sumaiyya, and Zainab, for their guidance, moral support, and for helping me achieve my goals, and my friends for their support throughout this project.

TABLE OF CONTENTS

LIST OF TABLES

LIST OF FIGURES

LIST OF APPENDICES

LIST OF ABBREVIATIONS

Ab	Antibody
APC	Allophycocyanin
BCG	*Bacille Calmette Guerin*
BDNF	Brain-Derived Neurotrophic Factor
BM	Bone Marrow
BSA	Bovine Serum Albumin
BSCB	Blood Spinal Cord Barrier
BBB	Blood Brain Barrier
CCR2	Chemokine Receptor 2
CCR7	Chemokine Receptor 7
cDC	Conventional Dendritic Cell
CD11a	αL Leukocyte Integrin α Subunit
CD11b	αM Leukocyte Integrin α Subunit
CD11c	αX Leukocyte Integrin α Subunit
CD11d	αD Leukocyte Integrin α Subunit
CD14	Lipopolysaccharide receptor
CD16	Low Affinity Fc Receptor
CD115	Macrophage-Colony Stimulating Factor Receptor
CD117	Stem-cell Factor Receptor
CD62L	Leukocyte Adhesion Molecule
CNS	Central Nervous System
DAPI	4',6'-diamidino-2-phenylindole hydrochloride

DC	Dendritic Cell
DMEM	Dulbecco's Modified Eagle's Medium
EAE	Experimental Allergic Encephalomyelitis
EGFP	Enhanced Green Fluorescent Protein
F4/80	Macrophage Specific Cell Surface Marker
FACS	Florescence Activated Cell Sorting
FMO	Fluorescence Minus One
FSC	Forward Scatter
GM-CSF	Granulocyte Macrophage Colony Stimulating Factor
HBSS	Hank's Balanced Salt Solution
HEPES	4-(2-hydroxyethyl)-1-piperazineethanesulfonic acid
hMØ	Hematogenous Monocyte-Macrophage
ICAM	Intercellular Adhesion Molecule-1
IL	Interleukin
LPS	Lipopolysaccharide
Ly6C/G	Neutrophil Cell Surface Marker
Lys-M	Lysozyme-M
M1	Classical Activated Macrophages
M2	Alternatively Activated Macrophages
mAb	Monoclonal Antibody
MCP-1	Monocyte Chemoattractant Protein-1
MHC	Major Histocompatibility Complex
MIP-1α, β	Macrophage Inflammatory Protein-1α, β

mMØ	Microglial Macrophage
mnMØ	Meningeal Macrophage
MP	Methylprednisolone
MPO	Myeloperoxidase
MPS	Mononuclear Phagocyte System
NGS	Normal Goat Serum
NK1.1	Natural Killer T cell marker
PDCA-1	Plasmacytoid Dendritic Cell Marker
pDC	Plasmacytoid Dendritic Cell
PE	Phycoerythrin
pMØ	Perivascular Macrophage
PBS	Phosphate Buffered Saline
PFA	Paraformaldehyde
RBC	Red Blood Cells
RT	Room Temperature
SA	Streptavidin
SCI	Spinal Cord Injury
SSC	Side Scatter
TGF-β	Transforming Growth Factor-β
TNF-α	Tumor Necrosis Factor-α
VCAM-1	Vascular Cell Adhesion Molecule-1
VP-SFM	Virus Production-Serum Free Medium

CHAPTER 1 – INTRODUCTION

1.1 OVERVIEW

Spinal cord injury (SCI) often results in lifelong disabilities of affected individuals *(1)*. The outcome of SCI depends on the severity of damage and can result in ambulatory, sensory, and autonomic dysfunctions *(1)* such as chronic pain, muscle spasticity, paralysis, poor cardiovascular control, and loss of bladder, bowel, and sexual functions *(2)*. In Canada, the annual incidence of SCI occurs at 42.4 per million population *(3, 4)*; 84% of these injuries are associated with people under the age of 34 although increasing numbers of elderly incur an SCI *(4)*. The most common causes of SCI are motor vehicle collisions (55%), sports injuries (27%), and falls (18%) *(4)*. At a societal level, SCI exerts a significant economic burden due to high levels of long-term disability resulting in unemployment of persons with SCI (62%) *(4)* and associated health care costs *(5)*. Thus, it is important to develop therapeutic interventions for SCI.

Current research efforts in SCI focus primarily on neuroprotective and neuroregenerative treatments *(6)*. Both areas aim to improve the outcome of SCI and thereby enhance the quality of life of affected individuals *(6)*. Neuroprotective research involves inhibiting pathological mechanisms occurring during ischemia that lead to calcium influx, activation of free radical reactions, and cell death, all of which lead to further neuronal and glial cell degeneration following SCI *(6, 7)*. Neuroregenerative research involves promoting the replacement of lost neuronal and glial cells in order to restore function *(6)*. The present study focuses on aspects of neuroprotection following SCI.

Two stages of injury occur after trauma to the spinal cord. The primary injury occurs at the time of trauma and is the result of mechanical events such as compression or laceration of the spinal cord *(8)*. The secondary injury occurs immediately following the primary injury and is characterized by events such as ischemia/reperfusion, edema, excitotoxicity, demyelination, free-radical production, and inflammation at the spinal cord lesion *(9, 10)*. These processes progressively result in further loss of neurons and glia in the areas adjacent to the primary lesion, thereby increasing lesion size leading to further neurological deterioration *(11)*. Thus, preventing the progression of secondary damage represents a significant target for therapeutic approaches to SCI.

1.2 THE ACUTE INFLAMMATORY RESPONSE TO SCI

Inflammation is a major contributing factor to secondary injury progression *(10, 11)*. However, the role of inflammation in SCI is controversial; evidence exists for both its beneficial as well as its harmful effects on the spinal cord *(12-14)*. The blood-spinal cord barrier (BSCB) that normally functions to restrict hematogenous leukocyte entry into the spinal cord is often disrupted following SCI *(15)* due to hemorrhage and release of cytokines from cells in and around the lesion *(16)*. Following SCI, pro-inflammatory cytokines such as interleukin (IL)-1β, IL-6, and tumor necrosis factor (TNF)-α are produced locally in the spinal cord by activated endothelial cells, neurons, astrocytes, oligodendrocytes, and microglia *(11, 13, 17)*. These cytokines alter endothelial cell permeability, compromise BSCB integrity, and induce endothelial cells to increase expression of selectins, intercellular adhesion molecules (ICAMs), and vascular cell adhesion molecules (VCAMs) *(11)*. Additionally, the above mentioned cytokines

trigger the release of various chemokines such as macrophage inflammatory protein (MIP)-1α, 1β, and monocyte chemotactic protein (MCP)-1 *(17)*, all of which, promote recruitment of hematogenous leukocytes such as neutrophils and monocyte-derived macrophages (hMØ) to the endothelial surface *(8, 11, 18)*. Generally, membrane-bound ligands expressed on the surface of hematogenous leukocytes bind selectins on the endothelial cell surface with weak affinity, resulting in rolling of leukocytes along the endothelium *(19)*. Inflammatory chemokines secreted from endothelial cells surrounding the SCI interact with their respective receptors on the surface of the rolling leukocytes resulting in activation of the β2 family of leukocyte integrins *(20)*. Hematogenous leukocytes express α4β1 and β2 (CD18) family integrins on their cell surface that interact with endothelial cells via binding to adhesion molecules [ICAM-1, ICAM-3, and VCAM-1] *(21, 22)*. Multiple β2 integrin-ligand high affinity interactions enable leukocytes on the endothelial surface to diapedese across the endothelial barrier, enter the underlying tissue, and migrate to the site of the SCI via a chemotactic gradient *(23)*. Thus, following SCI, the disrupted BSCB becomes permissive to the infiltration of hematogenous leukocytes which, together with the resident glial and neuronal cells contribute to the overall inflammatory response. A brief discussion on the inflammatory cells involved in the cellular inflammatory response to SCI is presented below.

1.3 NEUTROPHILS

Neutrophils are the first inflammatory cells to extravasate into the SCI lesion, with peak numbers in the rat model appearing at 1 day (d) post-SCI and then rapidly decreasing by 3d *(11, 24)*. The neutrophil response in the mouse is delayed with respect

to the rat model. In the mouse, neutrophil infiltration peaks at 1-3d post-SCI and drops dramatically by 7d *(25)*. In humans, neutrophil infiltration is similar to that seen in mice, with peak neutrophil numbers appearing in the lesion at 1-3d post-SCI and rapidly decreasing by 10d *(26)*.

Neutrophils produce a wide range of bioactive products that include lipids (Leukotriene B_4), cytokines (IL-1β,-6,-8, TNF-α, TNF-β), proteases (elastase), microbicidal agents [myeloperoxidase (MPO), lysozyme], and reactive oxygen intermediates, all of which play a critical role in neutrophil function *(27, 28)*. Neutrophils house many of the pro-inflammatory products listed above in secretory granules; the regulation of their release defines neutrophil function *(28)*. Neutrophil granules function by either fusing with a phagocytic vacuole to disarm the ingested contents or with the plasma membrane to release their products for a more widespread means of damage *(29)*. The latter process results in bystander damage of healthy neural tissue that exacerbates the loss of functional outcomes following SCI *(11, 30)*.

The damaging effects of neutrophils in the injured spinal cord are illustrated by studies carried out in nitrogen mustard-induced leukocytopenic rats. Following SCI, leukocytopenic animals exhibit significantly improved motor function and less MPO activity at the peak neutrophil infiltration time in rats *(30)*. In the same study, similar results were achieved when rats were treated with anti-P-selectin monoclonal antibody (mAb) that prevents leukocyte extravasation into the spinal cord. Additionally, both leukocytopenic and anti-P-selectin treated rats experienced less hemorrhage within the lesion compared to controls *(30)*. These results suggest that hemorrhage may be enhanced as a result of vascular damage facilitated by neutrophil free radical production and this

has been postulated to be critical in the breakdown of the BSCB *(30, 31)*. Hemorrhage within the spinal cord in turn results in: 1) uncontrolled entry of inflammatory cells; 2) extravascular release of red blood cells (RBC) into the CNS that release hemoglobin and thereby promote iron-mediated tissue damage *(32)*; and 3) disruption of blood flow creating ischemic regions within the lesion *(33, 34)*. It is becoming increasing clear that neutrophils play a largely destructive role in the acute inflammatory response to SCI.

1.4 T-LYMPHOCYTES AND DENDRITIC CELLS

T-lymphocytes are present in low numbers in the lesion post-SCI and are thought to be involved in both repair and secondary degenerative processes *(35)*. Activated T-lymphocytes can modulate macrophage function, endothelial integrity, and antibody production by B-lymphocytes, processes that could contribute to neurodestructive and neuroprotective effects *(35)*. Sroga et al. *(36)* have shown that T-lymphocytes enter the injured spinal cord at different times, depending upon the species and strain of animal. They showed that in the rat model, T-lymphocytes enter the SCI lesion at 3d and 7d post-SCI while mice exhibit a delayed onset of T-lymphocytes that infiltrate the lesion at 14d, and double in numbers at 6wks post-SCI *(36)*. Whether T-lymphocytes cause secondary degeneration or mediate wound repair after SCI remains highly controversial *(37-39)*.

Dendritic cells (DC) are potent antigen-presenting cells that have diverse functions including T-lymphocyte and B-lymphocyte activation, and immune tolerance *(36)*. Sroga et al. *(36)* showed that DC influx parallels that of T-lymphocytes in the SCI rat model. The functional nature of DC in response to SCI presently remains controversial *(36, 40)*.

1.5 THE MONONUCLEAR PHAGOCYTE SYSTEM

The mononuclear phagocyte system (MPS) consists of differentiated cell types such as kupffer cells, lung alveolar macrophages, microglia, peritoneal macrophages, DC, osteoclasts, and granuloma-forming macrophages that can be found at sites of inflammation *(41)*. Circulating monocytes derived from progenitor cells in the bone marrow (BM) give rise to the MPS (hematopoietic origin) *(41, 42)*. The MPS is thought to require continuous reconstitution of differentiated cells *(41)* which may be achieved by self-renewing progenitor cells *(43, 44)*, proliferation of BM-derived precursors in peripheral tissues *(45)*, or by the continuous extravasation and differentiation of circulating monocytes *(45, 46)*. These mechanisms possibly operate in parallel in the regeneration of the individual MPS subsets *(41)*. Heterogeneity of monocytes and macrophages has been recognized in the recent years, the discussion of which is presented below.

1.51 Monocyte heterogeneity in the blood

Monocytes have a bean-shaped nucleus and are defined as populations that 1) are mononuclear cells in the circulation, 2) carry out phagocytosis, and 3) have a propensity to differentiate into macrophages (MØ) or DCs in appropriate settings *(47)*. Monocytes represent about 5-10% of peripheral blood leukocytes in humans and mice *(48, 49)*. They originate from a myeloid precursor in the BM that is shared with neutrophils *(49)*. Monocytes are released from the BM into the circulation as non-dividing cells, and once they enter tissues, a differentiation program toward macrophages and DCs occurs *(49)*. The differentiated cell is then referred to as a monocyte-derived cell

(41, 48). The half-life of monocytes is believed to be relatively short, about 1d in mice and 3d in humans *(48)*. This short half-life in blood has fostered the concept that blood monocytes may continuously repopulate tissue macrophage or DC populations to maintain homeostasis and, during inflammation, fulfill critical roles in innate and adaptive immunity *(48, 49)*. However, other evidence suggests that macrophages in several different organs self-renew without input from blood precursors *(48)*.

Traditionally, monocytes were thought to express CD11b, CD11c, and CD14 in humans and CD11b, CD115, and F4/80 in mice, and lack B-cell, T-cell, Natural Killer (NK)-cell, and DC markers *(41, 48)*. However, in the recent years it has become clear that monocytes are morphologically and phenotypically heterogeneous *(41, 49)*. Two mouse monocyte subsets have been identified and share the surface expression of CD115, CD11b, and F4/80 antigens but are phenotypically distinguishable based on the use of the following combination of surface markers: Ly6C/G^{+}, CCR2^{+}, CD62L^{+}, CX$_3$CR1^{lo} and Ly6C/G$^{-/lo}$, CCR2^{-}, CD62L$^{-/lo}$, and CX$_3$CR1^{hi} *(41, 47)*. The former subset is referred to as the 'classical inflammatory' monocyte, while the latter subset is referred to as the 'non-classical resident' monocyte. Studies *(41, 48-50)* suggest that the 'classical inflammatory' monocytes are short lived and home to inflamed tissues mediated by expression of CCR2 and CD62L, where they participate in the ongoing immune response. The 'non-classical resident' monocytes have a longer half life and are the ones that home to non-inflamed tissues to become 'resident' cells that maintain tissue homeostasis *(41, 48-51)*. The accumulation of 'non-classical resident' monocytes in diverse tissues is thought to be facilitated by the expression of the chemokine receptor, CX$_3$CR1 *(48, 50, 51)*. To date, the development and differentiation pathway of monocytes is still poorly

understood *(48, 49)*. Gordon and Taylor *(49)* suggest that BM-derived Ly6C/G^{+} 'classical inflammatory' monocytes are released into circulation and, in the absence of inflammation, switch their phenotype to generate the Ly6C/G^{-} 'non-classical resident' monocytes by an unknown mechanism. This theory is supported by the observation of a monocyte subset in blood that expresses intermediate levels of Ly6C/G and has thus been termed 'intermediate' monocytes *(48, 52)*. The human counterparts of mouse monocyte subsets have been identified based on differential expression of CD14 and CD16 *(48)*. The 'classical inflammatory' CD14^{hi}, CD16^{-} monocytes, represent up to 95% of monocytes in healthy individuals and the 'non-classical resident' CD14^{lo}, CD16^{+} monocytes comprise the remaining fraction *(48, 49)*. These subsets share phenotype and homing potential similar to those described for the mouse monocyte subsets *(41, 47, 49)*.

The identification of monocyte subsets has led to the hypothesis that monocytes commit to specific functions while still in circulation *(49)* and has prompted investigations to determine their functional roles under homeostatic and inflammatory conditions *(41)*. Whether the monocyte subsets give rise to heterogeneous macrophage subsets that differentially participate in destruction and repair mechanisms remains unknown. The present study addresses the potential differential responses of monocyte subsets in the inflammatory response to SCI.

1.52 Macrophage heterogeneity and functionality

Hematogenous monocyte-derived macrophages (hMØ) are members of the innate immune response *(53)*. Studies have revealed that hMØs influence virtually every aspect of the immune response on the basis of their abundance in the body, their wide tissue

distribution, motility, and versatility *(53)*. hMØs show a high degree of heterogeneity reflecting their specialized function in different anatomical locations *(49)*. They have a broad role in the maintenance of tissue homeostasis, through the clearance of senescent cells *(49)*. hMØs function at the site of inflammation to kill invading microorganisms, remove debris, facilitate tissue repair, and help restore tissue homeostasis by secreting at least 100 known substances including polypeptide hormones (cytokines and growth factors), complement components, coagulation factors, proteases, lipases, lysozyme, hydrolases, deaminases, inhibitors of enzymes and cytokines, extracellular matrix or cell adhesion proteins, binding proteins, bioactive oligopeptides, bioactive lipids, sterol hormones, purine and pyrimidine products, and reactive oxygen and nitrogen intermediates *(53)*. It has been observed *in vitro* that under inflammatory conditions, hMØ polarize into one of two general phenotypes (M1 and M2) that acquire different functional properties in response to environmental signals *(49, 54-56)*. Macrophage exposure to interferon-γ (IFN-γ), LPS, or pro-inflammatory cytokines (TNF-α, GM-CSF) drives the classically activated M1 polarization resulting in cytotoxic, pro-inflammatory, and anti-tumoral effects *(49, 54-56)*. By contrast, the alternative M2 polarization induced by exposure to IL-4, IL-10, IL-13 or TGF-β, generally results in a phenotype that promotes immunoregulation, tissue repair/remodelling, and suppresses inflammation *(49, 54-56)*. Whether these phenotypes are distinct or indicate a continuum of physiological responsiveness currently remains unclear *(55, 56)*. Additionally, it is not known whether the functional macrophage phenotypes (M1/M2) are reflective of the monocyte subsets in the blood.

The response of hMØs to SCI involves their infiltration into the spinal cord at 3d reaching a plateau level at 7d post-SCI in rat models *(57)*. The hMØ response has a delayed onset in the mouse model with large numbers appearing at 7d post-SCI *(25)*. In humans, hMØ numbers gradually increase in the spinal cord starting at 1-3d and remain for up to 1 year post-SCI *(26)*. Several studies show that hMØs play different functional roles in the acute inflammatory response to SCI including phagocytosis of inhibitory proteoglycans and myelin in order to promote neural sprouting and axonal regeneration *(58-62)*. hMØs produce pro-inflammatory cytokines such as IL-1β, TNFα, and IL-6 following injury, and this results in a decrease in lesion size *(63)*. Finally, hMØs play a role in the clearance of toxic necrotic and apoptotic cells that exacerbate the inflammatory response in the SCI lesion *(62)*. While there is no doubt about hMØs' active participation in the acute inflammatory response to CNS injury, it is unclear whether they play a destructive or beneficial role in the recovery of the injured CNS. The infiltrating hMØ may polarize into M1 or M2 phenotype in the lesion thereby exhibiting neurodestructive and neurorepair functions respectively. However, this hypothesis remains to be investigated.

1.6 PERIVASCULAR (pMØ) AND MENINGEAL MACROPHAGES (mnMØ)

Perivascular MØ (pMØ) are ubiquitously distributed throughout body tissues including the central nervous system (CNS). pMØs are located between the basement membrane and the glia limitans (Virchow-Robin space), and on the surface of the small vessels, while tissue macrophages and microglia are located in the tissue parenchyma. pMØs exhibit oval or elongated cell bodies that conform to the shape of the vessel; some

studies have shown that they extend processes that wrap around the blood vessel *(64)*. pMØs are monocyte-derived, have a rapid rate of turnover compared to microglia, and studies have shown that pMØ repopulation is complete within 2 months following irradiation *(65)*. In addition, the same study showed that pMØs have antigen-presenting properties and are sufficient for presenting antigen in the induction of experimental allergic encephalomyelitis (EAE). The traditional MØ surface markers (CD68, CD11b, F4/80) are also expressed by pMØs; therefore, their location is the basis for their distinction *(64)* .

The meningeal MØ (mnMØ) are located in the subarachnoid space between the pia mater and the arachnoid, primarily on the surface of the pia with a few free floating in the cerebrospinal fluid *(66)*. They have typical MØ morphology and exhibit phagocytosis based on the uptake of horseradish peroxidase *(66)*. Like pMØs, the mnMØs are monocyte-derived and have a rapid turnover rate *(67)*.

Although very little is known about the roles of pMØs and mnMØs in the inflammatory response to SCI, studies using pMØ/mnMØ depleted mice have shown that they play a protective role in bacterial meningitis, as observed by increased illness, higher bacterial counts, and decreased leukocyte infiltration in infected mice lacking pMØ/mnMØ *(68)*. Another study found that the depletion of pMØs and mnMØs suppressed the clinical severity of EAE *(69)*. These studies suggest that pMØ and the mnMØ may be involved in the influx of leukocytes at the blood-brain-barrier (BBB).

1.7 MICROGLIAL MACROPHAGES (mMØ)

The microglial MØ (mMØ) are a specialized subset of tissue macrophages that reside in the CNS *(70)*. They were identified as a cell population distinct from other glial cells by Del Rio-Hortega in 1919 *(71)*. Microglial cells represent ~15% of the glial cell population, exhibit little or no turnover with hMØs in the homeostatic adult rodent CNS, and are ubiquitously found throughout the CNS *(72)*.

The origin of microglia has been an area of controversy spanning several decades. The most widely accepted theory is that a hematopoietic monocytic precursor to microglia arises early in development *(73)*. Microglia are thought to colonize the CNS in two waves; the first wave of microglia invades the embryonic and fetal CNS and derives essentially from the extramedullary sources of hematopoiesis, including the yolk sac *(73, 74)* . The second wave of microglia is formed by bone marrow (BM)-derived monocytic cells that colonize the CNS during early postnatal days (P0-P15) in rodents, or early prenatal days in humans *(73, 74)*.

The extent to which circulating monocytes or other BM hematopoietic precursors contribute to the adult microglial population in the CNS is still a matter of speculation *(73-75)*. Previous studies using irradiation-induced BM chimeric mice, in which BM cells were marked with GFP, MHC class II, Y chromosome, congenic CD45.1/CD45.2 molecules and others, showed that BM cells can enter the brain during postnatal development and differentiate into microglia *(65, 76)*, but not into other glial cell types *(77)*. However, chimeric mice in these studies were subjected to total body irradiation, thereby exposing the brain/spinal cord to potential irradiation-induced vascular changes that would allow for non-physiological engraftment of monocyte-

derived microglia. Recently, Mildner et al. *(75)* convincingly illustrated that in CNS disease models without BBB disruption, microglial engraftment only occurs in the presence of irradiation and that in this situation the Ly6C/G$^+$, CCR2$^+$ 'classical inflammatory' monocytes serve as precursors to microglia. However, whether monocytes contribute to microglial engraftment in CNS models with BBB disruption is currently unknown due to the fact that hMØ and mMØ are not easily distinguishable following CNS inflammation *(75, 78)*.

Microglia play a substantial role in CNS development by removing debris as well as acting as immunological sensors in the resting adult CNS *(70)*. Microglia are the resident immune cells of the CNS and become activated and mobilized in response to infectious diseases, inflammation, neurodegeneration, and trauma in an effort to protect the tissues in the CNS *(79)*. Resting microglia possess a distinct ramified morphology with extensive cell processes that radiate from the main cell body (Figure 1A). Upon homeostatic disturbances, microglia undergo a series of activation states (Figure 1B-D). The fully activated mMØs has a rounded morphology, is phagocytic and exhibits an increase in the expression of MHC and complement receptors (Figure 1E) *(79)*. The time course for mMØ activation is found to occur within 3-14d following CNS injury *(80)*.

Similar to hMØs, activated mMØs are known to secrete excitatory amino acids, reactive oxygen and nitrogen species, inflammatory cytokines, and proteases *(72)*. Human microglial cells prepared from embryonic telencephalon tissue have been found to express mRNA for IL-1β, -6, -8, -10, -12, -15 and TNFα, MIP-1α, -β, and MCP-1 in their unstimulated state; LPS stimulation increases the protein levels of IL-1β, IL-8, TNFα, and MIP-1 *(81)*. Microglia are known for their antigen presenting capabilities. For

Figure 1. Activation states of microglia. Microglial cells in their resting surveillance state have a ramified morphology with extensive cell processes radiating from the main cell body (A). Upon detection of homeostatic disturbances, they respond with a reorganization and retraction of their processes (B, C, D), to become fully activated MØ that are phagocytic and have a distinct rounded morphology (E). The schematic is extracted and modified from previous representations *(25, 70, 73, 82)*.

A

Resting Ramified Microglia

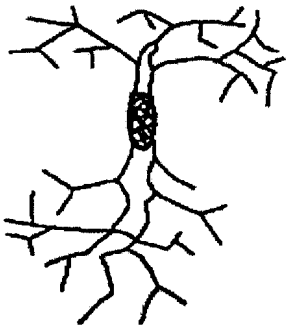

B

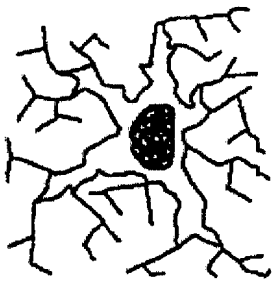

C

D

Activated Microglia

E

Phagocytic Microglia

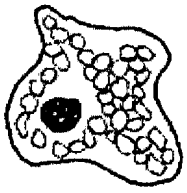

example, treatment with indomethacin (a cyclo-oxygenase blocker) induces cultured microglial cells to mediate specific allogenic proliferation of T-cells *in vitro (83)*. Microglia appear to be specialized and more efficient in the phagocytosis of myelin than hMØ *(84, 85)*. In culture, microglia phagocytose both opsonized and untreated myelin more efficiently than peritoneal MØs with respect to uptake time and concentration *(86)*. The role of microglia and mMØ in response to SCI currently remains unknown as these cells are morophologically and immunophenotypically indistinguishable from the hMØ.

Overall, the acute inflammatory response to SCI involves participation of an array of immune cells. As mentioned previously, the role of the ensuing acute inflammatory response to SCI is still a matter of debate; these dichotomous views are presented below.

1.8 POSITIVE EFFECTS OF THE ACUTE SCI INFLAMMATORY RESPONSE

A number of studies support the view that the acute inflammatory response is beneficial to recovery from SCI. Klusman and Schwab *(63)* investigated the effect of the local administration of pro-inflammatory cytokines IL-1β, IL-6, and TNF-α, in mice post-SCI. Their results showed that the cytokine treatment administered at 4d post-SCI recruited macrophages (MØ) to the lesion, and at 7d post-SCI, there was significantly more tissue sparing in the treated mice than in untreated controls. Their work suggests that additional MØ in the lesion may protect neural tissue that is normally lost following SCI. Frazen et al. *(87)* further showed that injecting unstimulated autologous peritoneal rat MØ directly into the lesion following SCI led to an increase in laminin, an axonal growth potentiating matrix substrate, and in neural sprouting one month later. These results suggest that MØ promote their beneficial effects by altering the microenvironment

of the injured spinal cord making it more favorable for neural regeneration. To investigate whether this effect could be enhanced by injecting activated MØ, Rapalino et al. *(58)* implanted MØ, pre-exposed *ex vivo* to peripheral nerve segments, into transected rat spinal cords. This resulted in tissue repair, increased numbers of intact axons traversing the lesion, and better functional recovery. Similar results were obtained in studies that incubated MØ with skin segments prior to injection caudal to the lesion *(58, 88)*. The beneficial effects of these activated MØ were proposed to be due to a decreased production of TNF-α and increased production of IL-1β and brain derived neurotrophic factor [BDNF], a neurotrophin that promotes neuronal survival and axon regeneration *(88)*. Thus these studies provided evidence supporting the concept that hMØ may play a beneficial role in spinal cord repair.

These observations were extended by Rabchevsky and Streit *(89)* who explored the possibility of whether mMØ might be better suited to promoting spinal cord repair. Microglial cells embedded in a gel foam matrix were engrafted into the lesion at the time of injury. This resulted in prominent neurite outgrowth within the transplanted matrix when compared to cell free matrix implants. Interestingly, no difference in neurite growth was observed between unstimulated and lipopolysaccharide (LPS) stimulated microglial cells, suggesting that the activation state of the implanted microglia may not play a role in regeneration, or that the initial purification of the microglial cells resulted in the same level of activation as the LPS stimulation. Together, the above findings suggest that acute inflammatory response involving augmented MØs from the blood or microglia may promote neuronal regeneration and functional recovery following SCI.

1.9 NEGATIVE EFFECTS OF THE ACUTE SCI INFLAMMATORY RESPONSE

Conversely, other studies have reported that the acute inflammatory response has adverse effects on the outcome of SCI. Activated MØ have been shown to contribute to demyelination and scarring of the injured spinal cord. Activated neutrophils release reactive oxygen and nitrogen species that damage endothelial cells and further facilitate extravasation of inflammatory leukocytes into the spinal cord lesion *(34, 90)*. Carlson et al. *(11)* correlated the presence of inflammatory leukocytes to the extent of tissue destruction by examining the location of neutrophils and MØ in the acutely injured rat spinal cord. Their study showed that neutrophils predominated in necrotic areas, and strictly localized to the injury epicenter and regions immediately rostral and caudal to the lesion. Regions with the highest MØ density corresponded to areas of tissue damage. Additionally, a human study *(26)* correlated areas of necrosis and cavitation in the injured spinal cord to presence of neutrophils in the acute stage and MØ in the chronic stage of injury. Studies have also determined the effect of MØ depletion on neurological outcomes following SCI. Depletion of MØ prior to, and immediately after SCI in the rat model led to a decrease in cavitation size and an improvement in myelinated axonal regeneration and functional recovery compared to controls *(91, 92)*. A study by Bethea et al. *(93)* suggests that early administration of IL-10, an anti-inflammatory cytokine, has protective effects on the injured spinal cord. Finally, targeted deletion of both P-selectin and ICAM-1, proteins responsible for leukocyte extravasation from the blood to the site of SCI, resulted in reduced inflammatory leukocyte infiltration, increased white matter sparing, and improved functional recovery following rodent SCI *(94, 95)*. Together, these studies illustrate that the acute inflammatory response can

contribute to negative outcomes following SCI. Anti-inflammatory therapies have thus been employed to improve SCI outcomes. Currently, the only approved but controversial anti-inflammatory treatment for SCI used in clinical settings is methylprednisolone (MP) *(96-98)*. Recently, it has been shown that MP affords no benefit to rodents or humans in recovery from SCI *(99-101)*. Thus, anti-inflammatory treatments with higher efficacies need to be developed.

Presently, there is no obvious reason as to why the acute inflammatory response has such dichotomous effects in different SCI treatment studies *(11, 63, 92)*. Differences may be attributed to the animal models used or to the timing of the administration of anti- or pro-inflammatory treatments. Schwartz *(102)* suggest that the dichotomy may in part be resolved by focusing on the regulation of the inflammatory response following SCI. Thus, anti-inflammatory treatments could play a neuroprotective role in SCI when its therapeutic approach addresses the regulation of the inflammatory response to SCI. One such anti-inflammatory strategy is the anti-CD11d mAb treatment that adopts the concept of integrin molecule blocking. Previous studies have shown that antibodies against integrin molecules result in significant anti-inflammatory effects by reducing leukocyte infiltration into the spinal cord lesion *(103)*.

Integrin molecules play a key role within multicellular organisms as many biological systems rely on their proper function. The immune system in particular requires a complex series of interactions with neighboring cells so as to effectively generate an immune response *(104)*. Integrins are cell surface transmembrane glycoproteins that bind to extracellular matrix ligands, cell-surface ligands, and soluble ligands *(105)*. Integrins associate as heterodimers composed of an α subunit non-

covalently bound to a β subunit *(106)*. Integrin subfamilies are categorized by their component β chain. There are 8 β chains in humans, and each associate with various α chains, of which there are 18 known human subunits *(107)*. Integrin β chains are able to pair with more than one specific α chain. There have been 24 distinct human integrin heterodimer conformations reported. The sub-family of β2 integrins contain the CD18 integrin β chain non-covalently associated with one of four distinct α-subunits to form, CD11a/CD18 (αLβ2, LFA-1), CD11b/CD18 (αMβ2, Mac-1), CD11c/CD18 (αXβ2), and CD11d/CD18 (αDβ2). These β2 integrin heterodimers mediate adhesion-dependent immunological responses *(108)*.

The CD11d/CD18 integrin is mainly found on neutrophils and monocytes/hMØ *(109, 110)*. Mabon et al. *(21)* first demonstrated that CD11d/CD18 integrin participates in facilitating the extravasation of leukocytes following SCI. The anti-CD11d strategy used for treatment in rodent SCI models involves administration of a mAb targeting the CD11d subunit of the CD11d/CD18 integrin *(21)*. The antibody blocks CD11d's interaction with its ligands, ICAM-3 and VCAM-1 in humans, and solely VCAM-1 in rodents *(108, 111)*. It was shown that the mAb specifically blocked the infiltration of neutrophils while only delaying entry of hMØ into the SCI lesion *(112)*. This reduction of inflammatory leukocyte infiltration led to numerous positive effects, including a reduction in lipid peroxidation and protein nitration *(113, 114)*, improvements in sensory, autonomic, and motor functions and reduced neuropathic pain in rats recovering from SCI *(112, 115)*. Importantly, these studies suggest that the dichotomous effects of hMØ may be determined by the timing of their influx into the lesion; early influx may result in harmful effects while later influx may result in beneficial effects. The possibility that the

early and later influx of hMØs are contributed by the differential response of monocyte subsets remains, and this issue is investigated in the present study. Together, studies on the anti-CD11d mAb treatment support the idea that regulating inflammation following SCI represents a valid therapeutic potential. Thus, the immunological basis behind its mechanism of neuroprotection needs to be understood.

1.10 DISTINGUISHING hMØ AND mMØ POPULATIONS FOLLOWING SCI.

A major obstacle in studying the acute inflammatory response to SCI is in distinguishing between the hMØs and the activated mMØs *(74, 92)*. As discussed previously these cells are morphologically distinct in their resting state, but become morphologically and phenotypically similar upon activation. Thus, distinguishing hMØ and mMØ using conventional histological and immunocytochemical techniques is difficult *(57, 92, 116)*. Studies of EAE and other CNS pathologies distinguished hMØ from mMØ based on CD45 expression with hMØ being $CD45^{hi}$ and mMØ being $CD45^{lo}$ *(117-119)*. It remains unclear whether such differences in fully differentiated and activated macrophages would hold true in a SCI model. Thus, in the present study, CD45 expression of the two cell types is also examined. Additionally, previous studies that aimed to distinguish between hMØ and mMØ involved the use of BM chimeric rats differing at the MHC locus. This approach led to the differential identification of hMØ and mMØ in the rat SCI lesion, with respect to time course of accumulation and their anatomical distribution *(57)*. However, as mentioned previously, irradiation of mice leads to BBB changes and allows for non-physiological donor monocytic engraftment as microglia in the CNS *(75)*. Thus, a simplified model system that directly permits the

distinction between the hMØ and mMØ would be advantageous. Our laboratory has proposed the use of *lys*-EGFP-*ki* mouse model for this purpose as is described below.

1.11 THE *LYS*-EGFP-*KI* MOUSE

The *lysozyme*-EGFP-*ki* (*lys*-EGFP-*ki*) transgenic mouse was created by Faust et al. *(120)* for studies of myeloid maturation and lineage specification of the hematopoietic system. The *lys*-EGFP-*ki* model involved the knock in of the gene for enhanced version of the green fluorescent protein (EGFP) into the first exon of the *lysozyme* gene by homologous recombination. Thus, in these mice, the *LysM* promoter drives the expression of EGFP specifically in mature myelomonocytic cells, which includes monocytes, macrophages, and neutrophils. *LysM* encodes for a protein that is not essential for the viability of mice, as such, the *lys*-EGFP-*ki* mice are reported to be normal in size, be fertile, contain all cells of the myeloid lineage, and show no overt defects in the hematopoietic system *(120)*. However, Ganz et al. *(121)* showed that these mice are more susceptible to certain bacterial infections due to ablation of the LysM protein in granulocytes and macrophages.

1.12 THE LYSOZYME M LOCUS

The expression of LysM has been extensively studied in the mouse because of its exclusive expression in hMØ and neutrophils *(122)*. Studies by *in situ* hybridization revealed that the transcription of *LysM* occurs in the majority of resting tissue hMØ *(123)*. Cross et al. *(124)* confirmed the absence of LysM mRNA or lysozyme activity in the brain tissue of normal mice, indicating that microglia do not express LysM

in the resting state. In order to assess the LysM expression in an activated state, mice were challenged with *Bacille Calmette Guerin* (BCG) and *Plasmodium yoelli* infectious agents *(122)*. Both infectious agents strongly induced LysM transcriptions in discrete subpopulations of hMØs in the spleen and liver, while the majority of tissues including the brain remained negative for LysM expression. This suggested that the *LysM* locus provides a target for transgenic expression exclusive to MØs and neutrophils. Furthermore, two previous studies have created transgenic mice using the *LysM* locus. The human LysM promoter has been used for specific expression of chloramphenicol acetyltransferase (CAT) enzyme in MØs and neutrophils *(124)*. Also, *LysM*Cre mice have been created by inserting cre recombinase cDNA into the *LysM* locus. These mice were later used for conditional gene targeting in double mutant mice with loxP-flanked target genes and were found to have a deletion efficiency of 98% in hMØ and 100% in neutrophils *(125)*. Together, these studies demonstrate the advantages of using the *LysM* locus as a target for creating transgenic animals with alterations in only hMØs and neutrophils. Overall, this mouse model system may be ideal for studies in which hMØ and mMØ populations in the SCI lesion are to be distinguished.

1.13 EVIDENCE VALIDATING THAT THE *LYS*-EGFP-*KI* MICE DISTINGUISHES hMØ AND mMØ FOLLOWING SCI.

Previously, our laboratory investigated whether the *lys*-EGFP-*ki* mouse model enables the distinction between hMØ and mMØ. Using immunohistochemical staining of spinal cord sections from the *lys*-EGFP-*ki* mice, we showed that while the $F4/80^+$, $EGFP^-$ cells were present in both the SCI and uninjured samples, the $F4/80^+$, $EGFP^+$ cells were

only found in SCI samples. This study suggested that microglia in resting state do not express EGFP (Figure 2) *(25)*. Furthermore, the administration of clodronic acid liposomes for hMØ depletion prior to, and following SCI in the *lys*-EGFP-*ki* mice revealed that the SCI spinal cords only contained $F4/80^+$, $EGFP^-$ cells suggesting that activated microglia lack EGFP expression *(25)*. Lastly, reciprocal bone marrow (BM) transplantation studies in which, the BM of *lys*-EGFP-*ki* mice transplanted into the C57BL/6 strain 6wks prior to SCI was performed. Immunohistochemistry of these SCI spinal cords revealed the presence of numerous $F4/80^+$, $EGFP^+$ and $F4/80^+$, $EGFP^-$ cells. In the reciprocal setting, where the C57BL/6 BM was transplanted into the transgenic mice, very little if any $F4/80^+$, $EGFP^+$ cells were observed; however, the spinal cords contained numerous $F4/80^+$, $EGFP^-$ cells. The few $EGFP^+$ cells observed are possibly residual EGFP cells in circulation as BM transplantation efficiency in this study was ~97% (Unpublished data, Karen Chan and Gregory Dekaban). Together, these studies demonstrated the potential usefulness of *lys*-EGFP-*ki* mouse model for differential study of the hMØ and mMØ in response to SCI.

1.14 FLOW CYTOMETRY

In the present study, we used flow cytometry as the primary method for examining the inflammatory response to SCI. Flow cytometry is a technique that allows simultaneous multiparametric analysis of the physical and/or chemical characteristics of single cells suspended in a stream of fluid *(126)*. However, flow cytometry of cells prepared from CNS tissue presents a challenge due to high lipid and myelin

Figure 2. Comparison of EGFP expression between hMØ and mMØ in the *lys*-EGFP-*ki* mice. Epi-fluorescent spinal cord sections of uninjured A) C57BL/6 and B) *lys*-EGFP-*ki* mice show lack of EGFP expression. Spinal cord sections at 3d post-SCI in the C) C57BL/6 and D) *lys*-EGFP-*ki* mice show extensive EGFP expression in the latter sample. Hatched yellow lines demarcate the outer edge of the spinal cord (A-D) and the gray and white matter (A-B). The contrast between gray and white matter is lost in injured samples (C-D). Spinal cord sections at 3d post-SCI were labeled with anti-GFP and anti-CD11b mAb's. E) Arrow indicates rounded $CD11b^+$, $EGFP^+$ hMØ while arrowhead indicates $CD11b^+$, $EGFP^-$ mMØ. F) A $CD11b^+$, $EGFP^-$ mMØ. Z-stacked images taken every 1μM and viewed from the bottom of E and F respectively to show the co localization of the EGFP (green) and the anti-CD11b (red) mAb's, with areas of co-localization appearing yellow (G-H). Scale bars in panels A-D represent 200μM and in E-H represent 5μM. The images were extracted from previous work by Leah Mawhinney *(25)*.

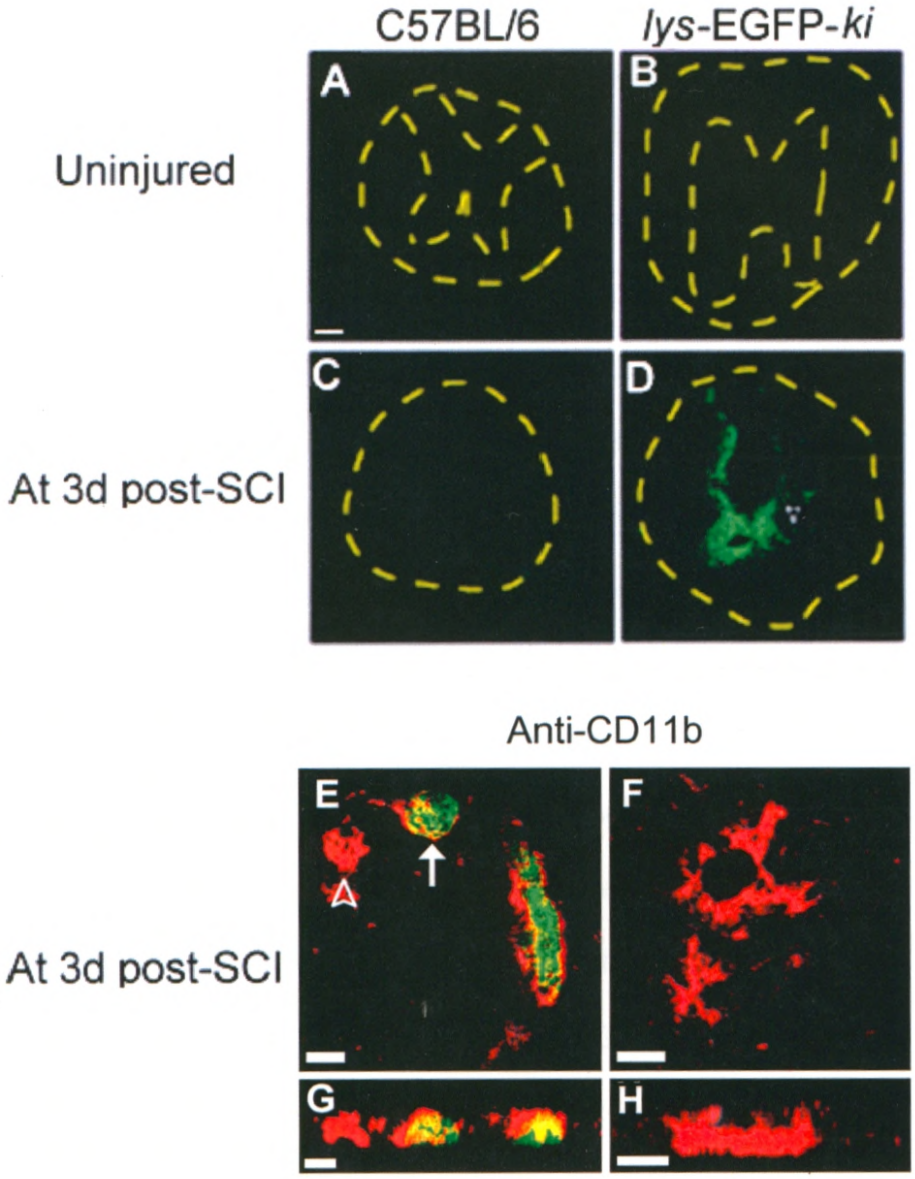
C57BL/6
lys-EGFP-ki
Uninjured
At 3d post-SCI
A
B
C
D
Anti-CD11b
At 3d post-SCI
E
F
G
H

content *(126)*. A number of studies in the past have processed rodent brain and spinal cord for flow cytometric analysis *(127-129)*. The common ground in these studies was the use of a gradient to enable separation of myelin and debris from the rest of the cells. In the present study, percoll gradient was used to process the spinal cords for flow cytometric analysis. Flow cytometry was also used to analyze the spleen and blood samples.

In this SCI study a general set of strategies was applied in analyzing cells by flow cytometry. A viable gate was placed on the forward scatter/side scatter (FSC/SSC) profiles of spleen, blood, and spinal cord samples such that any remaining RBC and debris normally found on the lower end of the SSC were excluded. Depending on the type of analysis to be performed, additional gates were placed on viable cells to analyze and define the nature of the cells based on fluorescence expression of EGFP and/or selected cell surface markers. Tissues contain resident-specific cells such that each tissue sample exhibits a unique FSC/SSC profile reflecting the heterogeneous cells it contains. These heterogeneous cells can be distinguished within their respective FSC/SSC profiles based on size (FSC) and granularity (SSC). In the present study, the FSC/SSC properties of cells were used as an additional tool to verify the identity and exclusive nature of cells of interest. Specifically, gated cells based on EGFP expression and various cell surface markers were overlaid onto their respective FSC/SSC to identify their location; this strategy is referred to as backgating *(126)*. Backgating served to compensate for the limitation of being able to analyze a maximum of four fluorescent channels on the fluorescence activated cell sorting (FACS) calibur. Thus, phenotypic analysis of cells of

interest was performed using a combination of antibodies and their identities confirmed by backgating.

Flow cytometry also allows the identification and separation of fractions of a single cell type from a multi-fluorescently labeled cell mixture that can then be studied in isolation *(126)*. In the present study, cell sorting was used to enable separation of hMØ and mMØ for the ultimate purpose of studying potential functional differences between the two cell types following SCI.

1.15 SUMMARY AND RATIONALE

The inflammatory response to SCI produces both beneficial and harmful effects on the outcome of the injury. Our laboratory has shown that in rodents, treatment of SCI with a mAb to CD11d leads to neurological improvements and neuroprotection by selectively blocking the neutrophil response and only delaying the hMØ influx into the lesion. These results suggest that neuroprotective and neurodegenerative hMØ effects may be determined by the timing of influx into the lesion, which in turn may be due to the differential response of monocyte/hMØ subsets. To date, the contribution of hMØs to SCI remains unclear because they cannot be readily distinguished from mMØ based on morphology and immunophenotypic markers. The present study makes use of the *lys*-EGFP-*ki* mouse model that enables the distinction between $EGFP^+$ hMØ and $EGFP^-$ mMØ. The first stage of this work aims to assess the cellular response of neutrophils, heterogeneous monocytes/hMØ, and mMØ post-SCI by flow cytometry. The second stage of this work aims to phenotypically characterize the heterogeneous subsets of monocytes in the blood, and hMØ and mMØ in the spinal cord. The third stage of this

work aims to develop a protocol for sorting hMØ and mMØ with the goal of examining differences in mRNA expression of these two populations following SCI.

1.16 HYPOTHESIS

A differential temporal appearance is exhibited by monocytes in the blood and by infiltrating hMØ and mMØ in the spinal cord lesion following SCI.

1.17 SPECIFIC GOALS

1) To assess the inflammatory response to SCI.
    a. To compare peripheral leukocyte populations between the *lys*-EGFP-*ki* and the wild-type strain, C57BL/6 mice.
    b. To examine the response of neutrophils in the blood and infiltrating neutrophils in the spinal cord in the acute (1d, 3d, 7d) and chronic (14d and 6wks) stages of SCI.
    c. To examine the response of heterogeneous monocyte and hMØ subsets in the acute and chronic stages of SCI.
    d. To examine the response of mMØ in the acute and chronic stages of SCI.
    e. To determine whether CD45 expression can distinguish between hMØ and mMØ following SCI.
2) To phenotype the heterogeneous subsets of monocytes in the blood, and hMØ and mMØ in the spinal cord following SCI.
3) To develop a protocol for sorting hMØ and mMØ for mRNA expression studies.

The first goal was accomplished as follows: analysis of EGFP expression, monocyte/hMØ, and neutrophil frequencies in the blood and spleens of *lys*-EGFP-*ki* and C57BL/6 were performed by flow cytometry. As well, analysis of the blood and spinal cords of SCI, sham injured, and uninjured mice at specific time points post-injury by flow cytometry were performed. The second goal was achieved by phenotyping blood and spinal cord samples at a specific time point post-SCI by flow cytometry. The last goal was achieved by optimizing cell sorting of hMØ and mMØ to yield sorted cells with acceptable purities and intact RNA.

CHAPTER 2 - MATERIALS AND METHODS

All protocols used for this study were approved by the University of Western Ontario Animal Use Subcommittee and conform to the Canadian Council on Animal Care guidelines (Appendix 1).

2.1 ANIMALS

Lys-EGFP-ki mice

The original heterozygous *lys*-EGFP-*ki* transgenic mice were provided by Thomas Graf, from the Albert Einstein College of Medicine (Bronx, NY) and initially bred for use in the Health Sciences Animal Facility at the University of Western Ontario Animal Care and Veterinary Services. Subsequently, they underwent embryo re-derivation and were bred in the mouse barrier facility at the Robarts Research Institute to produce homozygous mice so as to maximize EGFP expression. All experiments included a combination of male and female *lys*-EGFP-*ki* mice, an exception being the cell sorting/mRNA expression studies, in which, only males were used to exclude potential female hormonal influences on gene expression.

C57BL/6 mice

The wild-type strain, C57BL/6 mice (Charles River Laboratories, Wilmington, MA), were used as controls for comparing peripheral leukocyte profiles with *lys*-EGFP-*ki* mice. All mice used for experimental purposes were between 8-14 weeks old.

2.2 PRE - OPERATIVE TREATMENT

The *Lys*-EGFP-*ki* transgenic mice that were at least 10 weeks (wks) old and weighing 20g were prepared for surgery by anaesthetization with 4% Isofluorane (Abbott

Laboratories, Quebec) in oxygen. Isofluorane was maintained at 1% throughout surgery. The mice were placed on a heating pad during surgery to keep the body temperature at 37°C. The surgical area on the back was shaved and sterilized using 1% Proviodine.

2.3 ACUTE SPINAL CORD COMPRESSION INJURY

A dorsal laminectomy was performed to expose the spinal cord between the T4 and T5 thoracic vertebrae. A modified aneurysm clip with a closing force of 8x g was placed around the cord *(130)* to compress the region between T4-T5 and snapped close for 60sec, after which the clip was released. The muscles and skin were then sutured to close the surgical area. The spinal cord compression produced a moderately severe SCI in mice and resulted in immediate paraplegia.

2.4 SHAM INJURY

A deep incision was made to expose the vertebral column, after which, the surgical area was closed by suturing the muscles and skin. Mice returned to normal activities after recovering from anesthesia.

2.5 POST - OPERATIVE TREATMENT

All SCI and sham injured mice were placed under a heat lamp for recovery from the surgery and were subcutaneously administered with Buprenorphine (0.05 mg/kg), 1mL saline to prevent dehydration, and 0.01mL Baytril (Bayer, Toronto, ON) to prevent post-surgical infections. After recovery, SCI mice were placed in cages with a grid on the

bottom, which enabled mice to pull themselves around with their front limbs. Sham injured mice were also placed in cages and did not require grids.

For SCI mice, Baytril was administered twice daily for 3 days (d) post-surgery. In addition, urinary bladder was manually expressed twice daily to compensate for their innate loss of bladder function. For SCI mice kept past 4wks, urinary bladder was expressed once daily or until the mouse had independent bladder control. At each of these times, the general health of the mice was assessed; 1mL of saline: dextrose (1:1) [Baxter Corp., Toronto, ON] as well as additional doses of Baytril was administered as required, to counter dehydration and infections respectively.

2.6 SCI ENDPOINTS

For quantitative studies of the inflammatory response of circulating blood and infiltrating spinal cord leukocytes, *lys*-EGFP-*ki* mice were euthanized at 1d, 3d, 7d, 14d, and 6wks post-SCI and sham injury. At each of these times, uninjured control mice were also used. For each time point, a pool of mice (n=2-4) was used and experiments were replicated to be statistically relevant (N=3-4). For graphic displays, a mean of all uninjured values is used and is indicated as 'baseline levels'.

For phenotypic analysis of monocytes in the blood and hMØ and mMØ in the spinal cord, uninjured and SCI (at 7d post-SCI) *lys*-EGFP-*ki* and C57BL/6 mice were used. For these studies, individual mice were used and experiments were replicated to be statistically relevant (N=4-5 mice).

For cell sorting/mRNA expression studies, uninjured and SCI (at 7d post-SCI) *lys*-EGFP-*ki* mice were used. For these studies, a pool of mice (n=4-5) was used and experiments were replicated to be statistically relevant (N=3).

2.7 SPLENOCYTE PREPARATION FOR FLOW CYTOMETRY

Mice were deeply anesthetized with Isofluorane. The spleens were removed and individually processed. Each spleen was placed on a sterile metal screen (Small Parts Inc, Miami Lakes, FL), pore size approximately 120μM, and the cells were pushed through the screen into a sterile petri dish with a sterile 10cc plunger. The screen was rinsed intermittently with cold PBS 0.1% bovine serum albumin (BSA) [EMD Chemicals Inc., Savannah, GA). The cell suspension was transferred to a 50mL conical tube (BD Biosciences, Mississauga, ON) and the total volume was brought up to 20mL using cold PBS 0.1% BSA. The samples were then centrifuged at 6°C for 5min at 500g. The supernatant was removed and the cell pellet was resuspended in 2.5mL of ACK lysis buffer (Lonza Biowhittaker, Switzerland) before the addition of another 2.5mL of the lysis buffer. Samples were incubated for 3min at room temperature (RT) and gently mixed every minute. The volume was adjusted to 20mL with cold PBS 0.1% BSA and centrifuged at 6°C for 5min at 500g. The supernatant was discarded, cell pellet was resuspended using cold PBS 0.1% BSA, and the cell suspension was then filtered using a 70μm nylon filter (BD Biosciences, Mississauga, ON). Cells were washed 2 more times before non-specific binding was blocked by incubating the cells with 5% volume-to-volume (v/v) normal goat serum (NGS, Jackson ImmunoResearch Laboratories Inc, West Grove, PA) for 20min. Excess NGS was removed by washing once with cold PBS 0.1%

BSA. Cell counts were determined using a hemocytometer, and the cells were resuspended to a final concentration of $5.0x10^6$cells/mL. Primary antibodies, allophycocyanin (APC) conjugated anti-Ly6C/G (1:400, BD Biosciences, Mississauga, ON), phycoerythrin (PE) conjugated anti-CD115 (1:100, eBioscience, San Diego, CA), Percpcy5.5 conjugated anti-CD45.2 (1:100, BD Biosciences, Mississauga, ON), and biotinylated anti-F4/80 (1:100, Abd Serotec, NC, USA) were added to $5x10^5$ cells per 100μL in individual flow cytometry tubes (BD Biosciences, Mississauga, ON). Samples were incubated for 30min on ice in the dark, washed using 2mL of cold PBS 0.1% BSA and centrifuged at 6°C for 5min at 500xg. The supernatant was discarded and samples containing biotinylated antibody were resuspended with 100μL of streptavidin-phycoerythrin (SA-PE) or streptavidin-allophycocyanin (SA-APC) in PBS 0.1% BSA (1:2000, BD Biosciences, Mississauga, ON). Samples were incubated once again on ice for 30min in the dark. A summary of all antibodies, isotype-matched controls, and binding specificities are found in Table 1. Cells were washed a final time and resuspended in 400μL of 0.5% paraformaldehyde (PFA) fixative. Sample data were acquired by flow cytometry within 48hr of preparation as described in Section 2.12.

2.8 PERIPHERAL BLOOD PREPARATION FOR FLOW CYTOMETRY

Mice were deeply anesthetized with Isofluorane. Blood samples were obtained intracardially by first injecting 0.01mL of heparin into the left ventricle, and collected in a 1cc syringe fitted with a 20 gauge (G) needle. Blood was transferred into a 15mL conical tube and red blood cells (RBC) were lysed by the addition of 5mL of ACK lysis

Table 1. A list of antibodies used in this study, their isotype-matched controls, and binding specificities.

Antibody	Isotype-matched control	Binding Specificity
APC anti-Ly6C/G	APC rIgG2b,k	Inflammatory monocytes, Intermediate monocytes, Neutrophils, plasmacytoid DC *(41, 51, 131-133)*
APC anti-CD11c PE/Cy7 anti-CD11c	APC hIgG1,k PE/Cy7 hIgG1,k	DC, natural killer (NK) cells, 'monocyte-like' subset, mMØ *(127, 131-133)*
APC anti-CD11b	APC rIgG2b,k	Monocytes, Neutrophils, hMØ, and mMØ, DC *(41, 51, 131-133)*
APC anti-CD8α	APC rIgG2a,k	Plasmacytoid dendritic cells *(131-133)*
APC anti-CD45R/B220	APC rIgG2a,k	Plasmacytoid dendritic cells, B-cells *(131-133)*
PE anti-CCR7	PE rIgG2a,k	Mature DC *(51)*
PE anti-NK1.1	PE rIgG2a,k	NK, NKT cells *(134)*
PE anti-PDCA-1	PE rIgG2b,k	Plasmacytoid dendritic cells *(131-133)*
PE anti-CD62L	PE rIgG2a,k	Peripheral leukocytes, 'inflammatory monocytes' *(41, 51, 131-133)*
PE anti-CD115	PE rIgG2a,k	Monocytes, hMØ, mMØ *(51, 135)*
PE anti-CD117	PE rIgG2b,k	Myeloid precursors *(136)*
Percpcy5.5 anti-CD45.2 Alexa 700 anti-CD45.2	Percpcy5.5 mIgG2a,k Alexa700 mIgG2a,k	Hematopoietic cells *(137)*
Biotin anti-F4/80	Biotin rIgG2b, k	Monocytes, hMØ, and mMØ, DC *(41, 51, 131-133)*
7AAD		Dead cells *(126)*

buffer and incubated on ice for 5min. Samples were gently mixed every minute by inverting the tubes. Thereafter, the volume was brought up to 15mL by the addition of cold PBS 0.1% BSA and centrifuged at 6°C for 5min at 500g. Steps carried thereafter were as described for splenocytes in section 2.7.

2.9 SPINAL CORD PREPARATION FOR FLOW CYTOMETRY

Transcardial perfusions were performed at 1d, 3d, 7d, 14d, and 6wks after SCI and sham injury. All mice were deeply anesthetized with Isofluorane. The perfusion was performed with 50mL of cold oxygenated tissue culture medium at pH 7.4 Dulbecco's Modified Eagle's Medium (DMEM). A total of 5mm of spinal cord was removed (2.5mm rostral and dorsal to the site of lesion) from SCI, sham injured and uninjured mice (Figure 3A, B). Spinal cord tissue pooled per animal group was ground between frosted slides into a homogenous cell suspension. The slides were rinsed with 5mL of cold PBS 0.1% BSA, filtered through a 70μm strainer into a 50mL conical tube, and the cell suspension was then transferred to a 15mL conical tube. Percoll (Amersham Biosciences, Uppsala, Sweden), made with a pH 7.0-7.2 via addition of HEPES [4-(2-hydroxyethyl)-1-piperazineethanesulfonic acid), Invitrogen Corp., Carlsbad, CA], was added to the cell suspension to a final concentration of 30% v/v. The cell suspension was underlaid with 1mL of 70% percoll [made by addition of HEPES and HBSS (Hank's balanced salt solution), Invitrogen Corp]. The gradient was centrifuged at 1300g at 6°C for 30min and resulted in a density based cell separation (Figure 3A and B). For each sample, the collected layer was removed and divided into two 15mL falcon tubes to maximize cell

Figure 3. Density-based cell separation of spinal cord tissue. Approximately 5mm (~2.5mm rostral and caudal to the lesion site) of dissociated spinal cord tissue was centrifuged in a percoll gradient and resulted in separation of myelin, debris/dead cells (pellet), and RBC from leukocytes and CNS cells in SCI samples (A). Separation of myelin and debris/dead cells (pellet) from CNS cells was achieved in sham injured and uninjured samples (B).

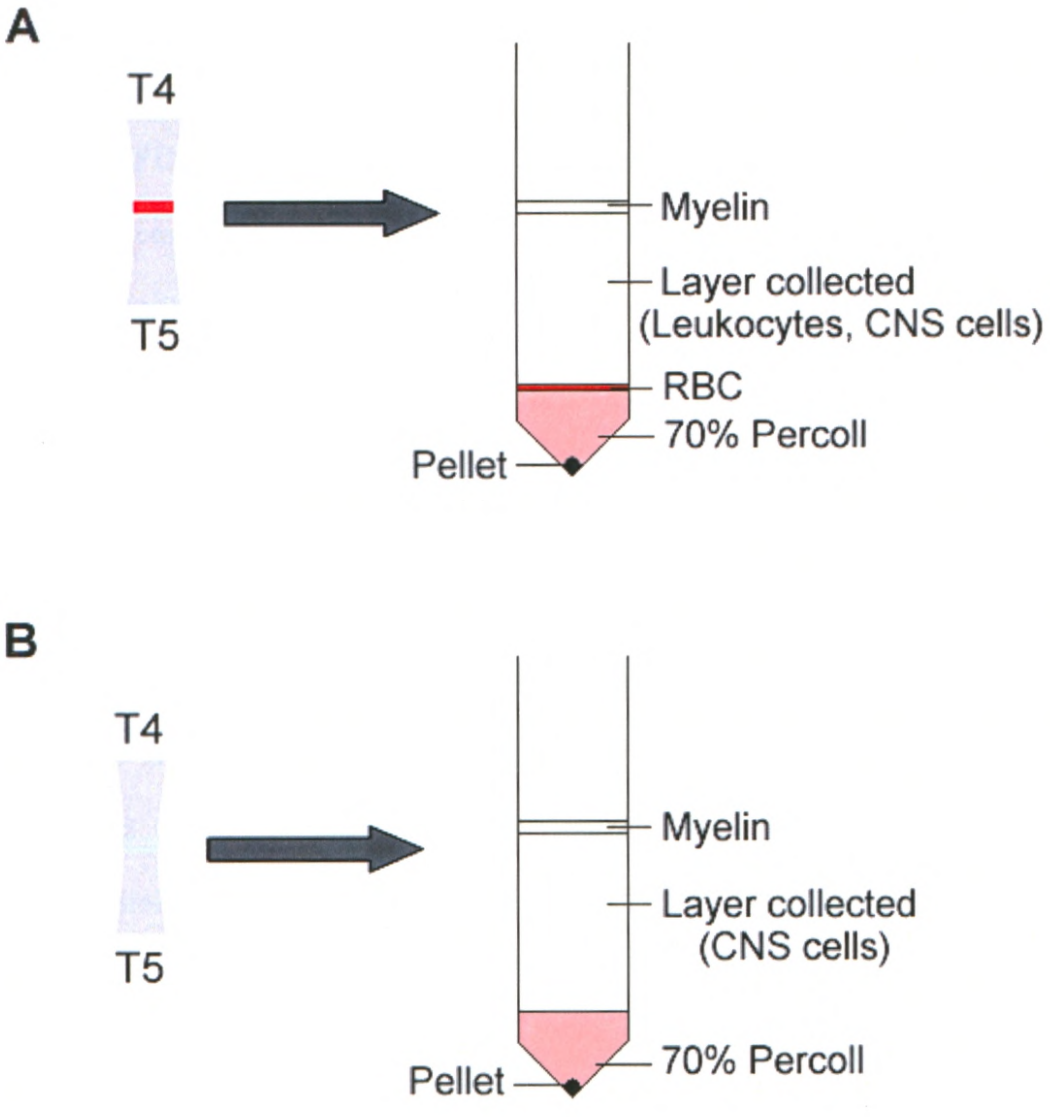
A
T4
T5
Myelin
Layer collected
(Leukocytes, CNS cells)
RBC
70% Percoll
Pellet
B
T4
T5
Myelin
Layer collected
(CNS cells)
70% Percoll
Pellet

recovery. The volume of each tube was brought to 15mL with addition of cold PBS 0.1% BSA. Cells were centrifuged at 6°C for 10min at 500g and the supernatants were discarded. Pellets from each sample were resuspended in PBS 0.1% BSA and pooled together. The remaining steps were carried out as described in section 2.7 except that centrifugation was done for 10mins.

2.10 PHENOTYPING BLOOD MONOCYTES

Blood processing of *lys*-EGFP-*ki* and C57BL/6 uninjured and mice at 7d post-SCI was done as described in section 2.8 except that additional antibodies were used to characterize the monocyte subsets: APC conjugated anti-CD11c (1:200, BD Biosciences), PE conjugated anti-CCR7 (1:200, BD Biosciences), and PE conjugated anti-CD62L (1:400, Biolegend, San Diego, CA). Further confirmatory phenotyping of monocytes was carried out in *lys*-EGFP-*ki* mice with PE/Cy7 conjugated anti-CD11c (1:200, Biolegend), PE conjugated anti-NK1.1 (1:100, Biolegend), PE conjugated anti-CD8α (1:1000, BD Biosciences), PE conjugated anti-CD45R/B220 (1:400, BD Biosciences), PE conjugated anti-PDCA-1 (1:400, Biolegend), PE conjugated anti-CD117 (1:800, Biolegend), and APC conjugated anti-CD11b (1:2000, BD Biosciences).

2.11 PHENOTYPING MICROGLIA, hMØ and mMØ IN THE SPINAL CORD

Spinal cord processing of *lys*-EGFP-*ki* and C57BL/6 uninjured and mice at 7d post-SCI was done as described in section 2.9 except that additional antibodies were used to characterize the resident and infiltrating macrophages as was done for blood monocytes in section 2.10.

2.12 FLOW CYTOMETRY

Spleen, blood, and spinal cord cells (10,000 or 35,000 cells/sample) were analyzed on a Becton Dickinson (BD) Biosciences fluorescence activated cell sorting (FACS) analog calibur equipped with an argon-ion laser and a helium laser that efficiently excites at 488nm and 635nm wavelengths respectively. Forward scatter (FSC-defines cell size) and side scatter (SSC-defines cell granularity) gates were set to include viable cells but to exclude RBC, debris, and remaining unbound particles. For all samples, EGFP was monitored on FL-1 channel whereas an array of antibodies was measured on the FL-2, FL-3, and FL-4 channels. Compensation was manually set, data acquisition was done using CELLQuest software (version 10, BD Biosciences, Franklin Lakes, NJ) and analysis was performed on FlowJo software version 7.1.2 (Tree Star, Inc., Ashland, OR). Detailed gating and analysis strategies used to define cells of interest will be addressed in the appropriate results section. The flow cytometry results in this work are presented as pseudocolor density plots, dot plot backgates, and histograms.

For initial studies, the viability of blood and spinal cord samples was determined using the viability marker, 7AAD. Regardless of the injury status of mice, viability was always consistent, with the frequency of $7AAD^+$ (dead) cells between 7-12% (Table 2).

2.13 QUANTIFICATION OF LEUKOCYTES IN THE SPINAL CORD

To quantify the absolute numbers of infiltrating neutrophils and hMØ, and resident microglia and mMØ in SCI, sham injured and uninjured spinal cords, the following calculation was performed:

	Blood (% 7AAD$^+$ cells)	Spinal Cord (% 7AAD$^+$ cells)
	Mean ± SEM	Mean ± SEM
Uninjured samples	8.58 ± 0.9	7.94 ± 2.0
Sham injured samples	8.68 ± 1.2	11.03 ± 2.9
SCI samples	10.08 ± 2.4	8.08 ± 2.0

$$\text{Absolute cell numbers} = *\frac{\text{cell frequency}}{100} \times \text{total cell number}$$

*Cell frequency and total cell numbers were determined by flow cytomtery results and calculations made during tissue processing respectively.

2.14 CELL SORTING

Blood and spinal cord cells were prepared as described in sections 2.8 and 2.9 except that HBSS 0.1% BSA was used as the washing buffer. After blocking, cells were stained with 3X the normal concentration of antibodies per 200µL to accommodate staining of large numbers of cells with biotinylated anti-F4/80, APC conjugated anti-CD11b, and Alexa 700 conjugated anti-CD45.2 (1:200, Biolegend) in the spinal cord; APC conjugated Ly6C/G was additionally added to the blood samples. The viability dye, 7-amino-actinomycin D (7AAD) was added (12µL 7AAD in 400µL of cells) to all samples. Additionally, anti-mouse and anti-rat compensation beads were used as per manufacturers' guidelines (BD Biosciences) for automated fluorescence compensation so as to maximize the number of cells in the sorting tubes. Sorting tubes contained at least $3.0x10^6$cells/400µL. Fluorescence minus one (FMO) and isotype-matched controls were used to accurately gate on cells of interest to be sorted. Cell sorting was done on live cells in a cooling chamber.

Cells were analyzed and sorted on a digital BD Biosciences FACSDiVa Vantage equipped with the DiVa software (BD Biosciences). Parameters of interest were detected either by the 488nm, 633nm, or UV laser. The sorter utilizes a custom fibre optic detector system and digital signal processing using FACSDiVa software for optimal signal detection, sample purity, and fast sort rates. In most applications, after a particle exits the

laser beam, it is sent to waste. Sorting allows capturing and collecting cells of interest for further analysis such as biochemical, microscopic, or functional studies. Population of interest is identified and a logical gate is placed on the region and loaded on to the software as the sort gate and this identifies the cells to be sorted out of the stream. Detailed explanation of cell sorting strategy is explained in the specific results section.

Sorted cells were collected in 100μL of serum free VP-SFM (Virus Production Serum Free Medium, Invitrogen). Immediately after cell sorting, 10μL of sorted sample was removed and mixed with sheath fluid in order to assess sorted cell purity. For spinal cords of uninjured and 7d post-SCI mice, the remainder of the sorted cells were mixed with 500μL of RNA protect cell reagent (Qiagen, Austin, Texas) to stabilize RNA and stored in -80°C until RNA extraction.

2.15 RNA EXTRACTION

RNA extraction of protected sorted cells was done using the RNeasy Plus Micro Kit (Qiagen) as per manufacturer's guidelines. Briefly, cell were thawed and centrifuged for 5mins at 5000g at 25°C and the supernatant was removed. Cells were disrupted by addition of Qiagen buffer RLT Plus and homogenized by vortexing for 1min. The homogenized lysate was transferred to a genomic DNA eliminator spin column placed in a 2mL collection tube. Samples were centrifuged for 30sec at ≥8000g and the columns were discarded. One volume of 70% ethanol was added to the flow-through and mixed by pipetting. The samples were then transferred to an RNeasy MinElute spin column placed in a 2mL collection tube and centrifuged for 15sec at ≥8000g. The flow-through was discarded and Qiagen buffer RW1 was added to the column and centrifuged again for

15sec at ≥8000g. The step was repeated again except that Qiagen buffer RPE was added to the column. Thereafter, the column was washed with 80% ethanol and centrifuged for 2mins at ≥8000g. The column was centrifuged a second time for 2mins to remove residual ethanol. Thereafter, the column was placed in 1.5mL collection tube with addition of 12μL of RNase-free water and centrifuged for 1min at full speed to elute RNA.

2.16 RNA QUALITY/QUANTITY CHECK

The quality and quantity of extracted RNA was assessed using a Bioanalyzer Pico kit (Agilent Technologies, Mississauga, ON). Generally, a ratio of 2:1 for 28S:18S RNA was considered to indicate samples with good RNA quality.

2.17 COMPUTATIONAL AND STATISTICAL ANALYSIS

Data are expressed as mean ± standard error of mean (SEM). Graphic displays of data and student t-test were performed using Graph pad prism (version 4.0, GraphPad Software, La Jolla, CA). Two-way analysis of variance (ANOVA) and one-way ANOVA were done using GB stat (version 7.0) and sigma stat (version 3.0) respectively followed by Fishers test for post-hoc analysis. For all analysis, statistical significance was accepted at $P \leq 0.05$ and refers to comparisons made either between SCI and uninjured mice, or sham injured and uninjured mice.

CHAPTER 3 – RESULTS

The results below are presented as follows: Firstly, peripheral leukocytes are compared between the *lys*-EGFP-*ki* and C57BL/6 mice. Secondly, the inflammatory response of neutrophils, monocytes/hMØ, and mMØ to SCI is determined. Additionally, the response of subsets of monocytes/hMØ to SCI is examined. Thirdly, phenotypic characterization of monocytes, hMØ, and mMØ subsets is presented. Lastly, the technique for sorting hMØ and mMØ in the spinal cord is described.

3.1 EXAMINATION OF PERIPHERAL LEUKOCYTES IN THE *LYS*-EGFP-*KI* AND C57BL/6 MICE

3.1.1 EGFP expression status of leukocytes in the blood and spleen

Faust et al. *(120)* examined the frequency of $EGFP^+$ cells in the peripheral blood of heterozygous *lys*-EGFP-*ki* mice using flow cytometry (14-44%). In the present study, EGFP expression of leukocytes in the blood and spleen of homozygous *lys*-EGFP-*ki* mice were compared to that of the wild-type strain, C57BL/6 mice. Results showed that on average, 27% and 4.3% of leukocytes were $EGFP^+$ in the *lys*-EGFP-*ki* blood (Figure 4A and C) and spleen (Figure 4D and F) respectively. EGFP expression was absent in the C57BL/6 blood (Figure 4B and C) and spleen (Figure 4E and F). Thus, the frequency of circulating $EGFP^+$ peripheral leukocytes in homozygous *lys*-EGFP-*ki* mice is consistent with that initially described of their heterozygous counterparts *(120)*.

Figure 4. Comparison of $EGFP^+$ peripheral leukocyte frequencies in the *lys*-EGFP-*ki* and C57BL/6 mice using flow cytometry. A viable gate was placed on the FSC/SSC plots of blood and spleen. Gated cells were examined for EGFP expression in the blood of *lys*-EGFP-*ki* (A) and C57BL/6 (B) mice. A similar analysis was done for the spleen of *lys*-EGFP-*ki* (D) and C57BL/6 (E) mice. Mean frequency of $EGFP^+$ leukocytes in the blood (C) and spleen (F) of *lys*-EGFP-*ki* and C57BL/6 mice are shown. Student's t-test, $*P \leq 0.05$. N=4-5.

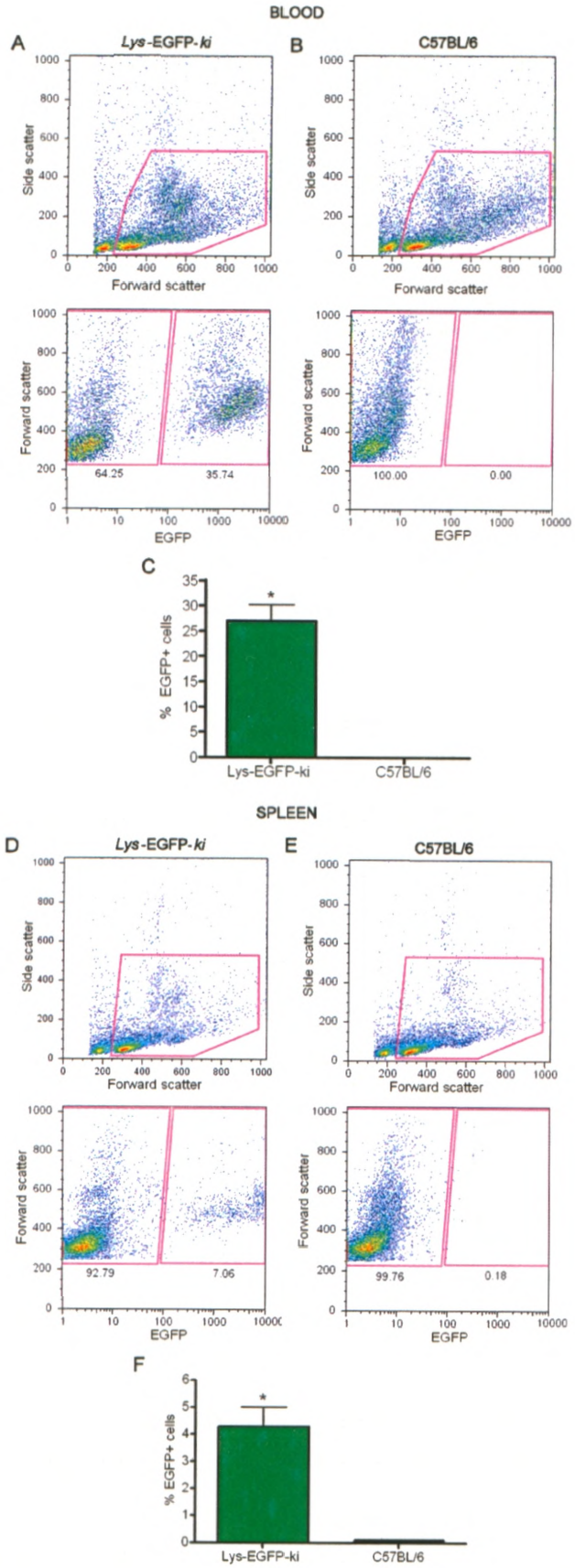
BLOOD
A
Lys-EGFP-ki
B
C57BL/6
Side scatter
Forward scatter
Forward scatter
EGFP
64.25
35.74
100.00
0.00
C
% EGFP+ cells
Lys-EGFP-ki
C57BL/6
SPLEEN
D
Lys-EGFP-ki
E
C57BL/6
92.79
7.06
99.76
0.18
F
% EGFP+ cells
Lys-EGFP-ki
C57BL/6

3.1.2 Frequency of circulating blood neutrophils and monocytes

Neutrophils have been identified as cells that express the Ly6C/G surface marker *(138)*. However, recent studies have shown that a subset of monocytes also express Ly6C/G *(41, 48)* in addition to F4/80 (pan monocyte/MØ marker) *(138-140)*. Thus, in the present study, neutrophils are identified as cells that are Ly6C/G$^+$ and F4/80$^-$, while peripheral monocytes/MØ are defined as cells that are F4/80$^+$ and CD115$^+$, both of which are pan monocyte/MØ markers. In order to enable examination of the absolute frequencies of peripheral neutrophils and monocyte/MØ relative to the total cell population, the EGFP expression of each population was not accounted for. Unless otherwise specified, this strategy holds true for all peripheral blood and spleen analysis presented in this work.

Using the strategy described above, the frequencies of blood neutrophils and monocytes were compared between the *lys*-EGFP-*ki* and C57BL/6 mice. Neutrophils were found to be two-fold higher in the *lys*-EGFP-*ki* mice (13%) (Figure 5A and F) than in the C57BL/6 (6%) mice (Figure 5B and F). The monocyte levels were similar between the *lys*-EGFP-*ki* (Figure 5C and F) and C57BL/6 (Figure 5D and F) mice having an average frequency of 16%. Backgating of each population showed that neutrophils appeared somewhat denser on the FSC/SSC plot of the *lys*-EGFP-*ki* (Figure 5A) than the C57BL/6 (Figure 5B) mice reflecting the differences seen in their neutrophil frequencies, while monocytes appeared to be similar between the two strains (Figure 5C and D). Although not shown, both the neutrophils and the monocytes of *lys*-EGFP-*ki* mice were EGFP$^+$.

Figure 5. Comparison of blood neutrophil and monocyte frequencies in the *lys*-EGFP-*ki* and the C57BL/6 mice using flow cytometry. Viable cells were gated for identification of neutrophils based on Ly6C/G^{+}, F4/80^{-} expression in the *lys*-EGFP-*ki* (A) and C57BL/6 mice (B). Monocytes were identified as F4/80^{+}, CD115^{+} cells in the *lys*-EGFP-*ki* (C) and C57BL/6 mice (D). Green represents neutrophils (A, B) and monocytes (C, D) backgated on to their respective FSC/SSC plots. Grey represents the rest of the cells present in the respective samples. Isotype-matched controls for neutrophil and monocyte antibody staining are shown (E). Frequency of circulating neutrophils and monocytes in the *lys*-EGFP-*ki* and C57BL/6 mice (F). Student's t-test, *$P \leq 0.05$. N=4-5.

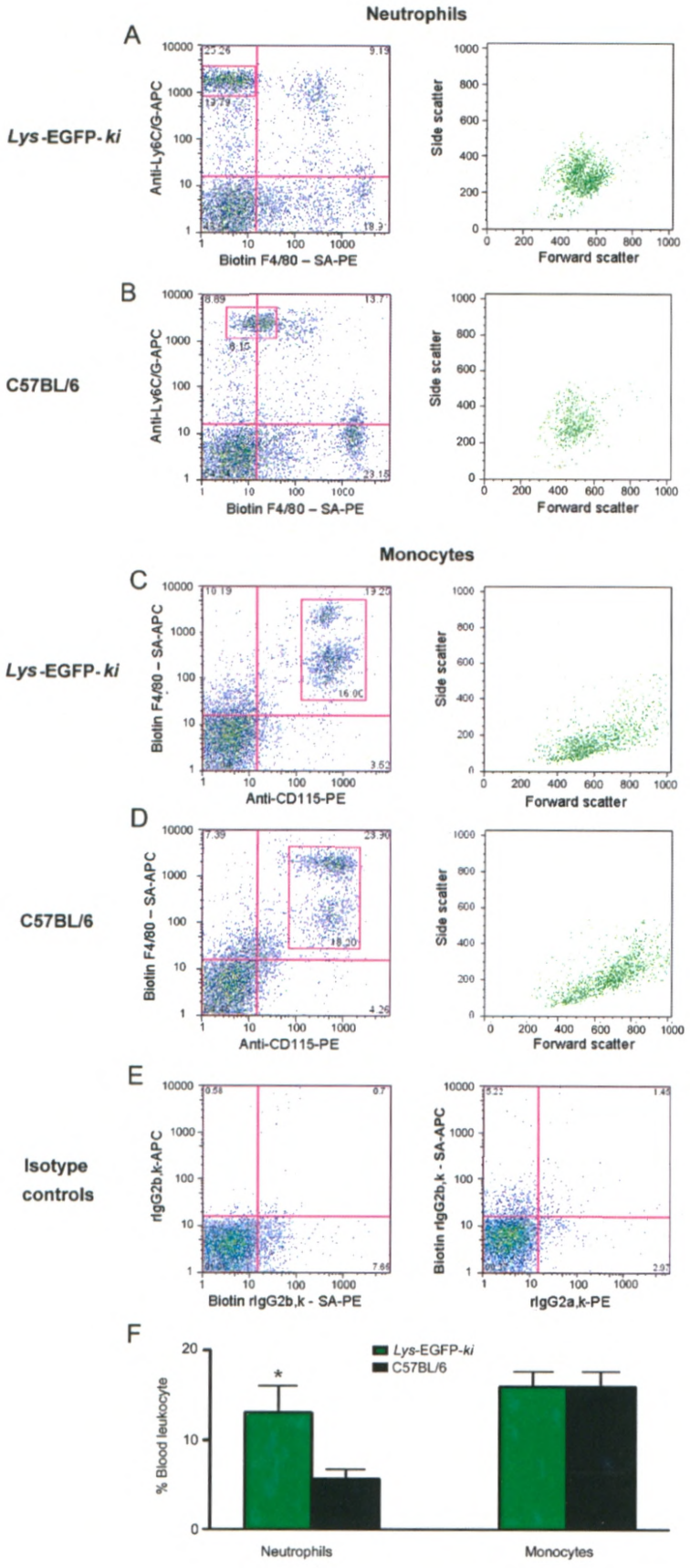
Neutrophils
A
Lys-EGFP-ki
Anti-Ly6C/G-APC
Biotin F4/80 – SA-PE
Side scatter
Forward scatter
B
C57BL/6
Anti-Ly6C/G-APC
Biotin F4/80 – SA-PE
Side scatter
Forward scatter
Monocytes
C
Lys-EGFP-ki
Biotin F4/80 – SA-APC
Anti-CD115-PE
Side scatter
Forward scatter
D
C57BL/6
Biotin F4/80 – SA-APC
Anti-CD115-PE
Side scatter
Forward scatter
E
Isotype controls
rIgG2b,k-APC
Biotin rIgG2b,k - SA-PE
Biotin rIgG2b,k - SA-APC
rIgG2a,k-PE
F
Lys-EGFP-ki
C57BL/6
% Blood leukocyte
Neutrophils
Monocytes

3.1.3 Frequency of splenic neutrophils and hMØ

The neutrophil and hMØ frequencies in the spleen of *lys*-EGFP-*ki* and C57BL/6 mice were compared next. Results revealed that neutrophil levels were not significantly different between the transgenic (2.1%) (Figure 6A and F) and C57BL/6 (2.5%) (Figure 6B and F) mice. The levels of splenic hMØs were also similar between the *lys*-EGFP-*ki* (3.0%) (Figure 6C and F) and C57BL/6 (3.5%) mice (Figure 6D and F). Additionally, backgating neutrophils (Figure 6A and B) and hMØ (Figure 6C and D) revealed similar FSC/SSC profiles between the two strains.

Overall, these results suggest that the peripheral leukocyte levels are comparable between the *lys*-EGFP-*ki* and C57BL/6 strain, although the former consists of higher circulating neutrophils. Thus using the *lys*-EGFP-*ki* mouse may be suitable for experimental SCI studies and will possibly be relevant to other SCI studies. Currently, the C57BL/6 strain is the standard mouse used for SCI research *(141)*.

3.2 THE NEUTROPHIL RESPONSE TO SCI

Previously, using immunohistochemistry we showed that neutrophils infiltrated the injured *lys*-EGFP-*ki* spinal cord at 1d, peaking at 3d, declining to baseline levels at 7d, and returning in reduced numbers at 14d post-SCI *(25)*. To validate our immunohistochemical approach, the present study examined the effect of SCI on the circulating neutrophil frequency in the blood, and the frequency and numbers of infiltrating neutrophils in the spinal cord lesion of *lys*-EGFP-*ki* mice. These responses were assessed in the acute (1d, 3d, and 7d) and chronic (14d and 6wks) stages of SCI using flow cytometry.

Figure 6. Comparison of splenic neutrophil and macrophage frequencies in the *lys*-EGFP-*ki* and the C57BL/6 mice using flow cytometry. Viable cells were gated for identification of neutrophils based on Ly6C/G^{+}, F4/80^{-} expression in the *lys*-EGFP-*ki* (A) and C57BL/6 mice (B). Macrophages were identified as F4/80^{+}, CD115^{+} cells in the *lys*-EGFP-*ki* (C) and C57BL/6 mice (D). Green represents neutrophils (A, B) and macrophages (C, D) backgated on to their respective FSC/SSC plots. Grey represents the rest of the cells present in the respective samples. Isotype-matched controls for neutrophil and macrophage antibody staining are shown (E). Frequency of splenic neutrophils and macrophages in the *lys*-EGFP-*ki* and C57BL/6 mice (F). N=4-5.

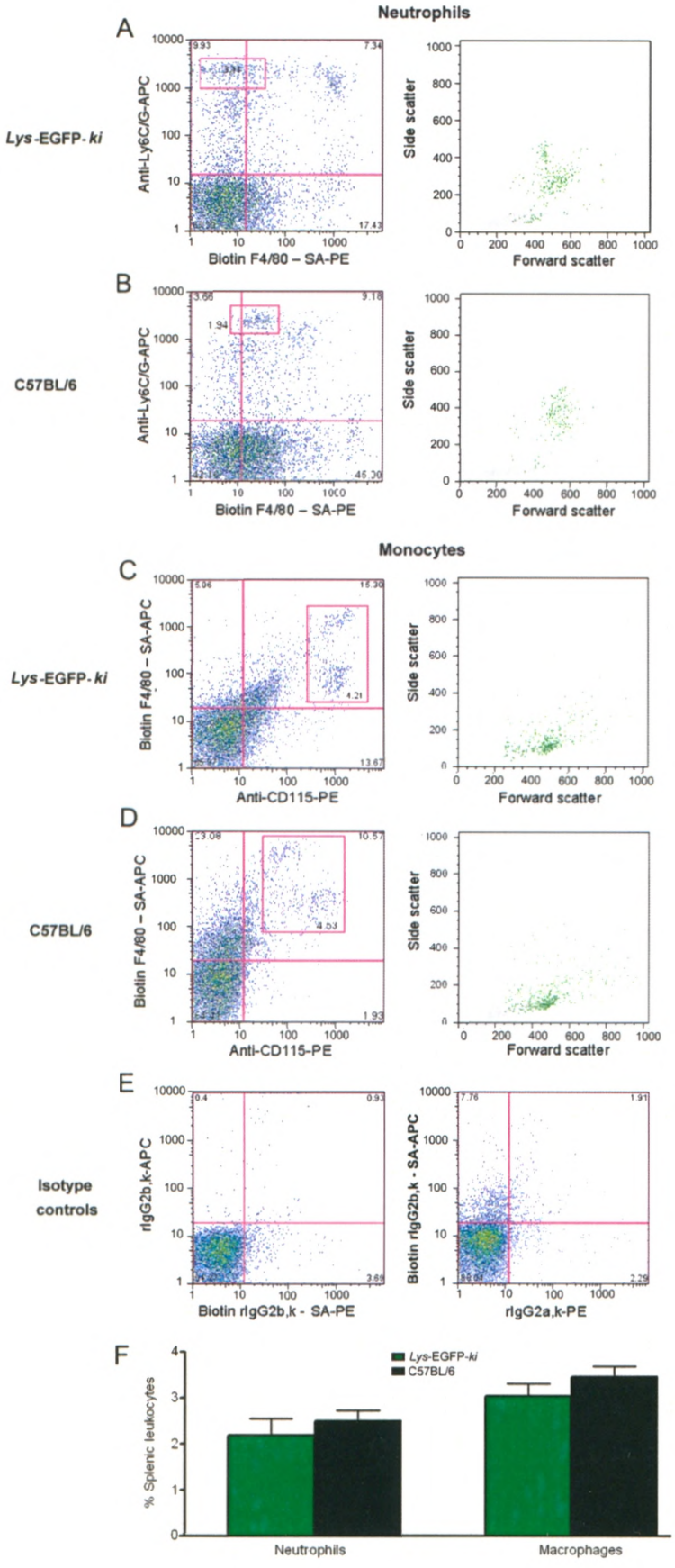
Neutrophils
A
Lys-EGFP-ki
Anti-Ly6C/G-APC
Biotin F4/80 – SA-PE
Side scatter
Forward scatter
B
C57BL/6
Monocytes
C
Lys-EGFP-ki
Biotin F4/80 – SA-APC
Anti-CD115-PE
D
C57BL/6
E
Isotype controls
rIgG2b,k-APC
Biotin rIgG2b,k - SA-PE
Biotin rIgG2b,k - SA-APC
rIgG2a,k-PE
F
Lys-EGFP-ki
C57BL/6
% Splenic leukocytes
Neutrophils
Macrophages

Results of the flow analysis revealed that the frequency of circulating blood neutrophils in SCI mice was significantly higher at all time points (1d, 3d, 7d, 14d, and 6wks) compared to uninjured mice (Figure 7C). The variable levels of neutrophils observed in the SCI blood samples over the time points examined, were not significantly different by a two-way ANOVA (Figure 7C). Neutrophil levels were similar between the uninjured and sham injured mice at all times except at 1d when the neutrophil frequency in the latter group was comparable to that of SCI mice (Figure 7C). This increase in blood neutrophil levels at 1d post-sham injury is probably due to the acute transient inflammation induced by the surgical procedure in these mice.

The frequencies and absolute numbers of neutrophils infiltrating into the injured spinal cord at 1d, 3d, 7d, 14d, and 6wks post-SCI were also examined. Results showed that the frequency of neutrophil infiltration into the SCI lesion significantly increased at 1d and 3d post-SCI and decreased thereafter (Figure 8C). The frequency of neutrophils was similar between sham injured and uninjured mice; the increase at 1d post-sham injury was not significantly different from uninjured mice (Figure 8C). When the absolute numbers of neutrophils were determined, neutrophil infiltration peaked at 1-3d, decreased at 7-14d, and persisted in reduced numbers to 6wks post-SCI (Figure 8D). The numbers of neutrophils in sham injured and uninjured mice were similar at all times (Figure 8D). Differences observed in the frequency and absolute numbers of infiltrating neutrophils into the spinal cord may be attributed to the fact that the former reflects the overall integrity of the spinal cord lesion. In the early time points post-SCI, the frequency of neutrophils increases as a result of the inflammatory response to tissue destruction

Figure 7. Examination of the circulating blood neutrophil response to SCI by flow cytometry. Viable gated cells in the blood (A) were further gated to identify neutrophils based on Ly6C/G^{+}, F4/80^{-} expression with the use of isotype-matched controls (B). Comparison of neutrophil levels in the uninjured, sham injured, and SCI samples at various times post-injury are shown (C). Representative dot plots for uninjured *lys*-EGFP-*ki* blood samples are shown (A-B). Two-way ANOVA followed by Fisher's test, *$P \leq 0.05$. N=3-4, n=2-4. Baseline levels represent a mean of uninjured samples.

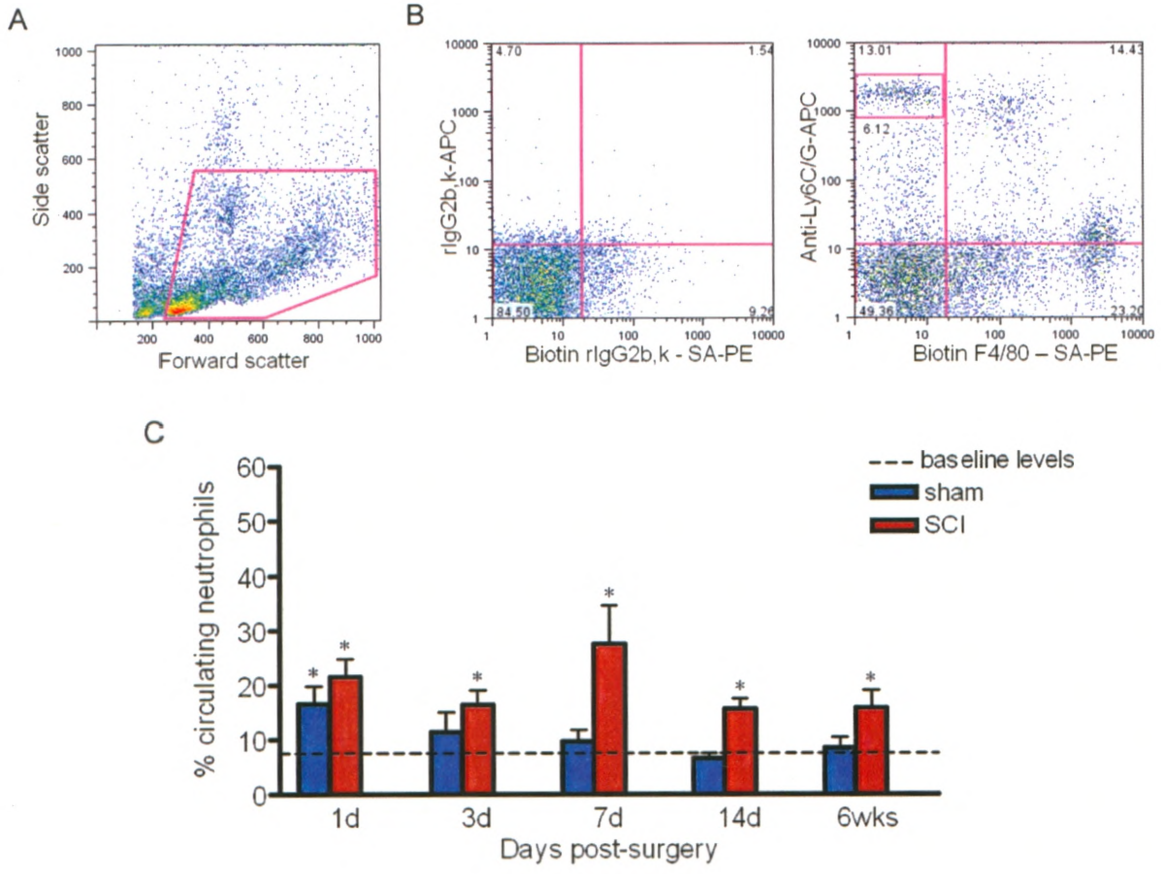
A
Side scatter
Forward scatter
B
rIgG2b,k-APC
Biotin rIgG2b,k - SA-PE
Anti-Ly6C/G-APC
Biotin F4/80 – SA-PE
C
% circulating neutrophils
baseline levels
sham
SCI
1d
3d
7d
14d
6wks
Days post-surgery

Figure 8. Examination of the infiltrating neutrophil response to SCI by flow cytometry. Gated cells in the spinal cord FSC/SSC (A) were further gated to identify neutrophils in the spinal cord lesion based on $Ly6C/G^{+}$, $F4/80^{-}$ expression with the use of isotype-matched controls (B). Comparison of neutrophil frequencies (C) and absolute numbers (D) in the spinal cords of uninjured, sham injured, and SCI samples at various times post-injury are shown. Representative dot plots from samples at 3d post-SCI, a time at which neutrophils peak in the lesion, are shown (A-B). Two-way ANOVA followed by Fisher's test, $*P \leq 0.05$. N=3-4, n=2-4. Baseline levels represent a mean of uninjured samples.

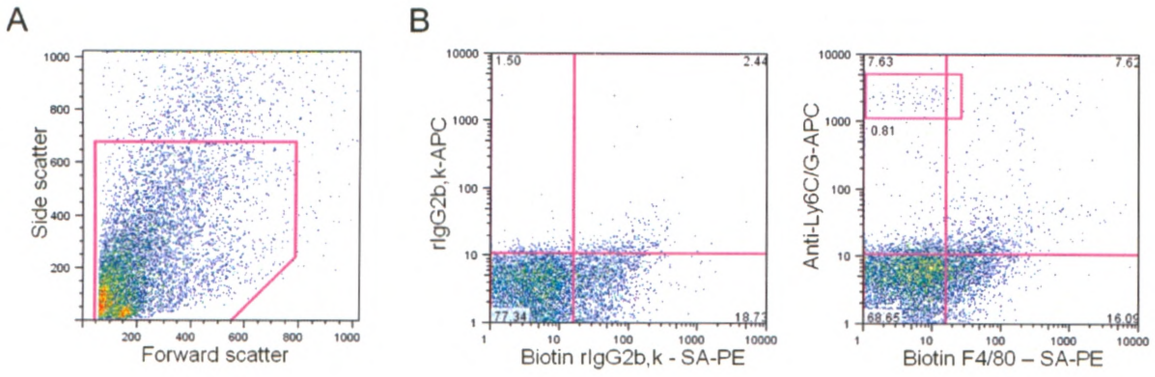
A
Side scatter
Forward scatter
B
rIgG2b,k-APC
Biotin rIgG2b,k - SA-PE
Anti-Ly6C/G-APC
Biotin F4/80 – SA-PE

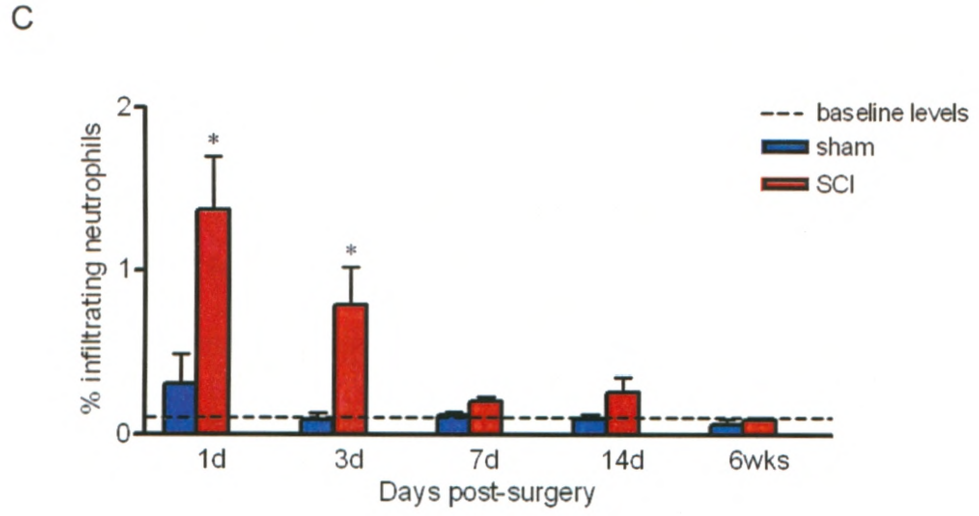
C
% infiltrating neutrophils
baseline levels
sham
SCI
1d
3d
7d
14d
6wks
Days post-surgery

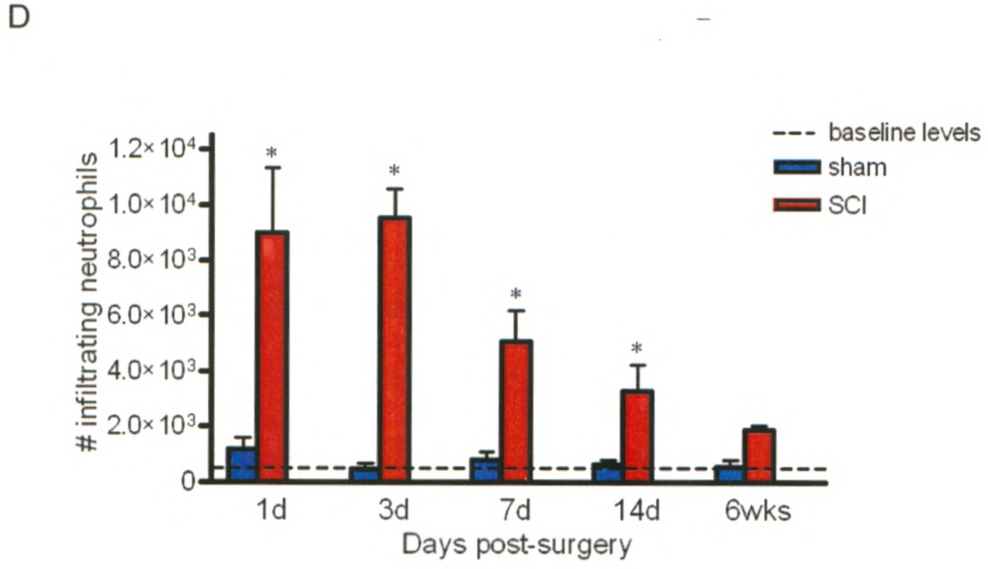
D
infiltrating neutrophils
baseline levels
sham
SCI
1d
3d
7d
14d
6wks
Days post-surgery

while in the later time points, the frequency of neutrophil decreases as a result of macrophages, microglia, and other cells that gather at the lesion site. Thus, the absolute numbers of neutrophils in the spinal cord appears to give a better representation of its infiltration pattern post-SCI.

Together, our results show that neutrophils respond to the acute and chronic stages of SCI pathology as seen by the increase in their levels in the circulation and their distinct infiltration pattern in the spinal cord lesion. Also, the pattern of neutrophil infiltration into the SCI lesion as obtained by flow cytometry in the present study are similar to that observed previously by immunohistochemistry *(25)*.

3.3 THE HEMATOGENOUS MONOCYTE AND MØ RESPONSE TO SCI.

Our previous immunohistochemical data indicate that post-SCI, hMØ numbers in the spinal cord lesion increase at 1-3d, peak at 7d, and decrease gradually thereafter *(25)*. In the present study, the response of monocytes in the blood as well as their corresponding infiltrating hMØs in the injured spinal cord was examined. Furthermore, investigation of the potential differential response of circulating monocyte subsets and infiltrating hMØ subsets to SCI was undertaken.

3.3.1 The circulating monocyte response to SCI

The flow analysis of the overall monocyte response to SCI revealed that circulating blood monocyte levels significantly increased at 3d, 14d, and 6wks post-SCI (Figure 9C). The monocyte frequency in SCI mice at 1d and 7d was similar to that observed in the corresponding control mice (Figure 9C). Monocyte levels were also

Figure 9. Examination of the circulating blood monocyte response to SCI by flow cytometry. Viable gated cells in the blood (A) were further gated to identify monocytes based on $F4/80^{+}$, $CD115^{+}$ expression with the use of isotype-matched controls (B). Comparison of monocyte frequencies between the uninjured, sham injured, and SCI samples at various times post-injury are shown (C). Representative dot plots from uninjured samples are shown (A-B). Two-way ANOVA followed by Fisher's test, $*P \leq 0.05$. N=3-4, n=2-4. Baseline levels represent a mean of uninjured samples.

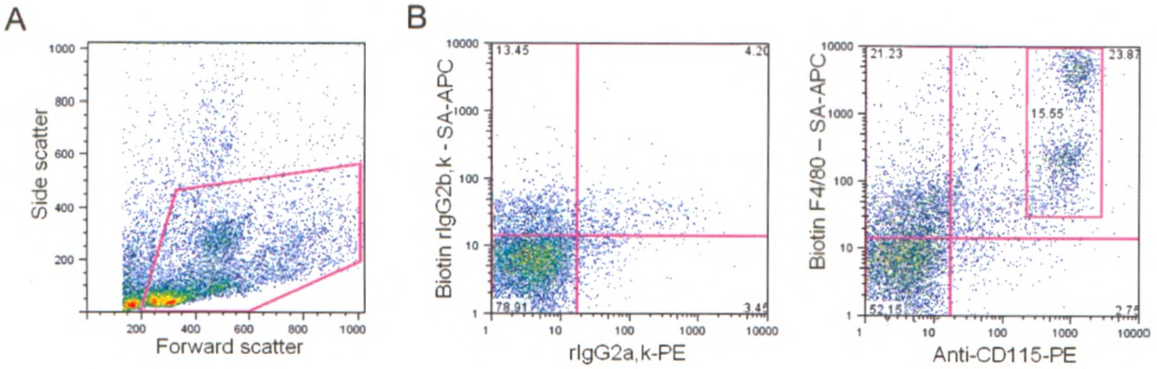
A
Side scatter
Forward scatter
B
Biotin rIgG2b,k - SA-APC
rIgG2a,k-PE
13.45
4.20
78.91
3.45
Biotin F4/80 – SA-APC
Anti-CD115-PE
21.23
23.83
15.55
52.18
2.75

C

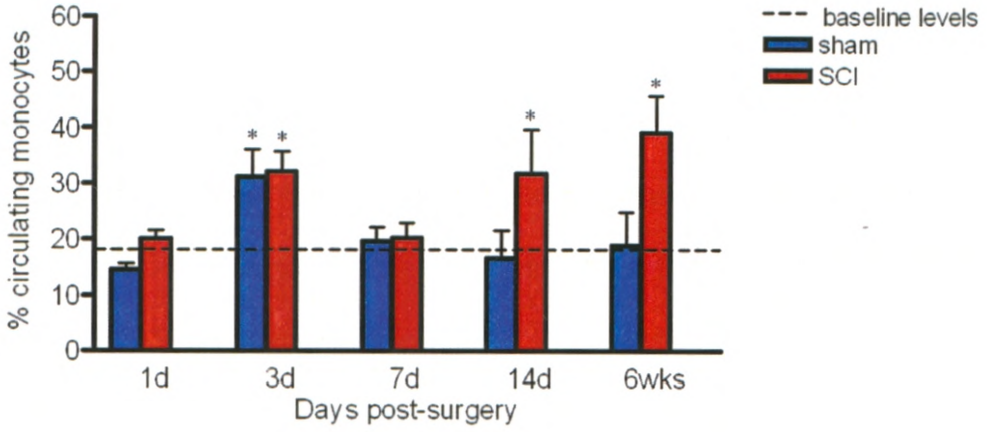
% circulating monocytes
Days post-surgery
1d
3d
7d
14d
6wks
baseline levels
sham
SCI

similar between uninjured and sham injured mice at all times except at 3d, when the frequency of monocytes in the latter was comparable to that of SCI mice (Figure 9C). This observation may be related to the acute response of the sham-injured mice to transient surgery-induced inflammation.

Tacke and Randolph *(48)* identified two blood monocyte subsets using the CX_3CR1/gfp mice: CX_3CR1^{lo}, $CCR2^{+}$, $Ly6C/G^{+}$, $CD62L^{+}$ (classical inflammatory) and CX_3CR1^{hi}, $CCR2^{-}$, $Ly6C/G^{-/lo}$, $CD62L^{-/lo}$ (non-classical resident) monocytes. In the present study, the two blood monocyte subsets were differentiated as $F4/80^{lo}$, $Ly6C/G^{+}$ (classical inflammatory) and $F4/80^{hi}$, $Ly6C/G^{-/lo}$ (non-classical resident) monocytes (Figure 10A). For simplicity, from here on, the $Ly6C/G^{-/lo}$ expression on the 'non-classical resident' monocytes is referred to as $Ly6C/G^{-}$. The same holds true with reference to CD62L expression. Examination of the two monocyte subsets in response to SCI showed that under resting conditions in the uninjured blood, the frequency of 'non-classical resident' monocytes was two-fold higher than that of the 'classical inflammatory' monocytes (Figure 10B). In response to SCI, the 'non-classical resident' monocytes increased at 3d, decreased at 7d, and then rose to higher levels at 14d and 6wks post-SCI (Figure 10B). Although a trend in the 'classical inflammatory' monocyte frequency towards increased levels was seen at 3d and 7d, statistical significance was achieved only at 7d post-SCI (Figure 10B). Interestingly, the 'non-classical resident' monocyte subset seems to contribute to the increase seen in overall monocyte levels at 3d, 14d, and 6wks post-SCI shown in Figure 9C. Similar to neutrophils, our results show that blood monocyte levels increase in response to the acute and chronic stages of SCI. However, the dynamics of monocyte subset responses differ substantially post-SCI.

Figure 10. Examination of blood monocyte subset responses to SCI by flow cytometry. Viable gated cells in FSC/SSC plots of blood were further gated to identify monocyte subsets based on F4/80^{lo}, Ly6C/G^{+} ('classical inflammatory' monocytes) and F4/80^{hi}, Ly6C/G^{-} ('non-classical resident' monocytes) with the use of isotype-matched controls (A). Comparison of the frequencies of each monocyte subset in the uninjured and SCI samples at various times post-injury is shown (B). The 'classical inflammatory' and 'non-classical resident' monocytes shown in (A) using red and blue gates respectively correspond to their representations in (B). Representative dot plots from uninjured samples are shown (A). Two-way ANOVA followed by Fisher's test, *$P \leq 0.05$. N=3-4, n=2-4. Baseline levels represent a mean of uninjured samples.

A

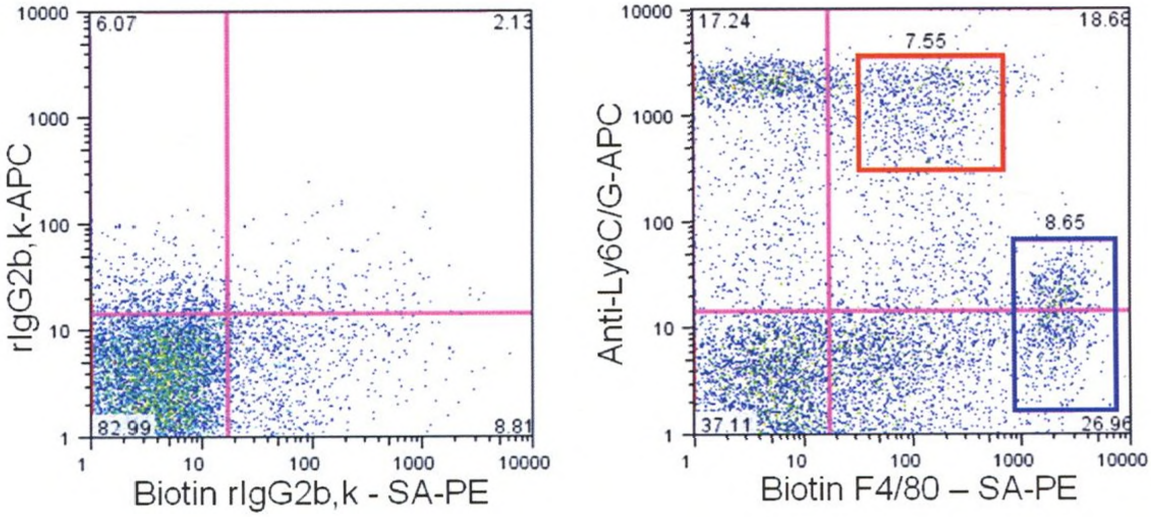
6.07
2.13
82.99
8.81
rIgG2b,k-APC
Biotin rIgG2b,k - SA-PE
17.24
7.55
18.68
8.65
37.11
26.96
Anti-Ly6C/G-APC
Biotin F4/80 – SA-PE

B

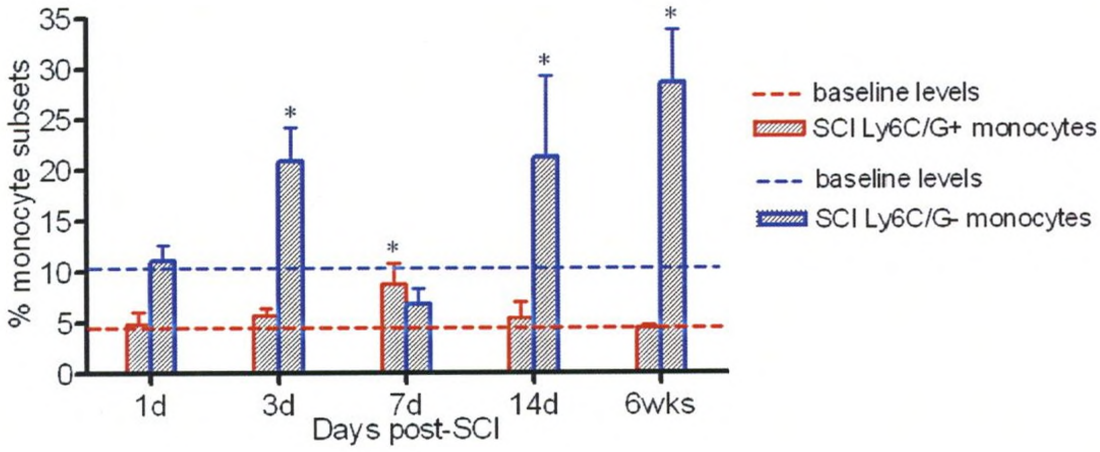
% monocyte subsets
Days post-SCI
1d
3d
7d
14d
6wks
baseline levels
SCI Ly6C/G+ monocytes
baseline levels
SCI Ly6C/G- monocytes

3.3.2 The infiltrating hMØ response to SCI

For spinal cord samples, total cells were examined for expression of F4/80 and EGFP to differentiate $F4/80^{+}$, $EGFP^{+}$ hMØ from $F4/80^{+}$, $EGFP^{-}$ mMØ. Thereafter, further analysis of each population was performed as required. The frequency of hMØ infiltration into the SCI lesion peaked at 1d, decreased at 3d, increased at 7d, dropped at 14d, and was similar to baseline levels at 6wks post-SCI (Figure 11C). When the absolute numbers of hMØ infiltration were examined, they increased at 1d and 3d, peaked at 7d, decreased at 14d, and persisted in reduced numbers at 6wks post-SCI (Figure 11D). Interestingly, at all times post-SCI, an inverse relationship of overall blood monocyte and infiltrating numbers of hMØ response is seen in the SCI lesion (Figures 9C and 11D).

The infiltrating hMØ were further analyzed to identify whether subsets of hMØ exists in the SCI lesion. Contrary to literature *(48, 50, 52)*, we observed that hMØ corresponding to the two blood monocyte subsets are present in the inflamed SCI lesion (Figure 12A-C). Examination of the hMØ subsets revealed that the 'non-classical resident' hMØ subset was found in reduced numbers in the SCI lesion at 1d and gradually increased thereafter up to 6wks post-SCI, at which time it was the predominant hMØ population in the lesion (Figure 12D). However, the 'classical inflammatory' hMØ subset was predominantly found in the lesion at 1d, and thereafter gradually decreased, such that it contributed to less than 10% of hMØ at 6wks post-SCI. At 3d post-SCI, both hMØ subsets were present in the lesion at similar levels (Figure 12D).

Overall, it seems that the 'classical inflammatory' monocytes and hMØ are the major monocytic population present in the acute response to SCI while the 'non-classical resident' monocytes and hMØ are involved in the chronic stages of SCI.

Figure 11. Examination of the infiltrating hMØ and resident mMØ response to SCI by flow cytometry. Gated cells in the spinal cord FSC/SSC plot (A) were further classified by placing gates on $F4/80^{+}$, $EGFP^{+}$ and $F4/80^{+}$, $EGFP^{-}$ cells to identify hMØ and mMØ respectively in the spinal cord lesion with the use of isotype-matched controls (B). Comparison of hMØ and mMØ frequencies (C, E) and absolute numbers (D, F) in the spinal cords of uninjured, sham injured, and SCI samples at various times post-injury is shown. Representative dot plots are from samples at 7d post-SCI, a time at which hMØ and mMØ peak in the spinal cord lesion (A-B). Two-way ANOVA followed by Fisher's test, $*P \leq 0.05$. N=3-4, n=2-4. Baseline levels represent a mean of uninjured samples.

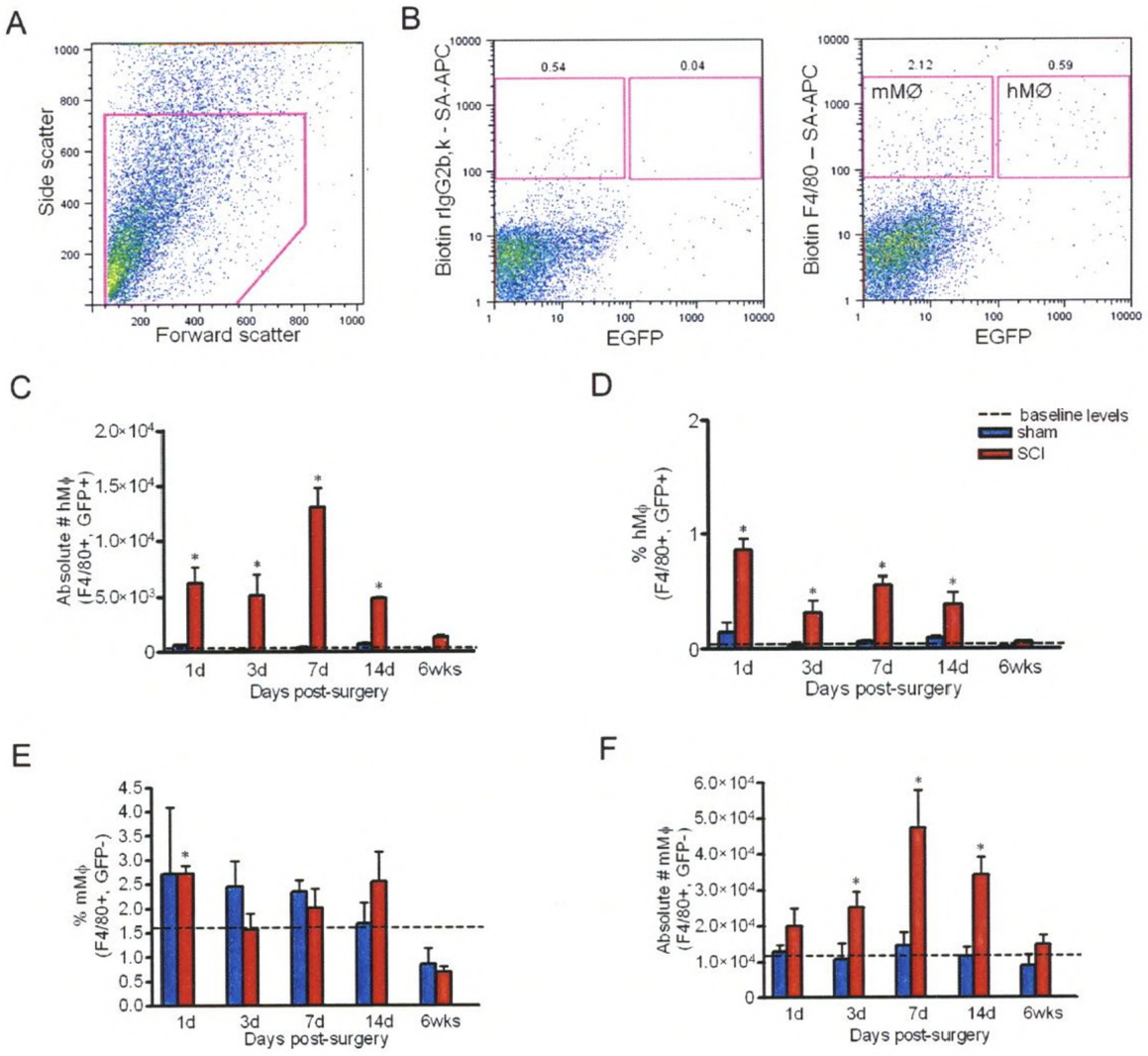
A
Side scatter
Forward scatter
B
Biotin rIgG2b,k - SA-APC
EGFP
0.54
0.04
Biotin F4/80 – SA-APC
mMØ
hMØ
2.12
0.59
C
Absolute # hMϕ (F4/80+, GFP+)
Days post-surgery
1d
3d
7d
14d
6wks
D
% hMϕ (F4/80+, GFP+)
baseline levels
sham
SCI
E
% mMϕ (F4/80+, GFP-)
F
Absolute # mMϕ (F4/80+, GFP-)

Figure 12. Examination of the hMØ subset responses to SCI by flow cytometry. The hMØ ($F4/80^{+}$, $EGFP^{+}$) in the SCI spinal cord samples were gated to identify the presence of 'classical inflammatory' ($F4/80^{lo}$, $Ly6C/G^{+}$) and 'non-classical resident' ($F4/80^{hi}$, $Ly6C/G^{-}$) hMØ subsets (A-C). Comparison of the differential presence of hMØ subsets in the SCI lesion at various times post-injury is shown (D). 'Classical inflammatory' and 'non-classical resident' hMØ subsets in (A-C) shown in red and blue gates respectively correspond to their representation in (D). Representative SCI samples in (A-C) are shown to reflect the trend seen in (D). Two-way ANOVA followed by Fisher's test, $*P \leq 0.05$.

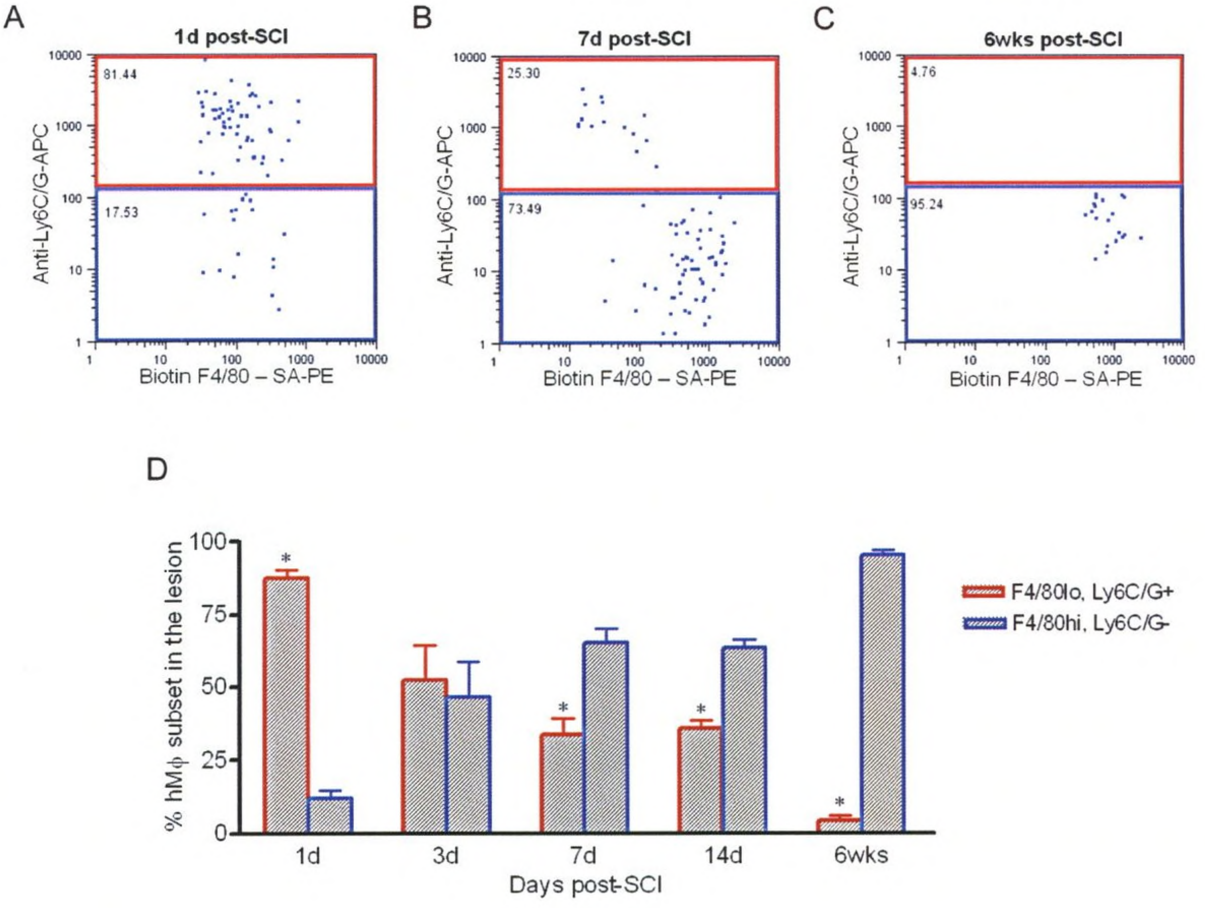
A
1d post-SCI
81.44
17.53
Anti-Ly6C/G-APC
Biotin F4/80 – SA-PE
B
7d post-SCI
25.30
73.49
Anti-Ly6C/G-APC
Biotin F4/80 – SA-PE
C
6wks post-SCI
4.76
95.24
Anti-Ly6C/G-APC
Biotin F4/80 – SA-PE
D
% hMϕ subset in the lesion
100
75
50
25
0
1d
3d
7d
14d
6wks
Days post-SCI
F4/80lo, Ly6C/G+
F4/80hi, Ly6C/G-

3.4 THE MICROGLIAL MACROPHAGE RESPONSE TO SCI.

The frequency and absolute numbers of mMØ responding to the SCI was investigated next. Results showed that the F4/80^{+}, EGFP^{-} mMØ frequency in the SCI lesion significantly increased at 1d post-SCI compared to uninjured controls (Figure 11E). When the absolute numbers of mMØ were examined, they increased at all times with significance achieved at 3d, 7d, and 14d post-SCI (Figure 11F). Similar to hMØ response, mMØ peaked at 7d, declined at 14d, and remained elevated at 6wks post-SCI (Figure 11F). The numbers of mMØ were always greater by at least 3-fold than those of hMØ in the SCI lesion (Figure 11D and F).

To confirm the distinctive nature of hMØ and mMØ in the lesion, backgating analysis of spinal cord samples were performed. Results showed that microglia (F4/80^{+}, EGFP^{-}) in the uninjured and sham injured samples localized as a unique population with uniform size and granularity on the FSC/SSC plot with little/no hematogenous contamination (Figure 13A and B). Backgating of hMØ (F4/80^{+}, EGFP^{+}) and mMØ (F4/80^{+}, EGFP^{-}) in the SCI samples illustrated the presence of two distinct populations that localized differentially on the FSC/SSC plot (Figure 13C). The hMØ appeared bigger in size than mMØ as judged by their higher FSC (Figure 13C). Also, the mMØ in the SCI sample were heterogeneous in granularity as judged by the range of SSC (Figure 13C) than microglia in the uninjured and sham injured samples (Figure 13A and B). This observation may reflect the differences in the activation states of microglia and mMØ, the former would be expected to be a uniform population while the latter would consist of heterogeneous cells that differ in morphology as described in Figure 1.

Figure 13. Identification of hMØ and mMØ populations at the SCI lesion site based on EGFP expression in the SCI *lys*-EGFP-*ki* mouse model. Gated cells in the spinal cord FSC/SSC plots were further classified by placing gates on $F4/80^{+}$, $EGFP^{-}$ cells to identify microglia in the uninjured (A) and sham injured (B) samples. hMØ and mMØ in the SCI samples were identified by placing gates on $F4/80^{+}$, $EGFP^{+}$ and $F4/80^{+}$, $EGFP^{-}$ cells respectively (C). Each cell population was backgated onto its respective FSC/SSC plot to identify the location of microglia in the uninjured (A) and sham injured (B) samples, and hMØ and mMØ in the SCI sample (C). Microglia/mMØ and hMØ are illustrated in blue and pink representations respectively.

A

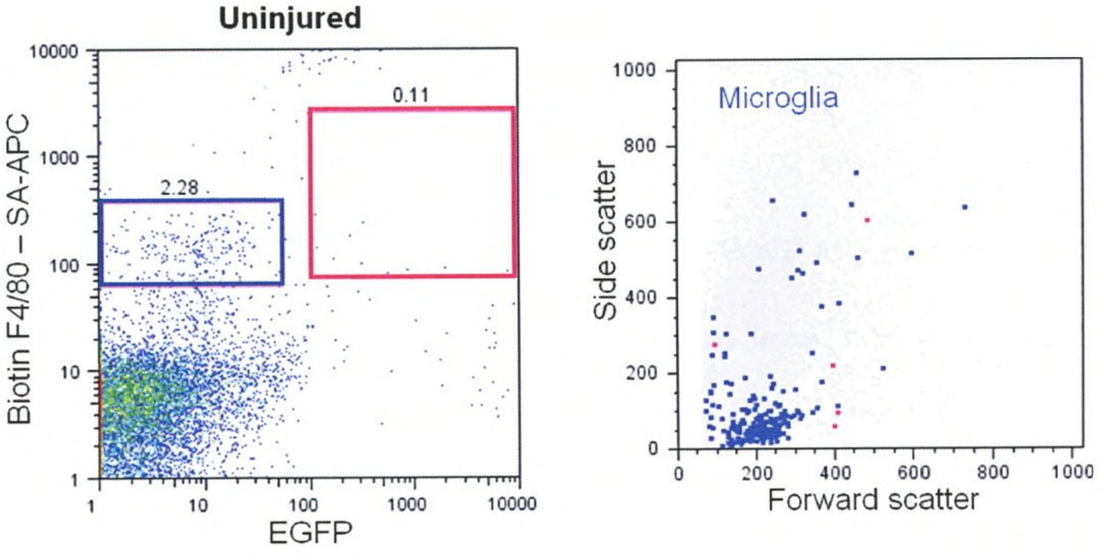
Uninjured
Biotin F4/80 – SA-APC
EGFP
2.28
0.11
Microglia
Side scatter
Forward scatter

B

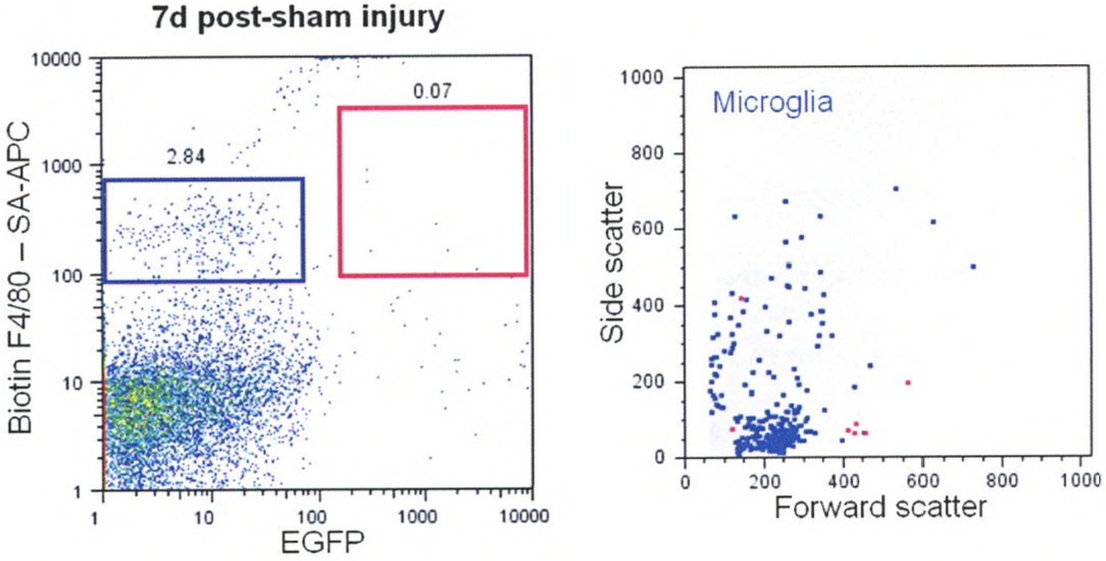
7d post-sham injury
Biotin F4/80 – SA-APC
EGFP
2.84
0.07
Microglia
Side scatter
Forward scatter

C

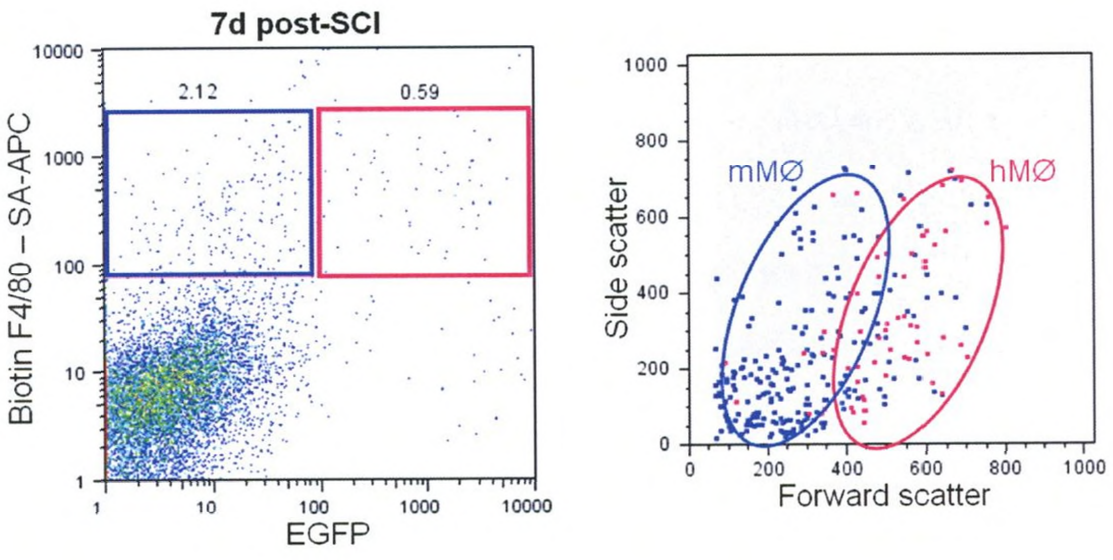
7d post-SCI
Biotin F4/80 – SA-APC
EGFP
2.12
0.59
mMØ
hMØ
Side scatter
Forward scatter

Overall, these results show that the microglial numbers increase post-SCI and predominate over that of hMØ; similar to hMØ, their maximal response occurs at 7d post-SCI. Also, our backgating results further sugget that hMØ and mMØ are distinguishable based on EGFP expression in the SCI *lys*-EGFP-*ki* mouse model. Thus, this model will be beneficial for future studies focused on investigating the functional differences between hMØ and mMØ following SCI.

3.5 IDENTIFICATION OF hMØ AND mMØ IN THE INJURED SPINAL CORD BASED ON CD45.2 EXPRESSION.

Previous studies on EAE and other CNS inflammation models have identified hMØ and mMØ based on differential CD45 expression; $CD45^{hi}$ and $CD45^{lo}$ for hMØ and mMØ respectively *(117-119)*. To investigate whether the same holds true in a SCI model, the present study examined the expression levels of CD45.2 in microglia from uninjured spinal cords and hMØ and mMØ from spinal cords at 7d post-SCI in the *lys*-EGFP-*ki* mice. Results showed that when the three populations were discriminated based on differential EGFP expression (Figure 14A, B), they exhibited variable levels of CD45.2 (Figure 14C). Microglia in the uninjured mice were $CD45.2^{lo}$ with an average mean fluorescence intensity (MFI) of 95. Conversely, the activated mMØ and infiltrating hMØ exhibited higher expression of CD45.2 with average MFI's of 166 and 608, respectively. Although the CD45.2 expression between microglia and mMØ did not reach statistical significance ($P=0.08$), the CD45.2 expression of hMØ was significantly higher than microglia and mMØ ($P \leq 0.05$). However, this difference was not apparent when hMØ

Figure 14. Identification of hMØ and mMØ populations based on CD45.2 expression in the SCI *lys*-EGFP-*ki* mouse model. Viable cells were gated to identify microglia ($F4/80^+$, $EGFP^-$) in the uninjured (A), and hMØ ($F4/80^+$, $EGFP^+$) and mMØ ($F4/80^+$, $EGFP^-$) in the SCI (B) spinal cord samples based on differential EGFP expression. Each cell population was then analyzed for expression of CD45.2 (C). Microglia (D), and hMØ and mMØ (E) were also analyzed based only on differential CD45.2 expression. However, hMØ and mMØ could not be distinguished on the pseudocolor dot plot (E). Isotype-matched controls are shown (F). The blue, green, and red representations in (A-C) correspond to microglia, hMØ, and mMØ respectively. Grey represents isotype control in (C). Analysis was done at 7d post-SCI, a time at which hMØ and mMØ numbers peak in the SCI lesion. N=5, n=2-4.

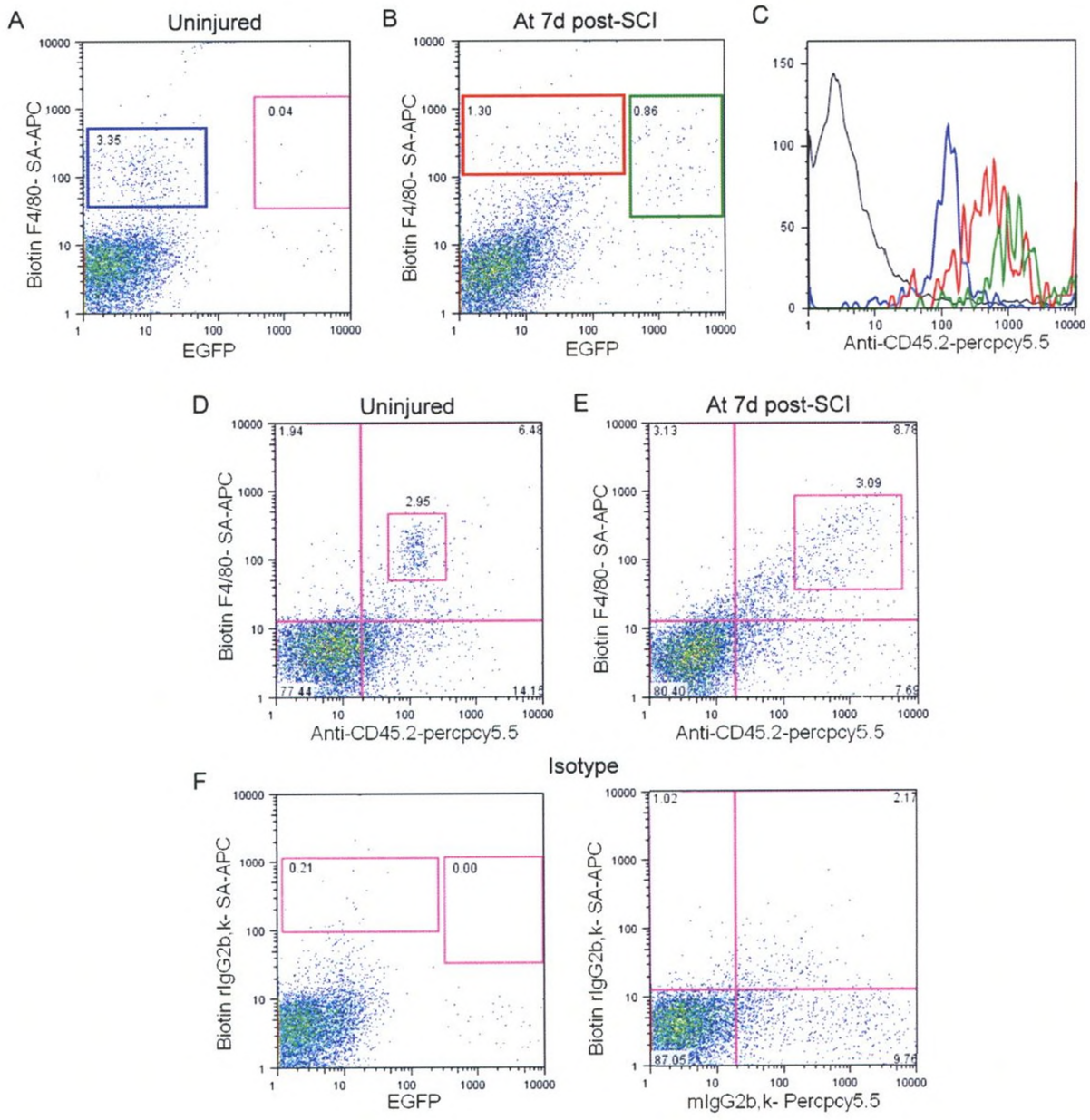
A
Uninjured
Biotin F4/80- SA-APC
EGFP
3.35
0.04
B
At 7d post-SCI
Biotin F4/80- SA-APC
EGFP
1.30
0.86
C
Anti-CD45.2-percpcy5.5
D
Uninjured
Biotin F4/80- SA-APC
Anti-CD45.2-percpcy5.5
1.94
6.48
2.95
77.44
14.15
E
At 7d post-SCI
Biotin F4/80- SA-APC
Anti-CD45.2-percpcy5.5
3.13
8.78
3.09
80.40
7.69
Isotype
F
Biotin rIgG2b,k- SA-APC
EGFP
0.21
0.00
Biotin rIgG2b,k- SA-APC
mIgG2b,k- Percpcy5.5
1.02
2.17
87.05
9.75

and mMØ were observed on pseudocolor dot plot with CD45.2 as the only distinguishing marker (Figure 14E). This may be due to overlapping mMØ and hMØ populations that have similar expression of CD45.2 (Figure 14C). Our results indicate that while it may be possible to distinguish hMØ and mMØ by CD45.2 expression post-SCI; it is not completely reliable for use when downstream applications that entail cell sorting (such as gene expression and functional studies) are required. Overall, our results do not support studies that use CD45 expression alone as the distinguishing criteria for hMØ and mMØ following CNS inflammation.

Together, the first stage of the present study demonstrates that neutrophils, monocytes, hMØ, and mMØ respond in distinct patterns during the acute and chronic stages of SCI. Furthermore, our results show that subsets of monocytes and hMØs respond differentially to SCI.

3.6 PHENOTYPIC ANALYSIS OF LEUKOCYTES IN SCI MICE

The differential response of monocyte/hMØ subsets to SCI led us to further examine the response of these cells in the blood and spinal cord lesion of SCI mice. Thus, additional phenotypic analysis of circulating subsets of monocytes and infiltrating hMØ and resident mMØ subsets in the lesion were conducted. These analyses were carried out at 7d post-SCI, a time at which, maximal numbers of infiltrating hMØ and resident mMØ are observed in the SCI lesion.

3.6.1 Phenotyping *lys*-EGFP-*ki* blood monocytes at 7d post-SCI

As mentioned previously, two main subsets of mouse monocytes have been identified, the 'classical inflammatory' and the 'non-classical resident' monocyte subsets based on differential expression of Ly6C/G, among other markers *(41, 48)* . An additional third monocyte subset, termed 'intermediate' monocyte, expressing an intermediate level of Ly6C/G has been reported *(48, 52)*. This intermediate subset has been proposed to be a transitional subpopulation between some Ly6C/G^{+} 'classical inflammatory' monocytes that give rise to Ly6C/G^{-} 'non-classical resident' monocytes *(48, 52)*.

In the present study, as shown in section 3.3.1, 'classical inflammatory' and 'non-classical resident' monocyte subsets were identified based on differential expression of F4/80 and Ly6C/G. We were further interested in examining whether these subsets differed in EGFP expression, in which case it would reflect their *LysM* activity. Additionally, we wanted to verify the absence of EGFP^{-} monocytes in the *lys*-EGFP-*ki* mouse. Thus, we examined EGFP^{+} and EGFP^{-} cells (Figure 15A) in the transgenic blood for expression of F4/80 and Ly6C/G (Figure 15B and C). Our analysis revealed the presence of 'classical inflammatory' (F4/80^{lo}, Ly6C/G^{+}, EGFP^{+}) subset, 'non-classical resident' (F4/80^{hi}, Ly6C/G^{-}, EGFP^{+}) subset, and a previously undescribed 'monocyte-like' (F4/80^{lo}, Ly6C/G^{-}, EGFP^{+}) subset (Figure 15B). Backgating of EGFP^{+} 'classical inflammatory' and 'non-classical resident' monocyte subsets showed that they are distinct; the latter subset has a higher FSC (bigger in size) than the former (Figure 15B). Additionally, the newly described 'monocyte-like' subset exhibits distinct FSC/SSC properties; it appears smaller and less granular than the other two EGFP^{+} subsets

Figure 15. Identification of blood monocyte subsets in the *lys*-EGFP-*ki* mouse model. Viable cells were selected for by placing a gate on the FSC/SSC plot and cells were further analyzed for expression of EGFP (A). Classification of $EGFP^+$ cells with the use of isotype-matched controls led to the identification of 'classical inflammatory' (pink), 'non-classical resident' (blue), and 'monocyte-like' (green) subsets (B). Classification of $EGFP^-$ cells with the use of isotype-matched controls led to the identification of $EGFP^-$ cells that correspond phenotypically to $EGFP^+$ 'classical inflammatory' (pink) and 'non-classical resident' (blue) monocytes, as well as the 'intermediate' (orange) monocyte subsets (C). Each of the identified monocyte subsets were examined for expression of Ly6C/G (D). Ly6C/G expression in (D) corresponds to the respective color coded monocyte subsets in (B-C). Shaded and non-shaded histograms represent $EGFP^-$ and $EGFP^+$ monocytes respectively (D).

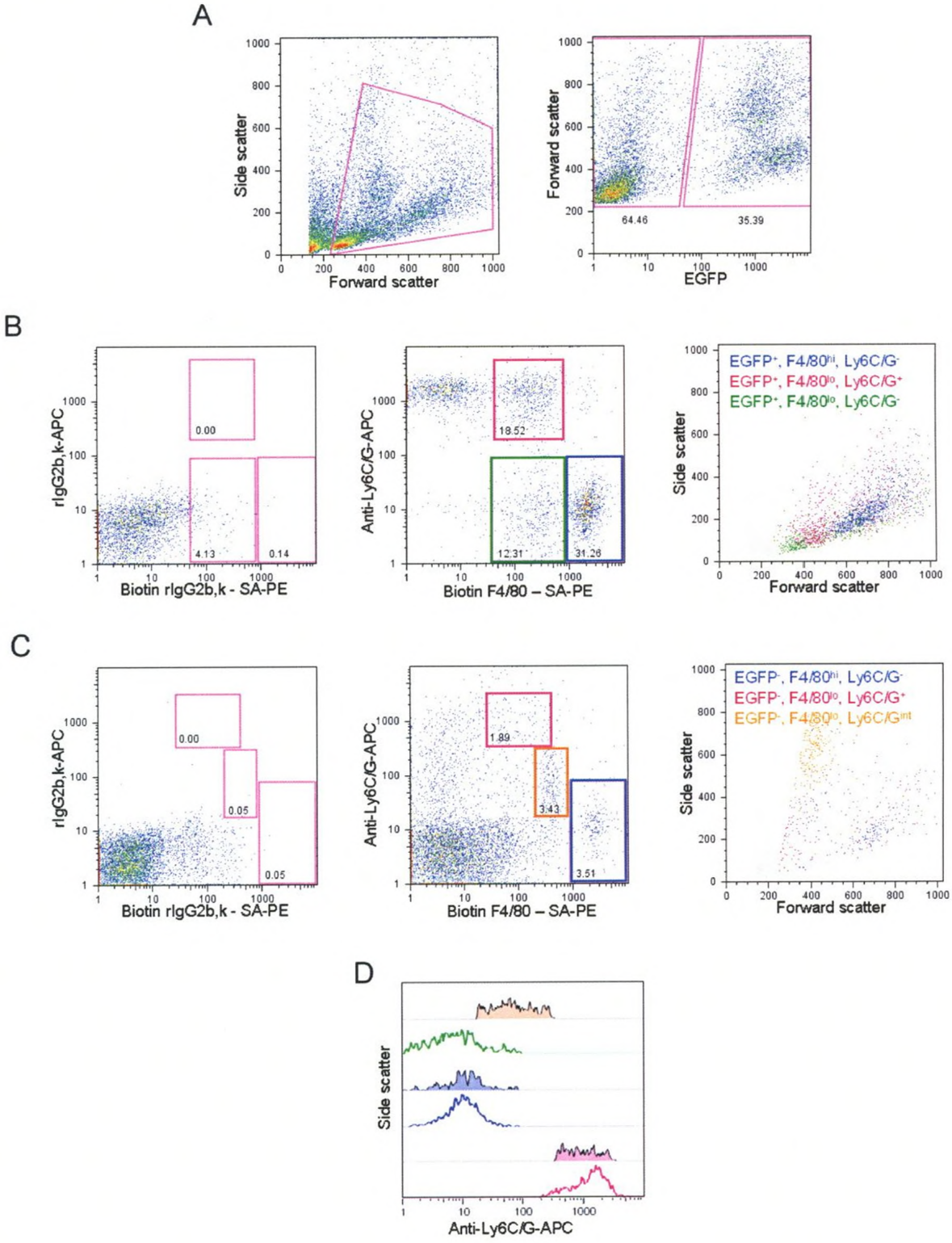
A
Side scatter
Forward scatter
Forward scatter
EGFP
64.46
35.39
B
rIgG2b,k-APC
Biotin rIgG2b,k - SA-PE
0.00
4.13
0.14
Anti-Ly6C/G-APC
Biotin F4/80 – SA-PE
18.52
12.31
31.26
EGFP+, F4/80hi, Ly6C/G-
EGFP+, F4/80lo, Ly6C/G+
EGFP+, F4/80lo, Ly6C/G-
Side scatter
Forward scatter
C
rIgG2b,k-APC
Biotin rIgG2b,k - SA-PE
0.00
0.05
0.05
Anti-Ly6C/G-APC
Biotin F4/80 – SA-PE
1.89
3.43
3.51
EGFP-, F4/80hi, Ly6C/G-
EGFP-, F4/80lo, Ly6C/G+
EGFP-, F4/80lo, Ly6C/Gint
Side scatter
Forward scatter
D
Side scatter
Anti-Ly6C/G-APC

(Figure 15B). Together, these results indicate presence of three distinct $EGFP^+$ blood monocyte subsets in the *lys*-EGFP-*ki* mouse.

Examination of the $EGFP^-$ blood cells revealed the presence of the 'intermediate' monocyte subset ($F4/80^{lo}$, $Ly6C/G^{int}$, $EGFP^-$) and two minor subsets defined as $F4/80^{lo}$, $Ly6C/G^+$, $EGFP^-$ and $F4/80^{hi}$, $Ly6C/G^-$, $EGFP^-$ (Figure 15C). These two minor subsets appear to phenotypically correspond to the 'classical inflammatory' and 'non-classical resident' monocyte subsets but lack EGFP expression. Backgating of the three $EGFP^-$ monocyte subsets revealed that the 'intermediate' subset was highly granular (high SSC) compared to the $EGFP^+$ subsets (Figure 15B) and the two $EGFP^-$ minor subsets (Figure 15C). Additionally, the two $EGFP^-$ minor subsets exhibit FSC/SSC properties similar to those of $EGFP^+$ 'classical inflammatory' and 'non-classical resident' monocytes, further suggesting that they may be counterparts (Figure 15B and C). The existense of $EGFP^-$ monocyte subsets indicates either absence of or very low *LysM* promoter activity such that the EGFP cannot be detected by flow cytometry. Since the *LysM* promoter is strongly expressed in mature myelomonocytic cells *(120)*, our results suggest that these $EGFP^-$ subsets possibly represent monocyte precursor cells. A summary of the monocyte subsets identified is shown in Figure 15D. The histogram illustrates the differential expression of Ly6C/G among monocyte subsets. The 'classical inflammatory' monocytes and their $EGFP^-$ counterparts exhibit a high Ly6C/G expression relative to the intermediate expression by 'intermediate' monocytes and the negative expression by 'non-classical resident' monocytes and their $EGFP^-$ counterparts. The newly identified 'monocyte-like' subset appears negative for Ly6C/G expression.

Our results appear to be consistent with the description of 'classical inflammatory', 'non-classical resident', and 'intermediate' monocyte subsets *(48, 52)*. To further confirm the identification of the monocyte subsets, we next investigated the expression of CD62L, a peripheral leukocyte marker that is only expressed by 'classical inflammatory' monocytes *(41, 48)*. Our results on CD62L expression by monocyte subsets were consistent with previous reports (Figure 16A). Additionally we also examined the expression of CD11c, a DC-specific marker on the monocyte subsets and found that while the 'classical inflammatory' and 'non-classical resident' monocytes were $CD11c^-$, the newly identified 'monocyte-like' subset was $CD11c^+$ (Figure 16B). These results suggest that the 'monocyte-like' subset are possibly DCs. Examination of total $CD11c^+$ populations in the blood showed an absence of CCR7 expression, a marker characteristic of mature DCs (Figure 16C) suggesting that the 'monocyte-like' subset did not contain mature DCs.

We next investigated what impact SCI had on the phenotype of the blood monocyte subsets; the focus was on the $EGFP^+$ monocytes as EGFP enables us to track them in the lesion post-SCI. Also, the analysis was conducted at 7d post-SCI, a time at which maximal numbers of hMØ and mMØ are observed in the spinal cord. Results revealed that there was no statistically siginificant changes in the 'classical inflammatory' and 'non-classical resident' blood monocyte levels in response to SCI; however, the 'monocyte-like' subset significantly decreased in the SCI blood (table 3A). The result for 'classical inflammatory' monocytes appears to be contradictory to that obtained in Figure 10B, where a siginificant increase in their frequency was observed. These differences may be be resolved by increasing the number of experimental replicates.

Figure 16. Phenotypic characterization of $EGFP^+$ blood monocyte subsets in the uninjured and 7d post-SCI *lys*-EGFP-*ki* mice. The $EGFP^+$ cells in the uninjured and SCI samples were analyzed for expression of CD62L (A), CD11c (B), and CCR7 (C) with the use of appropriate isotype-matched controls. A representative FACS sample is shown in (A-B); colored gates represent the 'classical inflammatory' (pink), 'non-classical resident' (blue), and 'monocyte-like' (green) subsets. A sample of isotype controls for the SCI samples is shown in (A-C). N=4-5.

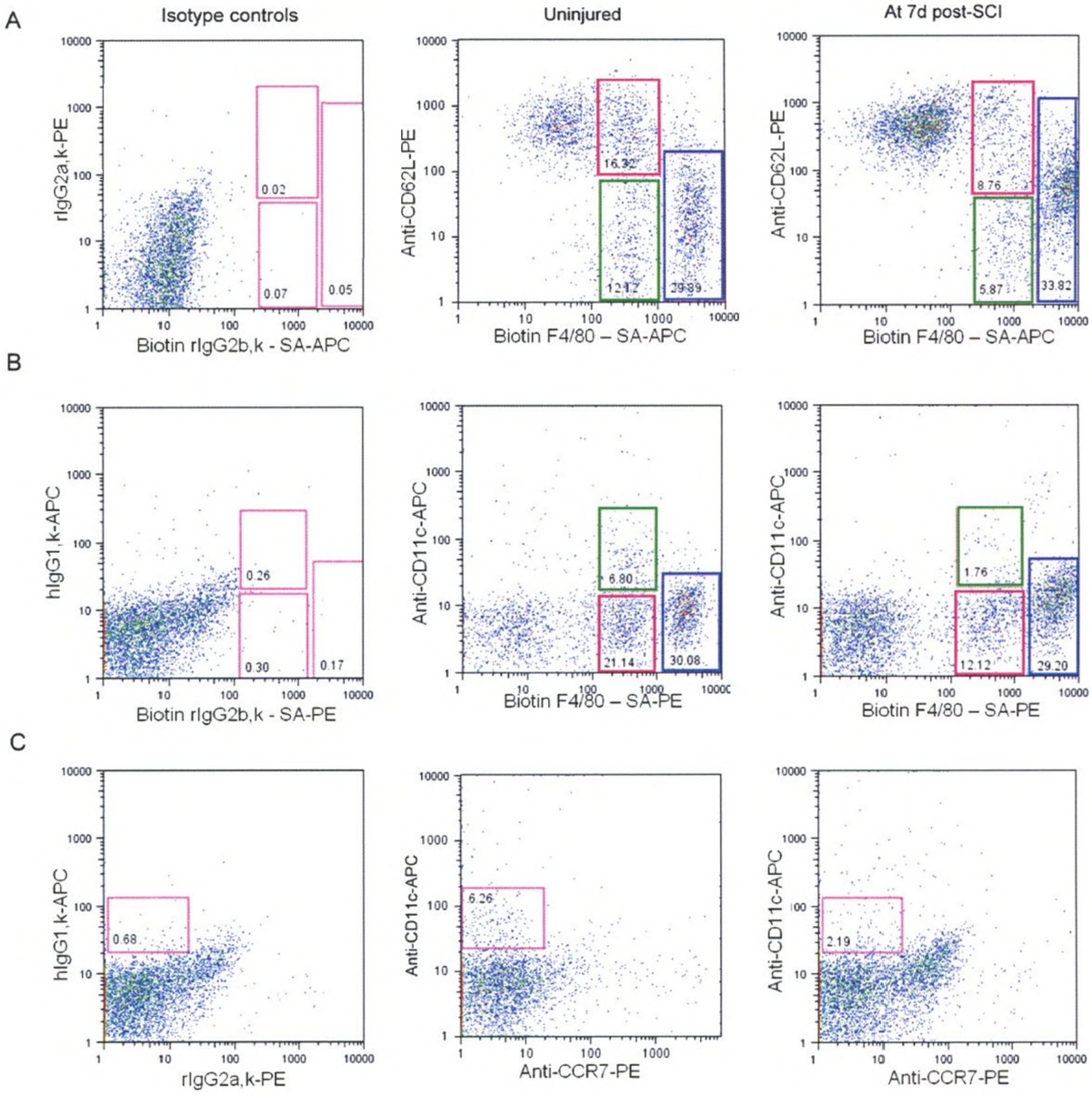
A
Isotype controls
Uninjured
At 7d post-SCI
rIgG2a,k-PE
Anti-CD62L-PE
Biotin rIgG2b,k - SA-APC
Biotin F4/80 – SA-APC
0.02
0.07
0.05
16.32
12.12
29.89
8.76
5.87
33.82
B
hIgG1,k-APC
Anti-CD11c-APC
Biotin rIgG2b,k - SA-PE
Biotin F4/80 – SA-PE
0.26
0.30
0.17
6.80
21.14
30.08
1.76
12.12
29.20
C
hIgG1,k-APC
Anti-CD11c-APC
rIgG2a,k-PE
Anti-CCR7-PE
0.68
6.26
2.19

Table 3. Changes in frequencies of monocyte subsets between uninjured and mice at 7d post-SCI. Frequencies of circulating 'classical inflammatory' monocytes, 'non-classical resident' monocytes, and 'monocyte-like' subsets in the *lys*-EGFP-*ki* (A) and C57BL/6 (B) mice. N=4-5, Students t-test, *P≤ 0.05.

A

Lys-EGFP-*ki* mice

	Uninjured	7d post-SCI
	Mean ± SEM	Mean ± SEM
'Non-classical Resident' Monocytes ($F4/80^{hi}$, $Ly6C/G^{-}$)	37.0 ± 2.8	28.9 ± 5.1
'Classical inflammatory' Monocytes ($F4/80^{lo}$, $Ly6C/G^{+}$)	15.7 ± 1.7	14.4 ± 2.8
'Monocyte-like' Subset ($F4/80^{lo}$, $Ly6C/G^{-}$)	10.9 ± 1.0*	5.6 ± 1.0*

*$P \leq 0.05$, Student's t-test.

B

C57BL/6 mice

	Uninjured	7d post-SCI
	Mean ± SEM	Mean ± SEM
'Non-classical Resident' Monocytes ($F4/80^{hi}$, $Ly6C/G^{-}$)	43.44 ± 2.5	30.79 ± 6.6
'Classical inflammatory' Monocytes ($F4/80^{lo}$, $Ly6C/G^{+}$)	22.07 ± 3.9	25.37 ± 4.7
'Monocyte-like' Subset ($F4/80^{lo}$, $Ly6C/G^{-}$)	25.24 ± 2.9	30.51 ± 4.0

Overall, we confirmed the presence of 'classical inflammatory', 'non-classical resident', and 'intermediate' monocyte subsets in circulation. Additionally, we identified a possibly new 'monocyte-like' subset that responds to SCI by being present at a reduced frequency in the injured mice. To confirm that these subsets are not unique to the *lys*-EGFP-*ki* mouse, we performed similar phenotyping on the wild-type strain, C57BL/6 mice.

3.6.2 Phenotyping C57BL/6 blood monocytes at 7d post-SCI

Phenotyping of uninjured C57BL/6 blood revealed the presence of all four monocyte subsets obtained for the *lys*-EGFP-*ki* strain (Figure 17B), with Ly6C/G expression being high in 'classical inflammatory' monocytes, absent in the 'non-classical resident' and 'monocyte-like' subsets, and having intermediate expression in the 'intermediate monocyte' subset (Figure 17B). Additionally, the 'classical inflammatory' monocytes were $CD62L^+$, $CD11c^-$, 'non-classical resident' monocytes were $CD62L^-$, $CD11c^-$, and the 'monocyte-like' subset were $CD62L^-$, $CD11c^+$ (Figure 18B-G). However, unlike the *lys*-EGFP-*ki* mice (Figure 16), the levels of the 'monocyte-like' subset did not differ significantly between the uninjured and 7d post-SCI C57BL/6 mice (Table 3B). This observation may be a reflection of the differential gating strategies used to identify the monocyte subsets between the two strains; analysis of the *lys*-EGFP-*ki* mice was based only on $EGFP^+$ cells (mature myelomonocytic cells) while analysis of the C57BL/6 mice was based on the total blood leukocyte population. Hence, it is possible that the 'monocyte-like' subset with active *LysM* promoter activity is the one that participates in SCI.

Figure 17. Blood monocyte subsets in the C57BL/6 mice are similar to that observed in the *lys*-EGFP-*ki* mice. The FSC/SSC blood plot with isotype-matched controls (A). Gating placed on the four monocyte populations in the blood and histogram showing Ly6C/G expression levels of each monocyte population identified (B). Color representations correspond to 'classical inflammatory' monocytes (pink), 'non-classical resident' monocytes (blue), 'intermediate' monocytes (orange), 'monocyte-like' subset (green), and 'isotype-matched' control (grey).

A

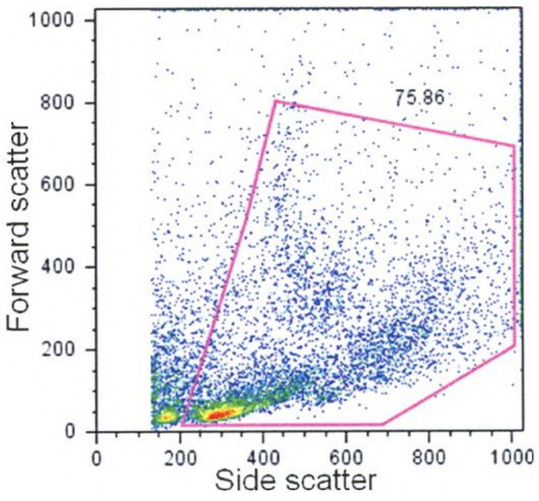
Forward scatter
Side scatter
75.86
0
200
400
600
800
1000

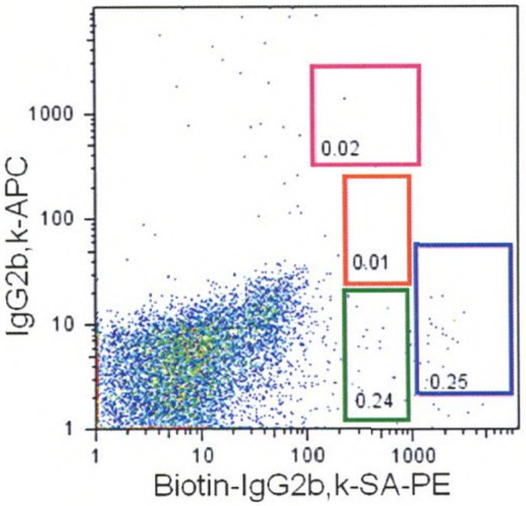
IgG2b,k-APC
Biotin-IgG2b,k-SA-PE
0.02
0.01
0.24
0.25
1
10
100
1000

B

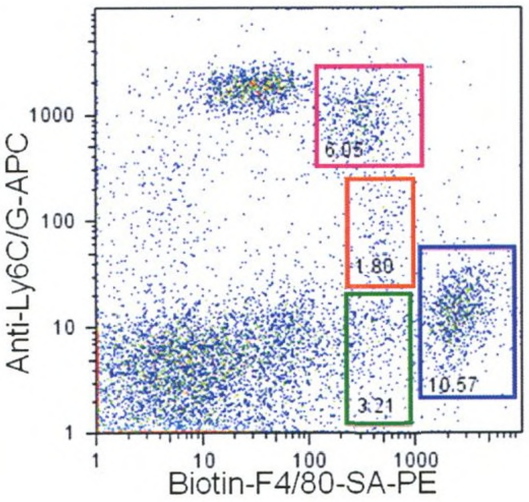
Anti-Ly6C/G-APC
Biotin-F4/80-SA-PE
6.05
1.80
3.21
10.57
1
10
100
1000

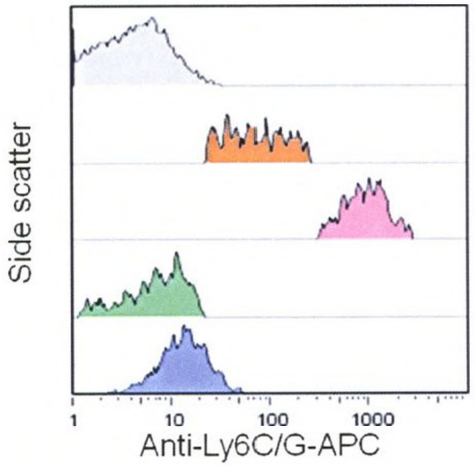
Side scatter
Anti-Ly6C/G-APC
1
10
100
1000

Figure 18. Phenotypic characterization of blood monocyte subsets in the uninjured and 7d post-SCI C57BL/6 mice. Viable cells were gated for expression of F4/80 with the use of an isotype-matched control (A). The gated cells in the uninjured (B-D) and SCI (E-G) samples were further analyzed for expression of Ly6C/G, CD62L, and CD11c. Representative FACS plots are shown in (B-G); the colored gates represent the 'classical inflammatory' (pink), 'non-classical resident' (blue), and 'monocyte-like' (green) subsets. N=4-5.

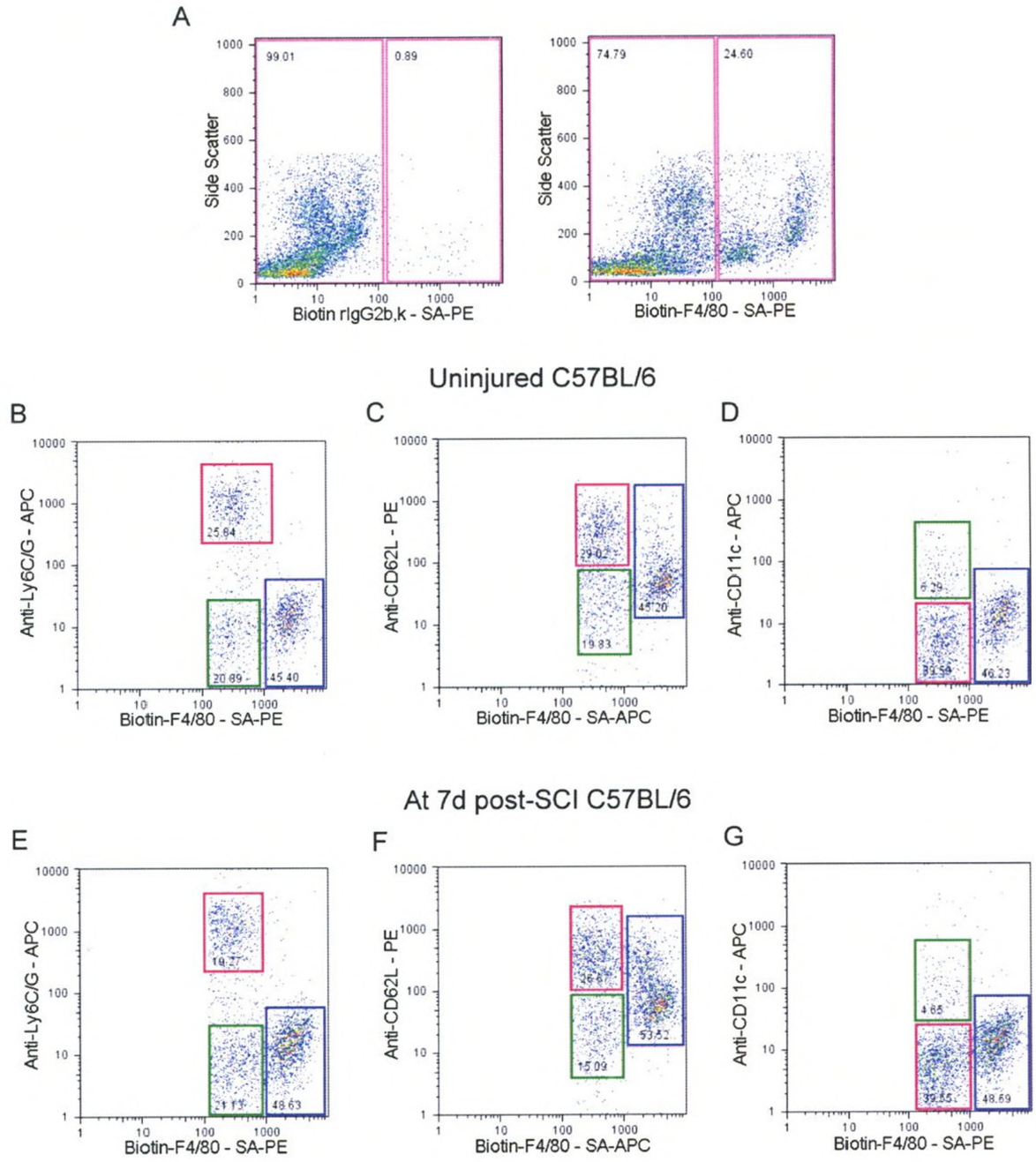
A
99.01
0.89
74.79
24.60
Side Scatter
Biotin rIgG2b,k - SA-PE
Biotin-F4/80 - SA-PE
Uninjured C57BL/6
B
C
D
25.84
20.89
45.40
29.02
19.83
45.20
6.29
39.59
48.23
Anti-Ly6C/G - APC
Anti-CD62L - PE
Anti-CD11c - APC
Biotin-F4/80 - SA-PE
Biotin-F4/80 - SA-APC
At 7d post-SCI C57BL/6
E
F
G
19.27
21.13
48.63
15.09
53.52
4.65
39.55
48.69

Together, our results confirm that the monocyte subsets identified in the *lys*-EGFP-*ki* mice are not affected by the presence of EGFP expression. Due to the fact that the newly identified 'monocyte-like' subset plays a role in response to SCI in the *lys*-EGFP-*ki* mice, we conducted a further extensive phenotypic analysis of monocyte subsets in the uninjured *lys*-EGFP-*ki* mice in an effort to characterize the 'monocyte-like' subset.

3.6.3 Characterizing the 'monocyte-like' subset in uninjured *lys*-EGFP-*ki* mice

As shown in Figure 16, the 'monocyte-like' subset expresses markers for monocytes (F4/80) as well DCs (CD11c). In Figure 16C, we show that the circulating $CD11c^+$ cells are negative for DC maturation marker, CCR7. These results suggest that the 'monocyte-like' subset are not mature DCs. However, it does not eliminate the possibility of the 'monocyte-like' subset belonging to other DC subsets, NK cells (also express CD11c), or premyeolocytes (BM-derived monocyte precursor). Thus, we performed phenotypic analysis of the 'monocyte-like' subsets to address the above possibilities. To examine whether the 'monocyte-like' subset belongs to DC subsets, we investigated the expression of CD11b, CD8α, CD45R, and PDCA-1 surface markers. Studies have described at least two DC subsets: plasmacytoid DC (pDC) and conventional DC (cDC) *(131-133)*. In mice, pDCs are defined as $CD11c^+$, $CD11b^-$, $Ly6C/G^+$, $CD45R^+$, $CD8\alpha^+$, and $PDCA\text{-}1^+$, while cDCs are defined as $CD11c^+$, $CD11b^+$, $Ly6C/G^-$, $CD45R^-$, $CD8\alpha^-$, and $PDCA\text{-}1^-$ *(131-133)*. Results indicated that a small proportion of the $CD11c^+$ 'monocyte-like' subset was positive for CD8α (Figure 19D), CD45R (Figure 19E), and PDCA-1 (Figure 19F) indicating that a minor subpopulation of

Figure 19. Phenotypic characterization of $EGFP^+$ blood monocyte subsets in the uninjured *lys*-EGFP-*ki* mice. Viable cells were gated for expression of EGFP in the uninjured blood (A). The $EGFP^+$ cells were classified for identification of 'classical inflammatory' (pink), 'non-classical resident' (blue), and 'monocyte-like' (green) subsets with the use of isotype controls (B). Each monocyte subset was further analyzed for expression of CD11b (C), CD8α (D), CD45R (E), PDCA-1 (F), NK1.1 (G), and CD117 (H) with the use of appropriate isotype controls. The grey, pink, blue, and green representations in (C-H) correspond to isotype controls, 'classical inflammatory', 'non-classical resident', and 'monocyte-like' subsets respectively. Representative FACS plots and histograms are shown (A-H). N=4-5.

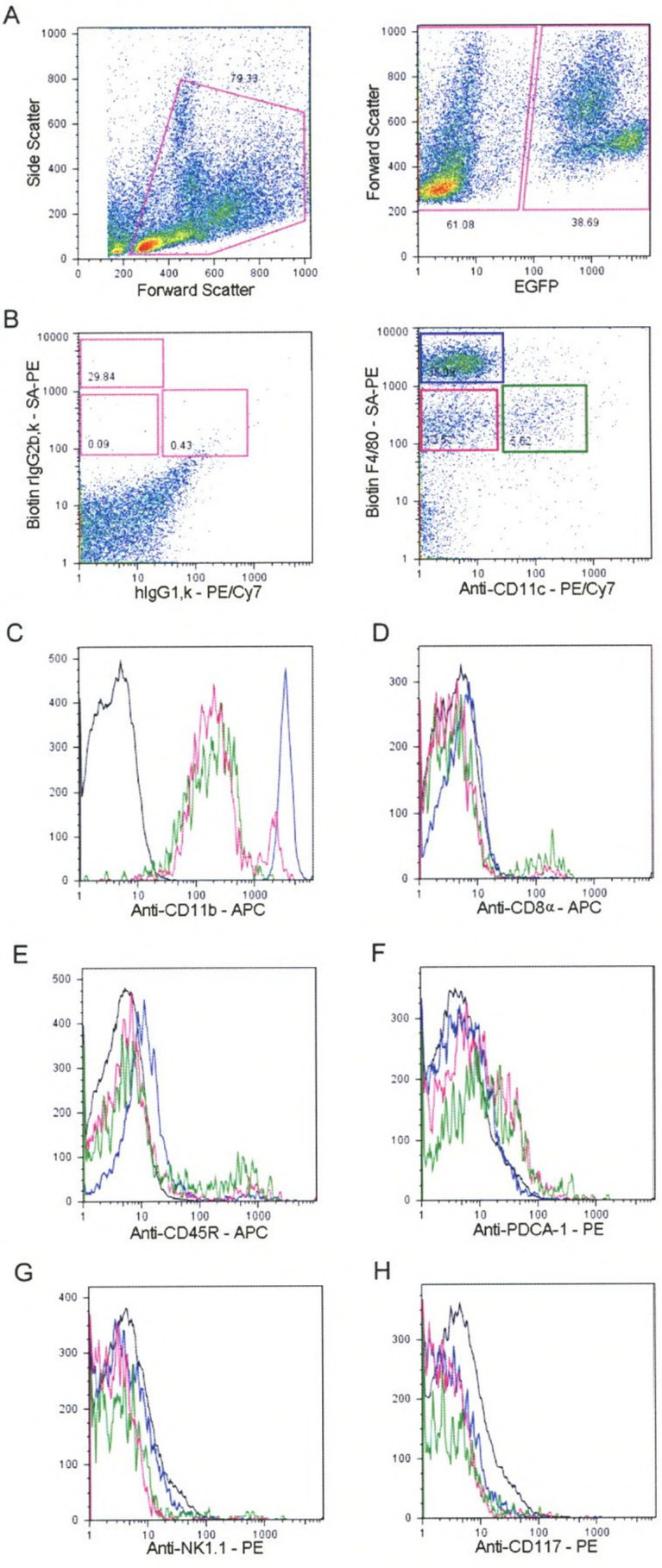
A
Side Scatter
Forward Scatter
79.33
Forward Scatter
EGFP
61.08
38.69
B
Biotin rIgG2b,k - SA-PE
hIgG1,k - PE/Cy7
29.84
0.09
0.43
Biotin F4/80 - SA-PE
Anti-CD11c - PE/Cy7
C
Anti-CD11b - APC
D
Anti-CD8α - APC
E
Anti-CD45R - APC
F
Anti-PDCA-1 - PE
G
Anti-NK1.1 - PE
H
Anti-CD117 - PE

the 'monocyte-like' subset may be pDC, although we previously showed that the 'monocyte-like' subset was Ly6C/G$^-$ (Figure 15D). As shown in Figure 19C, the CD11c$^+$ 'monocyte-like' subset was positive for CD11b, as were the 'classical inflammatory' and the 'non-classical resident' monocytes (Figure 19C). Although it may seem that the majority of 'monocyte-like' subset are cDCs, we cannot make this conclusion based on exclusive expression of CD11b, a pan monocyte/granulocyte marker *(138)*. Thus, additional phenotyping may need to be conducted in the future.

To address the possibility of the 'monocyte-like' subset being an NK-cell or a premyelocyte cell, we examined for expression of NK1.1 and CD117 respectively. Results showed that the population was negative for NK1.1 (Figure 19G) and CD117 (Figure 19H). Together, these results confirm that the 'monocyte-like' subset does not contain pDCs, NK cells, or premyelocytes. However, the possibility of the 'monocyte-like' population containing largely cDC remains.

In summary, the phenotypic analysis of the *lys*-EGFP-*ki* mouse revealed the presence of circulating 'classical inflammatory', 'non-classical resident', and 'intermediate' blood monocytes in both uninjured and SCI mice. Additionally, a potentially new 'monocyte-like' subset was identified that responds to SCI. Of interest next was to examine whether the EGFP$^+$ monocyte subsets were present in the SCI lesion.

3.6.4 Phenotyping the *lys*-EGFP-*ki* spinal cord at 7d post-SCI

3.6.4.1 Hematogenous macrophages

Phenotypic analysis of the macrophage populations in the lesion was performed on the spinal cords taken from the same mice used to characterize the phenotypes of the blood monocyte populations. Due to limitations on the number of markers that can simultaneously be analyzed, inferences on the phenotype of hMØ subsets were based on backgating. Two distinct populations of $F4/80^+$, $EGFP^+$ hMØ were observed in the spinal cord lesion at 7d post-SCI based on CD45.2 and differential expression of Ly6C/G (Figure 20B), CD62L (Figure 20C), and CD11c (Figure 20D). Backgating of each population onto the FSC/SSC plot suggested that the $Ly6C/G^+$ hMØ may possibly be $CD62L^+$, $CD11c^-$ while the $Ly6C/G^-$ hMØ are possibly for the most part $CD62L^-$, $CD11c^-$ (Figure 20C, D), although a fraction of these cells may be $CD11c^+$ (Figure 20D). Additionally, these analyses suggest that the $Ly6C/G^-$, $CD62L^-$, $CD11c^-$ hMØ are bigger in size (high FSC) than the $Ly6C/G^+$, $CD62L^+$, $CD11c^-$ hMØ (lower FSC) (Figure 20B, C, and D). However, the above inferences are based on backgating and need to be confirmed using instrumentation that allows analysis of more than four simultaneous parameters.

Overall, heterogeneous subsets of hMØ are present in the lesion. Our results suggest that both the 'classical inflammatory' and 'non-classical resident' monocytes migrate to the SCI lesion site and differentiate to hMØ.

Figure 20. Phenotypic characterization of $EGFP^+$ hMØ subsets at 7d post-SCI in the spinal cord lesion of *lys*-EGFP-*ki* mice. Gated cells in the spinal cord FSC/SSC plot were further classified to identify hMØ and mMØ by placing gates on $F4/80^+$, $EGFP^+$ and $F4/80^+$, $EGFP^-$ cells respectively with the use of isotype-matched controls (A). The hMØ were analyzed based on CD45.2 staining for differential expression of Ly6C/G (B), CD62L (C), and CD11c (D). The $CD11c^+$ cells in the spinal cord lesion were analyzed for expression of CCR7 (E). Representative FACS plots are shown (A-E); in (B-E), the pink and blue gates correspond to their respective backgates. N=4-5.

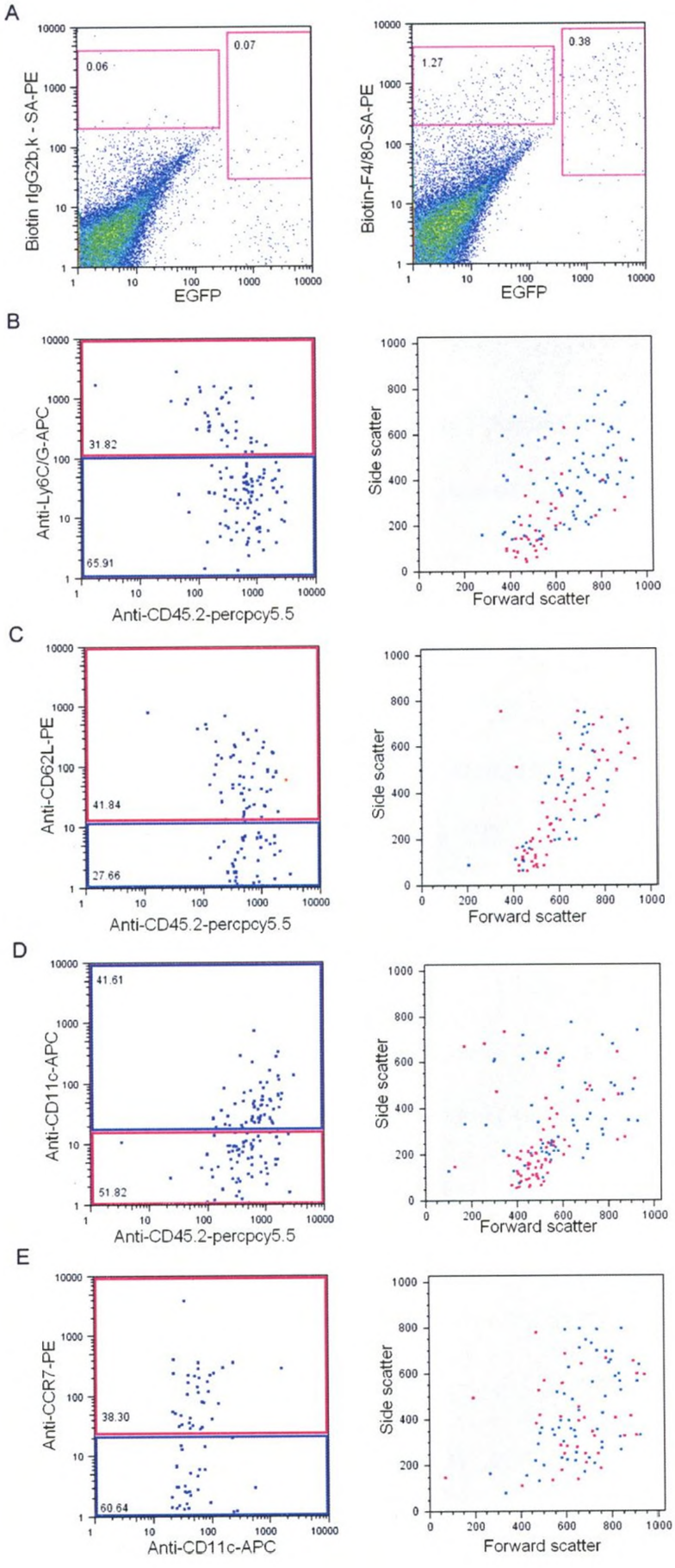
A
Biotin rIgG2b,k - SA-PE
EGFP
0.06
0.07
Biotin-F4/80-SA-PE
EGFP
1.27
0.38
B
Anti-Ly6C/G-APC
Anti-CD45.2-percpcy5.5
31.82
65.91
Side scatter
Forward scatter
C
Anti-CD62L-PE
Anti-CD45.2-percpcy5.5
41.84
27.66
Side scatter
Forward scatter
D
Anti-CD11c-APC
Anti-CD45.2-percpcy5.5
41.61
51.82
Side scatter
Forward scatter
E
Anti-CCR7-PE
Anti-CD11c-APC
38.30
60.64
Side scatter
Forward scatter

3.6.4.2 Dendritic cells (DC)

A $CD11c^+$ population was observed in the lesion at 7d post-SCI (Figure 20D). Approximately 40% of the $CD11c^+$ cells found in the lesion were $CCR7^+$ (Figure 20E), indicating the presence of mature DCs in the lesion. Due to limitations in being able to simultaneously analyze only four fluorescence channels, it is not possible to directly identify whether the $F4/80^{hi}$, $Ly6C/G^-$, $CD62L^-$, $CD11c^+$, $EGFP^+$ cells are $CCR7^+$. However, based on backgating, there appeared a separate population of $CD11c^+$, $CCR7^+$ cells (Figure 20D and E). Our results suggest the presence of DCs in the lesion at least at 7d post-SCI.

3.6.4.3 Microglial Macrophages

Phenotyping of $F4/80^+$, $EGFP^-$ mMØ subset was done similar to that of the hMØ. The analysis reveals the presence of at least two subsets of mMØ based on differential expression of CD62L and CD11c (Figure 21B, C). The $CD62L^+$ mMØ appear bigger in size as judged by a higher FSC than the $CD62L^-$ mMØ (Figure 21B). Based on backgating, it seems that there may be a small fraction of $CD62L^+$ mMØ that are $CD11c^+$ (Figure 21B and C). Also, the mMØ subsets do not express the Ly6C/G marker (Figure 21A). These results suggest the presence of heterogeneous populations of mMØ at the lesion site post-SCI.

3.6.4.4 Microglia

Phenotyping $F4/80^+$, $EGFP^-$ microglia in the uninjured spinal cords showed that resting microglia also may possibly be of two phenotypes: $Ly6C/G^-$, $CD62L^-$, $CD11c^-$ and $Ly6C/G^-$, $CD62L^+$, $CD11c^-$ (Figure 22B, C, and D). Additionally, it seems that the microglia subsets may differ in the expression of CD45.2 (Figure 22B, C, and D).

Figure 21. Phenotypic characterization of $EGFP^-$ mMØ subsets at 7d post-SCI in the spinal cord lesion of *lys*-EGFP-*ki* mice. The $F4/80^+$, $EGFP^-$ mMØ were analyzed based on CD45.2 staining for differential expression of Ly6C/G (A), CD62L (B), and CD11c (C). Representative FACS plots are shown in (A-C); the red and green gates correspond to their respective backgates. N=4-5.

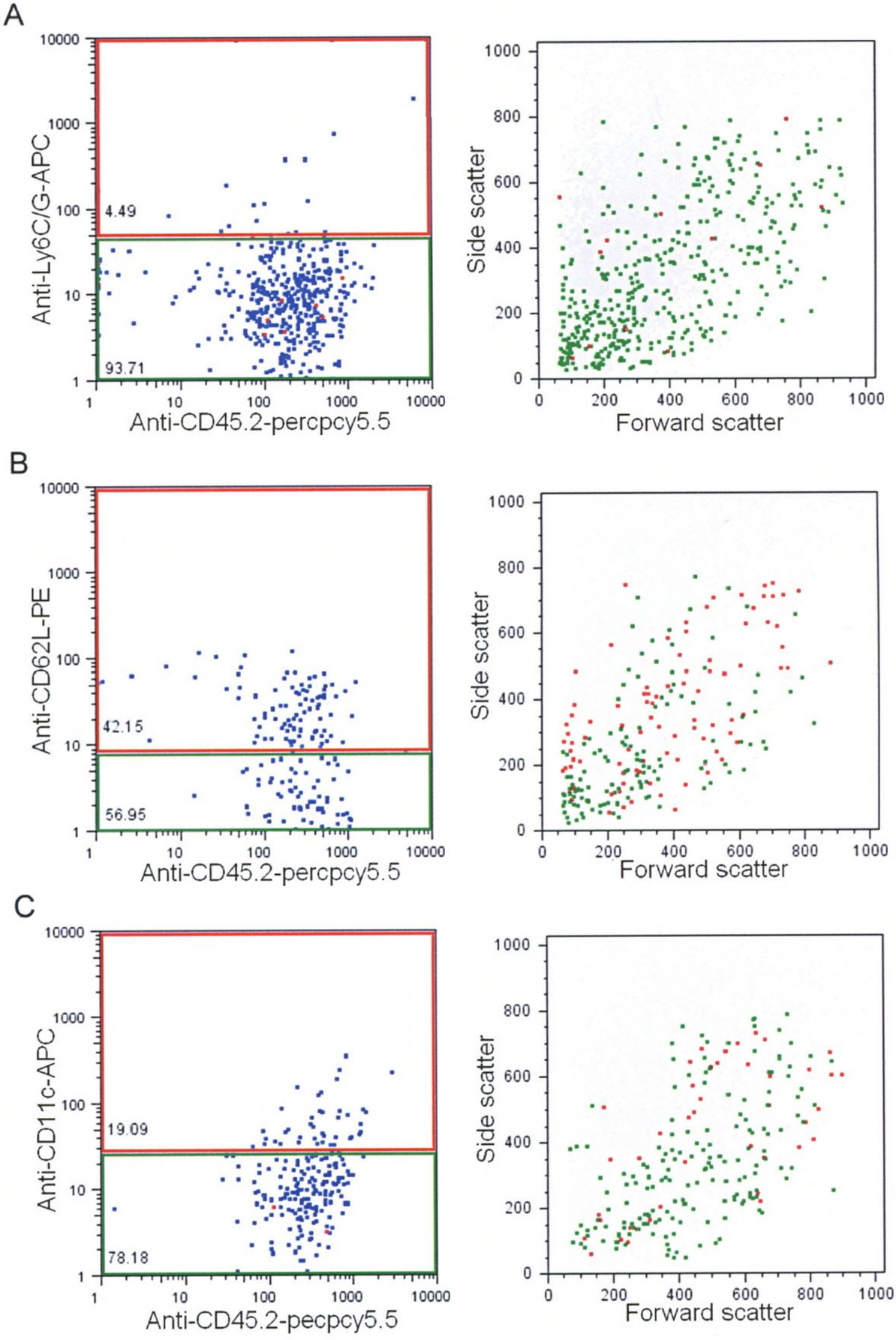
A
Anti-Ly6C/G-APC
4.49
93.71
Anti-CD45.2-percpcy5.5
Side scatter
Forward scatter
B
Anti-CD62L-PE
42.15
56.95
Anti-CD45.2-percpcy5.5
Side scatter
Forward scatter
C
Anti-CD11c-APC
19.09
78.18
Anti-CD45.2-pecpcy5.5
Side scatter
Forward scatter

Figure 22. Phenotypic characterization of EGFP$^-$ microglia in the uninjured spinal cords of *lys*-EGFP-*ki* mice. Gated cells in the spinal cord FSC/SSC plot were classified to identify microglia by placing a gate on F4/80$^+$, EGFP$^-$ cells with the use of isotype-matched controls (A). The microglia were analyzed based on CD45.2 staining for differential expression of Ly6C/G (B), CD62L (C), and CD11c (D). Representative FACS plots are shown in (A-D); the red and green gates in (B-D) correspond to their respective backgates. N=4-5.

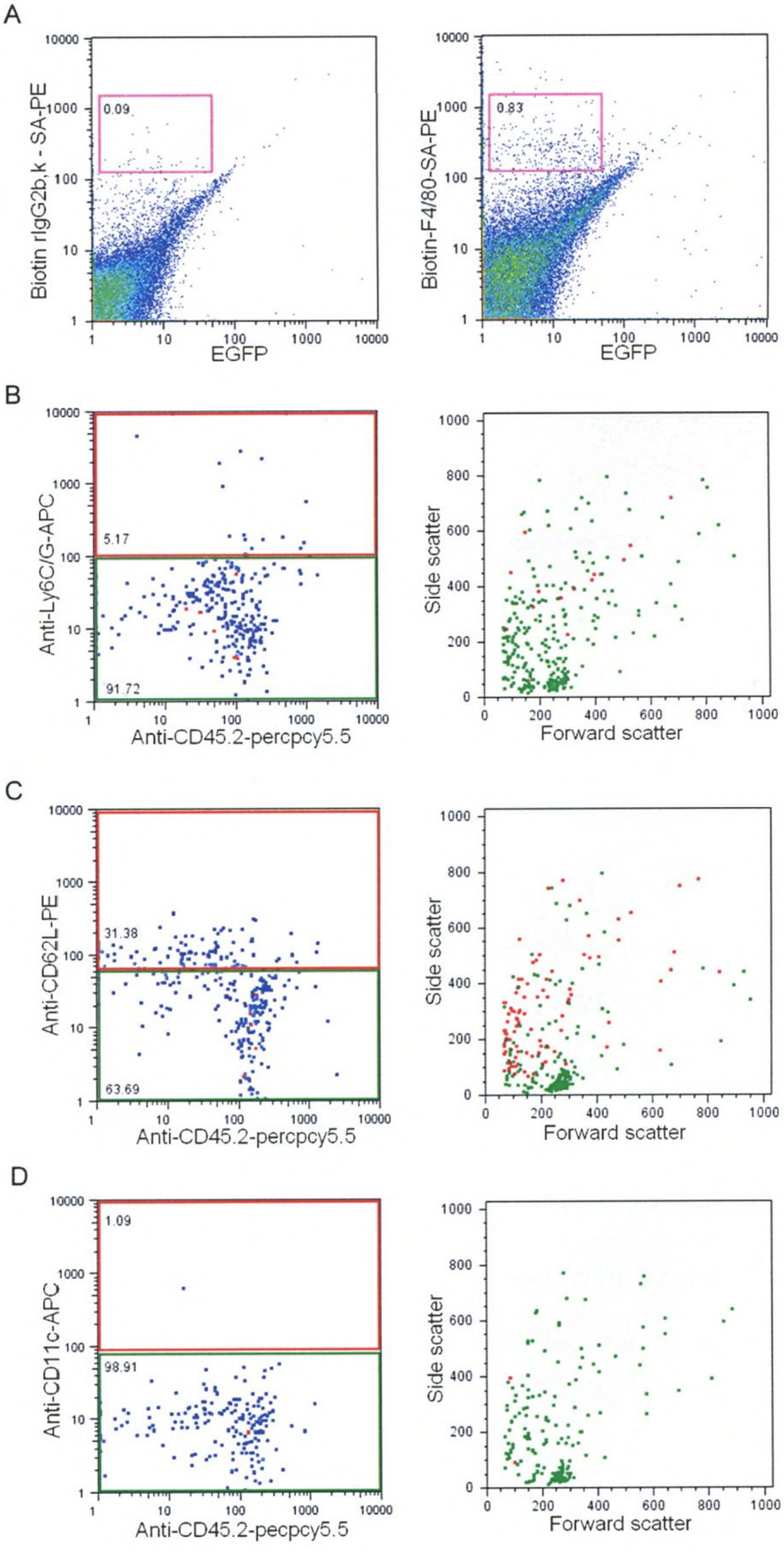
A
Biotin rIgG2b,k - SA-PE
EGFP
0.09
Biotin-F4/80-SA-PE
EGFP
0.83
B
Anti-Ly6C/G-APC
Anti-CD45.2-percpcy5.5
5.17
91.72
Side scatter
Forward scatter
C
Anti-CD62L-PE
Anti-CD45.2-percpcy5.5
31.38
63.69
Side scatter
Forward scatter
D
Anti-CD11c-APC
Anti-CD45.2-pecpcy5.5
1.09
98.91
Side scatter
Forward scatter

However, backgating of the microglia subsets indicate that the $CD62L^+$ subset is found on the lower left quadrant of the FSC/SSC plot, a spot typical of debris (Figure 22C). Similar observations are made for Figure 22B and D that suggest differential expression of CD45.2 among microglia. Our previous data point to a distinct FSC/SSC profile for microglia in the uninjured spinal cord (Figure 13A). Thus, additional studies using the 7AAD viability marker needs to done in combination with the surface markers to confirm whether or not microglia subsets are indeed found in the uninjured spinal cords.

Overall, the second stage of the present study indicates the presence of DCs and heterogeneous subsets of hMØ and mMØ suggesting the complexity of the immunological response to SCI. Ultimately the functional analysis of these cells needs to be conducted. Of particular interest is determining the individual functional roles of hMØ and mMØ in response to SCI. Thus, we established a protocol for cell sorting of these two cell types following SCI, as is discussed next.

3.7 SORTING OF INFLAMMATORY CELLS FOLLOWING SCI.

Cell sorting of hMØ and mMØ was performed with the aim of being able to process these cells for mRNA preparation. Additionally, attempts were made to sort 'classical inflammatory' from the 'non-classical resident' monocytes in the *lys*-EGFP-*ki* blood as future studies may consider examining functionality of the monocyte subsets in response to SCI. The cell surface markers and gating strategies used for sorting of spinal cord cells is discussed first.

3.7.1 Cell surface markers and gating strategies for cell sorting of spinal cord samples

The spinal cord tissue consists of cells such as neurons, astrocytes, oligodendrocytes, and microglia and is rich in lipid and myelin content. Microglia and mMØ represent only ~15% of the total cell population *(72)*. Also, in response to SCI, the infiltrating hMØ are present in the lesion in minute numbers relative to the total spinal cord cells. As such, flow cytometry of the spinal cord is challenging. Ideally, sorting of rare populations requires additional steps that enrich for cells of interest; in our study, these being the hMØ and mMØ in the injured spinal cord and microglia in the uninjured spinal cord.

A first method of enrichment is removal of unwanted components from the single cell suspension. In our study, a percoll gradient served to remove debris, myelin, and RBC from the spinal cord samples (Figure 3A and B). A second method of cell enrichment is negative selection of unwanted populations by cell surface marker staining. However, currently, antibodies to the cell surface of neurons, oligodendrocytes, and astrocytes are not available and as such they could not be excluded from the spinal cord samples. However, microglia, hMØ, and mMØ are hematopoietic in origin with microglia/mMØ being the only CNS cell of this origin *(41, 75)*. Thus, we focused on positive selection of hematopoietic cells in the spinal cord.

Our pilot studies used uninjured spinal cord cells spiked with 5μL of blood as this closely compares to the SCI lesion. In these samples, we observed that hematopoietic cells backgate to a specific location on the FSC/SSC plot (Figure 23B and D). Also, our results showed that the total frequency and numbers of $CD45.2^+$ (hematopoietic marker)

Figure 23. Blood-spiked spinal cord samples processed with percoll gradient (top panel) show enrichment of hematopoietic CD45.2^{+} cells compared to samples processed without percoll gradient (bottom panel). Blue boxed regions highlight the total frequency and numbers of hematopoietic cells in samples processed with (B) and without (D) percoll. Isotype-matched controls are shown in (A) and (C). Grey, purple, red, and orange colors represent background populations, hematopoietic gated cells, live cells, and CD45.2^{+} cells respectively. N=3.

With percoll gradient

A

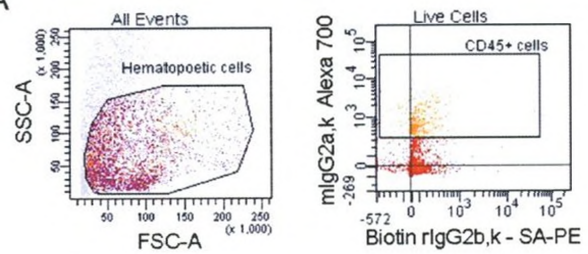

Population	#Events	%Parent	%Total
All Events	10,000		100.0
Hematopoetic cells	4,237	42.4	42.4
Single Cells	3,980	93.9	39.8
Live Cells	3,595	90.3	35.9
CD45+ cells	519	14.4	5.2

B

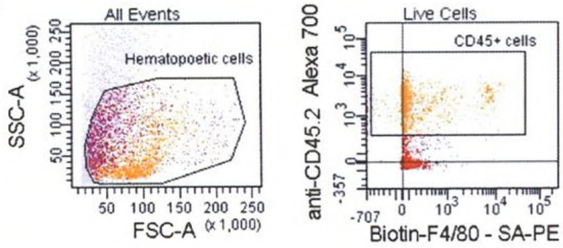

Population	#Events	%Parent	%Total
All Events	10,000		100.0
Hematopoetic cells	4,204	42.0	42.0
Single Cells	3,961	94.2	39.6
Live Cells	3,574	90.2	35.7
CD45+ cells	1,682	47.1	16.8

Without percoll gradient

C

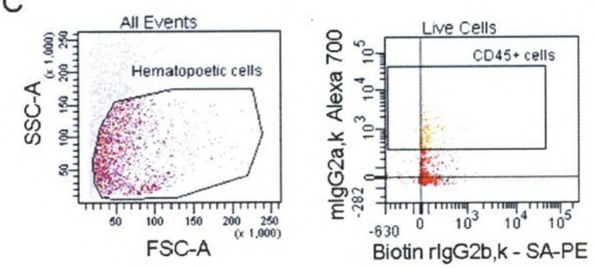

Population	#Events	%Parent	%Total
All Events	10,000		100.0
Hematopoetic cells	2,453	24.5	24.5
Single Cells	2,372	96.7	23.7
Live Cells	2,249	94.8	22.5
CD45+ cells	290	12.9	2.9

D

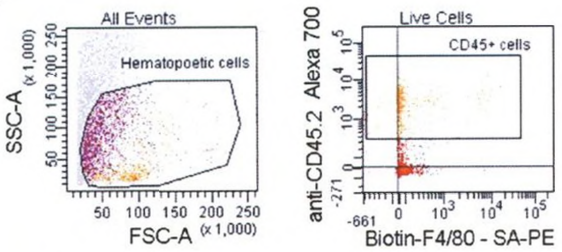

Population	#Events	%Parent	%Total
All Events	10,000		100.0
Hematopoetic cells	2,243	22.4	22.4
Single Cells	2,172	96.8	21.7
Live Cells	2,077	95.6	20.8
CD45+ cells	529	25.5	5.3

cells were 3-fold higher in samples that were run through the percoll gradient than samples that were not (Figure 23B and D) confirming that the percoll gradient efficiently enriches for hematopoietic cells.

We applied the above results to our sorting strategies. Generally, for all spinal cord sorting experiments, we first backgated CD45.2^{+} cells and placed a gate on the hematopoietic cells in the FSC/SSC plot to reduce contributions of unwanted components (Figure 24A and 25A). Thereafter, the 'area' versus 'width' dimension *(126)* was used to only gate on singlet cells and exclude doublets (Figure 24A and 25A). Additionally, the viability dye, 7AAD was used to exclude dead cells (Figure 24A and 25A). Cells meeting all these parameters were then examined for F4/80 and EGFP expression to discriminate hMØ (F4/80^{+}, EGFP^{+}) from mMØ (F4/80^{+}, EGFP^{-}) in the SCI samples (Figure 24B). Similarly, microglia were identified as F4/80^{+}, EGFP^{-} cells in the uninjured samples (Figure 25B). Each cell type was further analyzed for expression of CD45.2 and CD11b (Figure 24C, D and 25C, D). The CD11b marker was used as its expression is common although not exclusive to hMØ, mMØ, and microglia. The combination of CD45.2 and CD11b more specifically enabled further discrimination of hematopoietic cells from the unwanted components. Thus the required population had to meet all the above parameters for it to be sorted.

Cell sorting of the blood monocyte populations was performed similar to that of the spinal cords except that the monocyte subsets were differentiated based on EGFP, F4/80, and Ly6C/G expression (Figure 26). The 'classical inflammatory' monocytes were F4/80^{lo}, Ly6C/G^{+}, EGFP^{+} while the 'non-classical resident' monocytes were

Figure 24. Cell sorting of hMØ and mMØ in the spinal cord lesions of *lys*-EGFP-*ki* mice at 7d post-SCI. A gate was placed on the FSC/SSC plot to outline hematopoietic cells, which were further refined by gating on singlet and live cells (A). Identification of hMØ and mMØ was made by placing gates on $F4/80^{+}$, $EGFP^{+}$ and $F4/80^{+}$, $EGFP^{-}$ cells respectively with the use of an isotype control (B). To reduce background scatter, an $EGFP^{+}$ and $EGFP^{-}$ gate was placed around hMØ and mMØ respectively (B). Cells were further classified for positive expression of CD11b and CD45.2 so as to sort mMØ (C) and hMØ (D). Light grey: background scatter, maroon: hematopoietic cells, dark grey: singlet cells, red: live cells, green: hMØ, and blue: mMØ. N=3, n=4-5.

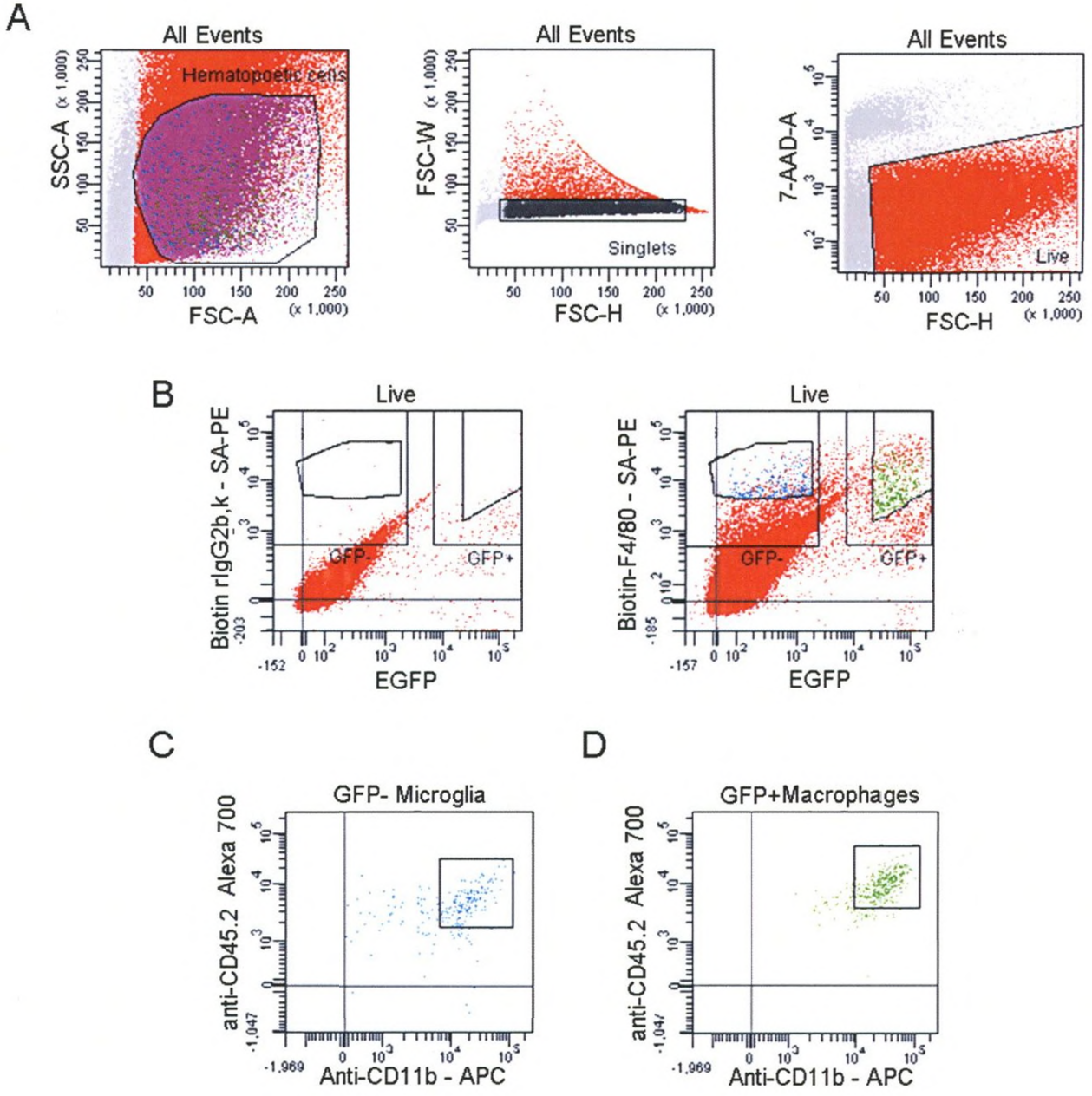
A
All Events
Hematopoetic cells
SSC-A (x 1,000)
FSC-A (x 1,000)
All Events
Singlets
FSC-W (x 1,000)
FSC-H (x 1,000)
All Events
Live
7-AAD-A
FSC-H (x 1,000)
B
Live
GFP-
GFP+
Biotin rIgG2b,k - SA-PE
EGFP
Live
GFP-
GFP+
Biotin-F4/80 - SA-PE
EGFP
C
GFP- Microglia
anti-CD45.2 Alexa 700
Anti-CD11b - APC
D
GFP+Macrophages
anti-CD45.2 Alexa 700
Anti-CD11b - APC

Figure 25. Cell sorting of microglia in the uninjured spinal cords of *lys*-EGFP-*ki* mice. A gate was placed on the FSC/SSC plot to outline hematopoietic cells, which were further refined by gating on singlet and live cells (A). Identification of microglia was made by placing a gate on $F4/80^{+}$, $EGFP^{-}$ cells with the use of an isotype control (B). To reduce background scatter, an $EGFP^{+}$ and $EGFP^{-}$ gate was placed around the areas of hMØ and microglia (B) as was done for SCI samples. Cells were further classified for positive expression of CD11b and CD45.2 so as to sort microglia (C) and hMØ (D). The lack of hMØ in (B, D) indicates absence of contamination. Light grey: background scatter, maroon: hematopoietic gate, dark grey: singlet cells, red: live cells, green: $EGFP^{+}$ cells, blue: microglia. N=3, n=4-5.

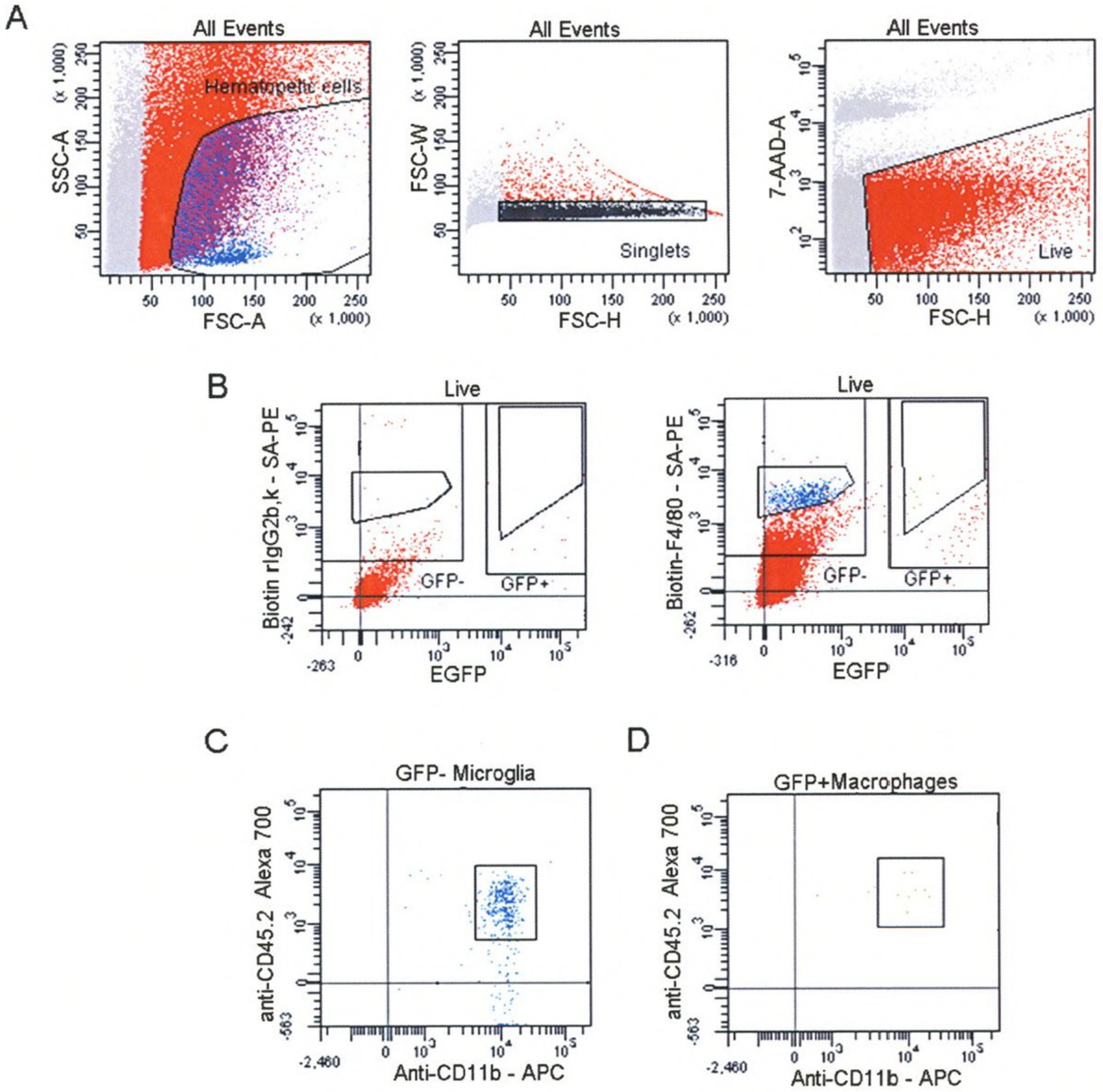
A
All Events
Hematopoetic cells
SSC-A
FSC-A
(x 1,000)
All Events
Singlets
FSC-W
FSC-H
(x 1,000)
All Events
Live
7-AAD-A
FSC-H
(x 1,000)
B
Live
Biotin rIgG2b,k - SA-PE
GFP-
GFP+
EGFP
Live
Biotin-F4/80 - SA-PE
GFP-
GFP+
EGFP
C
GFP- Microglia
anti-CD45.2 Alexa 700
Anti-CD11b - APC
D
GFP+Macrophages
anti-CD45.2 Alexa 700
Anti-CD11b - APC

Figure 26. Cell sorting of blood monocyte subsets in the uninjured *lys*-EGFP-*ki* mice. A gate was placed on the FSC/SSC plot to outline hematopoietic cells, which were further refined by gating on singlet and live cells (A). Identification of 'classical inflammatory' (P4) and 'non-classical resident' (P5) monocytes were made by placing gates on $F4/80^{lo}$, $EGFP^{+}$ and $F4/80^{hi}$, $EGFP^{+}$ cells respectively with the use of an isotype control (B). The P4 and P5 cells were further classified for expression of Ly6C/G so as to sort the 'classical inflammatory' (P1) from 'non-classical resident' monocyte (P3) (C). Light grey: background scatter, maroon: hematopoietic gate, dark grey: singlet cells, red: live cells, green: $EGFP^{+}$ cells, pink: 'classical inflammatory' monocytes, blue: 'non-classical' resident monocytes. N=3, n=4-5.

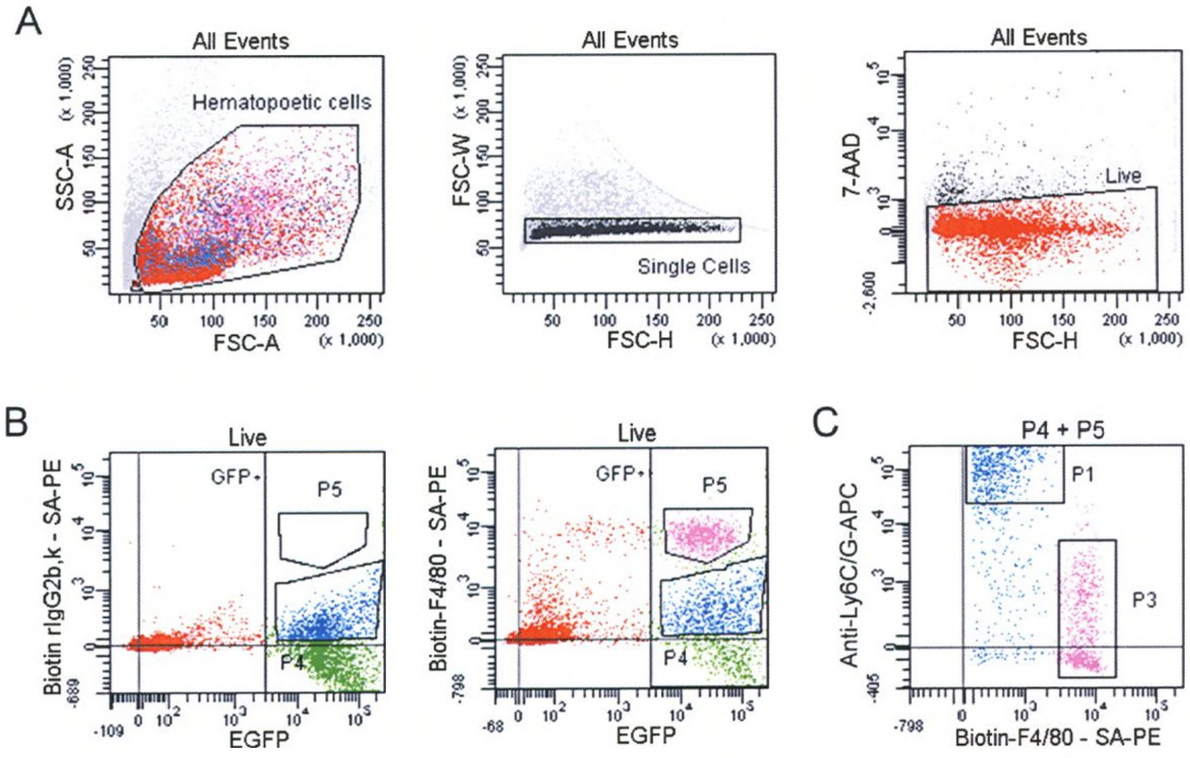
A
All Events
Hematopoetic cells
SSC-A (x 1,000)
FSC-A (x 1,000)
All Events
Single Cells
FSC-W (x 1,000)
FSC-H (x 1,000)
All Events
Live
7-AAD
FSC-H (x 1,000)
B
Live
GFP+
P5
P4
Biotin rIgG2b,k - SA-PE
EGFP
Live
GFP+
P5
P4
Biotin-F4/80 - SA-PE
EGFP
C
P4 + P5
P1
P3
Anti-Ly6C/G-APC
Biotin-F4/80 - SA-PE

F4/80^{hi}, Ly6C/G^{-}, EGFP^{+}. Also, the use of CD11b and CD45.2 markers were not needed for cell sorting as monocytes are not rare populations in the blood.

Overall, the above strategies were applied to sort mMØ, hMØ, microglia, and monocytes subsets, the results of which are discussed below.

3.7.2 Cell sorting of hMØ and mMØ at 7d post-SCI.

Three independent experiments of cell sorting of hMØ and mMØ from the spinal cord lesion at 7d post-SCI were done. The 7d time point was chosen because maximumnumbers of hMØ and mMØ were observed in the lesioned spinal cord at that time (Figure 11D, F). Using the gating strategies described, hMØ and mMØ were sorted from the injured spinal cord samples. Figure 24 shows a representative sorting experiment of the lesioned spinal cord. The numbers of hMØ and mMØ sorted were 5886 and 2175, respectively. The purity of sorted cells was assessed by taking an aliquot of the sorted population and re-running it through the cell sorter to determine whether the population met within the parameters used to define it (Appendix 2). In order to maximize the number of cells for downstream applications, only 5µL of the 100µL of serum free media -containing sorted cells was taken and diluted with sheath fluid to assess the purities. This fact contributes to the very low numbers of cells shown in Appendix 2. The DiVa software generated numbers for hMØ and mMØ sorted purities were 96.6% and 94.4%, respectively. These numbers represent the frequency of 'sorted cells meeting defined parameters' relative to the parent population. Generally, the purities of sorted hMØ and mMØ were over 90% for all experiments conducted.

3.7.3 Cell sorting of microglia in the uninjured spinal cord

Three independent experiments for sorting of microglia was performed, a representation of which is shown in Figure 25. The actual numbers of sorted microglia for that particular experiment was 3383 and was obtained with a purity of 93.5% (Appendix 2). Generally, the purities of microglia were also over 90% for all experiments conducted.

3.7.4 Cell sorting of blood monocytes

Three independent experiments using uninjured blood were performed to sort 'classical inflammatory' from 'non-classical resident' monocytes (Figure 26). In that experiment 25,783 'classical inflammatory' and 39,771 'non-classical resident' monocytes were isolated; the respective cell purities obtained were 94.7% and 98.5% (Appendix 2).

3.7.5 RNA extraction of sorted microglia, hMØ and mMØ

The aim of sorting microglia, hMØ and mMØ was to assess differences in mRNA expression following SCI. The RNA obtained from some of the sorted cells of the spinal cord showed that they were of good quality as determined by the 28S/18S rRNA ratio (Figure 27A and B). However, many of the samples contained degraded and/or non-detectable levels of RNA (Figure 27C and D).

Figure 27. Samples of extracted RNA showing RNA quality and quantity obtained from sorted cells in the spinal cord samples. RNA extracted from sorted mMØ (A) and hMØ (B) post-SCI exhibit properties of good RNA quality with the 28S:18S rRNA ratio close to 2.0. RNA extracted from sorted microglia (C) and hMØ (D) show negligible and/or degraded RNA. This figure shows a sample of representative RNA extractions.

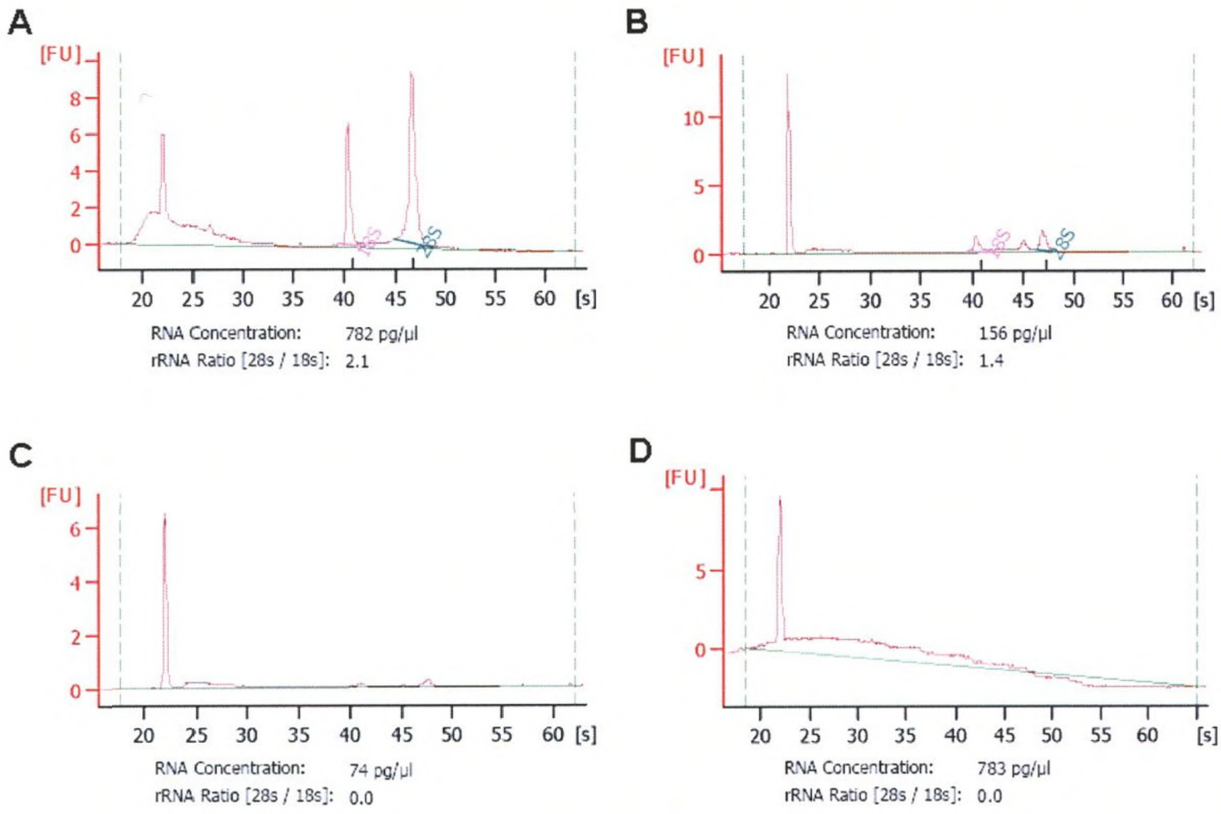
A
[FU]
8
6
4
2
0
20 25 30 35 40 45 50 55 60 [s]
RNA Concentration: 782 pg/µl
rRNA Ratio [28s / 18s]: 2.1
B
[FU]
10
5
0
20 25 30 35 40 45 50 55 60 [s]
RNA Concentration: 156 pg/µl
rRNA Ratio [28s / 18s]: 1.4
C
[FU]
6
4
2
0
20 25 30 35 40 45 50 55 60 [s]
RNA Concentration: 74 pg/µl
rRNA Ratio [28s / 18s]: 0.0
D
[FU]
5
0
20 25 30 35 40 45 50 55 60 [s]
RNA Concentration: 783 pg/µl
rRNA Ratio [28s / 18s]: 0.0

A possible explanation for our results is that the RNA from our sorted cells was extracted almost 8 weeks post sorting. Thus, due to the low yield of sorted cells, the RNA may have degraded faster than anticipated. This suggests that while it is possible to obtain good RNA from sorted cells, steps to optimize better yields of sorted cells and/or better/immediate RNA extraction of sorted samples is required before attempting to carry out gene profiling studies.

CHAPTER 4 – DISCUSSION

4.1 THE INFLAMMATORY RESPONSE TO SCI

Inflammation of the injured CNS is partly mediated by infiltrating neutrophils *(11, 24, 31)* and hMØ *(10, 11)*, and resident microglia *(70, 79, 142)*. Previously, our laboratory showed that administration of a mAb against CD11d/CD18 integrin minimizes progression of secondary SCI by selectively blocking the neutrophil influx and only delaying the extravasation of hMØ into the spinal cord lesion *(21, 109)*. This treatment resulted in neuroprotection and improved sensory, autonomic, and motor functions in an experimental rodent model of SCI *(109, 112, 143)*. These results suggested that hMØ may have varying effects depending on the timing of their influx into the injured spinal cord. In light of the recent discovery of heterogeneous monocyte subsets *(41, 48)*, the possibility of these subsets migrating differentially into the lesion and differentiating into hMØ with neurodegenerative or neuroprotective effector function remains. However, the individual roles of hMØ and mMØ remain unclear as they are morphologically and immunophenotypically similar in their activated states following SCI *(63, 92)*. This limitation has been an obstacle in the investigation of differential temporal and spatial roles of hMØ and mMØ in the inflammatory response to SCI *(57, 92, 116)*.

Recently, our laboratory has used the *lys*-EGFP-*ki* transgenic mouse as a model system that is able to differentiate hMØ from mMØ following SCI. Originally created by Faust et al. *(120)*, the transgenic mice express EGFP under the *LysM* promoter; thus, in these mice, EGFP is only expressed in mature myelomonocytic cells (neutrophils, monocytes, and hMØ). However, their study did not examine the nature of EGFP

expression in the CNS microglia, which are hematopoietic in origin *(70, 71, 73)* and are a part of the mononuclear phagocyte system *(41, 70)*.

Our laboratory investigated the expression of EGFP in the microglia of *lys*-EGFP-*ki* mice. Using immunohistochemical staining of spinal cord sections, we showed that the SCI lesions of transgenic mice contained F4/80$^+$, EGFP$^+$ and F4/80$^+$, EGFP$^-$ cells. However, the uninjured spinal cords only contained F4/80$^+$, EGFP$^-$ microglia, suggesting that under resting conditions, microglia in the adult transgenic mice do not express EGFP. Additionally, studies in which hMØs were depleted by administration of clodronic acid liposomes prior to, and following SCI, showed exclusive presence of F4/80$^+$, EGFP$^-$ cells in the lesion of SCI *lys*-EGFP-*ki* mice. This study suggested that activated microglia and mMØ do not express EGFP. Lastly, BM transplantation studies of *lys*-EGFP-*ki* BM transplanted into the C57BL/6 strain showed the presence of numerous F4/80$^+$, EGFP$^+$ and F4/80$^+$, EGFP$^-$ cells in the lesion following SCI. In the reciprocal setting, numerous F4/80$^+$, EGFP$^-$ cells but only negligible numbers of F4/80$^+$, EGFP$^+$ cells were observed in the SCI lesion. This study further supported the evidence that activated microglia and mMØ are EGFP$^-$. Together, these studies demonstrated that the *lys*-EGFP-*ki* mouse model enables the distinction of EGFP$^+$ hMØ from EGFP$^-$ mMØ following SCI.

The study presented in this thesis used the transgenic *lys*-EGFP-*ki* mice in a model of SCI to investigate the cellular inflammatory response in the blood and in the spinal cord lesion. I conducted a three part study. The first part of the study involved examining the response of inflammatory cells to the acute (1d, 3d, and 7d) and chronic (14d and 6wks) phases of SCI. Specifically, I examined the response of circulating neutrophils and monocytes in the blood, as well as, infiltrating neutrophils and hMØ, and

resident mMØ in the injured spinal cords. Furthermore, the differential response of monocyte and hMØ subsets was examined following SCI. The second part of the study involved phenotypic characterization of subsets of monocytes in the blood, and hMØ and mMØ in the SCI lesion. The third part of the study involved developing a protocol for sorting hMØ and mMØ for the purpose of examining potential differences in their mRNA expression post-SCI. The results obtained from the three parts of the study are discussed below.

4.1.1 The neutrophil response to SCI

To my knowledge, the present study is the first to investigate the levels of circulating blood neutrophils in response to SCI. I demonstrated that neutrophils in circulation are consistently elevated in response to the acute and chronic phases of SCI. Simultaneously, an increase in neutrophil numbers in the spinal cord lesion occurs at 1-3d post-SCI; these numbers gradually decrease but remain above the control levels for up to 6wks following SCI. These flow cytomteric results on the infiltration pattern of neutrophils into the lesion of SCI *lys*-EGFP-*ki* mice are qualitatively similar to those previously obtained by our laboratory using immunohistochemistry *(25)*. However, inferences on the quantitative aspects of neutrophil infiltration between the two methodologies cannot be made; the flow cytometric approach is based on absolute numbers while the immunohistochemical approach is based on the mean ratio of immunoreactive cells. Additionally, the present study used a monoclonal antibody while the immunohistochemical approach used a polyclonal antibody for neutrophil identification. Overall, our infiltration pattern agrees with literature that suggest a late

onset of neutrophil infiltration for the mouse model as compared to the rat model of SCI *(11, 24)*. Importantly, the mouse neutrophil infiltration pattern during the acute stage is quite similar to that seen in humans with SCI *(26)* strongly suggesting that using an experimental mouse model of SCI is relevant to the human condition.

Together, our results on the neutrophil response to SCI suggest that unlike damage in peripheral nervous system that resolves over time, the CNS damage (dependent on severity of injury) remains unresolved over the course of injury *(144)*, and is associated with a constant presence of neutrophils in the spinal cord lesion. These incoming neutrophils may further exacerbate the effects of the trauma by facilitating secondary injury processes *(11, 30)* However, Kigerl et al. *(141)* have shown that strain-dependent neuroinflammation is observed after SCI. Thus, the response of neutrophils in the SCI *lys*-EGFP-*ki* mice may possibly be affected by its transgenic nature. I used the homozygous transgenic strain that constitutively expresses high levels of EGFP in mature myelomonocytic cells (neutrophils and monocyte/hMØ) raising the possibility that high EGFP expression may alter the functionality of these cells. Recently, Bou-Abdallah et al. *(145)* showed that green fluorescence protein (GFP) can potentially quench superoxide radicals and exhibit antioxidant properties in corals naturally expressing GFP-like proteins. This effect may have implications especially on neutrophil function; presence of EGFP may reduce neutrophil reactive oxygen species (ROS) production, and this may contribute towards a differential response to SCI. Although the original study *(120)* on the *lys*-EGFP-*ki* mice established the viability and completeness of hematopoietic system in the transgenic mice, detailed examination of specific macrophage and neutrophil functions (such as phagocytic capacity and bactericidal action) of the mice were not

performed. In the present study, we observed that circulating neutrophils were elevated by 2-fold in the *lys*-EGFP-*ki* mice as compared to the wild-type strain, C57BL/6 mice. A caveat to these data was the use of C57BL/6 mice alone as controls; a more appropriate control would be the use of mice containing contributions from the non-transgenic parental strains C57BL/6 and 129Sv mice, such as their F1 cross. Overall, additional studies that compare the levels of neutrophil infiltration in SCI transgenic mice and the standard strain used for SCI studies, the C57BL/6 mice *(141)* need to be conducted to determine whether the inherent elevated numbers of neutrophils in the *lys*-EGFP-*ki* mice affects their neurological recovery following SCI.

4.1.2 The monocyte/hMØ response to SCI

Circulating blood monocytes are heterogeneous in that they encompass subtypes differing in the expression of CX_3CR1, CCR2, CD62L, and Ly6C/G *(41, 48, 52)*. 'Classical inflammatory' monocytes are CX_3CR1^{lo}, $CCR2^{+}$, $CD62L^{+}$, $Ly6C/G^{+}$ and are preferentially recruited to sites of inflammation due to their recognition of CCL-2 and CD62L-mediated interaction with endothelial cells, both of which facilitate extravasation to sites of acute inflammation *(41, 48, 52)*. Conversely, the 'non-classical resident' monocytes are CX_3CR1^{hi}, $CCR2^{-}$, $CD62L^{-/lo}$, $Ly6C/G^{-/lo}$ and are thought to migrate into non-inflamed tissues where they may function in homeostatic maintenance; their migration is facilitated by the expression of the chemokine receptor, CX_3CR1 *(41, 48, 52)*. Studies support the idea that monocytes newly released from the BM are $Ly6C/G^{+}$ (classical inflammatory) and have the capacity to undergo maturation in the blood to give

rise to the Ly6C/G$^{-/lo}$ (non-classical resident) monocytes *(48, 49, 52)*. This theory is supported by evidence that a monocyte subset with intermediate expression of Ly6C/G is observed in the blood and is termed the 'intermediate' monocyte *(48, 52)*.

In the present study, the overall circulating monocyte levels significantly increased in the SCI blood samples at 3d, 14d, and 6wks; this increase was specifically due to the rise in the 'non-classical resident' monocytes. In contrast, the levels of the 'classical inflammatory' monocytes did not significantly change in the SCI blood over time post-SCI except at 7d when their levels increased. To my knowledge, the present study is the first to examine blood monocytes and their subsets in response to SCI. Studies that examine the response of monocyte subsets to inflammation in general are also few. Sunderkötter et al. *(52)* showed that in mice, *Listeria monocytogenes* infection had no effect on the monocyte subset ratio in the blood at 2d; however, at 3d post-infection, the 'classical inflammatory' monocytes exhibited a higher frequency in the blood. Similarly, chronic parasitic infection in mice also led to a shift towards the 'classical inflammatory' monocytes in the blood. Thus, my results on the ratio of monocyte subsets at the onset of the acute phase (1d) of SCI corroborates with their study; however, data obtained for the chronic phase of SCI are essentially the opposite of what was reported *(52)*. The differences observed in the ratio of monocyte subsets in the blood during the chronic SCI stage may be due to the nature of inflammation induced; peripheral and CNS inflammation may involve differential mechanisms that presently remain unknown.

The present study also examined the hMØ influx into the SCI lesion. I showed that hMØ numbers in the lesion peaked at 7d post-SCI, decreased thereafter, but persisted

at an elevated level for up to 6wks post-SCI. An effort was also made to identify the source of these hMØ at each of the time points following SCI. My results provide evidence that the acute phase of SCI (1d, 3d, and 7d) involves predominantly the 'classical inflammatory' derived hMØ; however, the chronic phase (14d and 6wks) involves the 'non-classical resident' derived hMØ. My data with regards to the nature of acute inflammation are consistent with studies showing the presence of 'classical inflammatory' hMØ at sites of inflammation including the brain *(52, 146)*. However, at present, little is known about the fate of hMØ during the chronic stages of CNS inflammation. A recent study examined the nature of acute and chronic inflammation in the brains of hepatitis virus infected mice. Consistent with my work, Templeton et al. *(127)* report that while the acute stage of brain inflammation involves the presence of the 'classical inflammatory' hMØ, the chronic stages involves presence of the 'non-classical resident' hMØ. They propose that the presence of the latter population during the chronic stage of inflammation reflects the maturation of Ly6C/G^{+} ('classical inflammatory') hMØ to Ly6C/G^{-} ('non-classical resident') hMØ. This maturation process may parallel that seen in the blood for monocyte subsets in which CD62L and Ly6C/G expression are down-regulated to generate the Ly6C/G^{-} resident monocytes *(127)*. However, they report that the expression of CD43, a monocyte maturation marker, that is upregulated on the 'non-classical resident' monocyte subset in the blood *(52)* is not upregulated in the corresponding hMØ subset in response to brain inflammation *(127)*. Thus, to confirm whether hMØ maturation occurs at the lesion in response to SCI, the expression of known macrophage maturation markers such as MHC II, CD40, CD43 and CD86 *(127)* could be examined in the lesion during the acute and the chronic stages of SCI. Overall,

my results indicate that the monocyte/hMØ response is persistent in the chronic phase of SCI. Similar to neutrophils, the observation reflects ongoing inflammation of the lesion following SCI. Previously, our laboratory has shown that delaying the influx of hMØ into the lesion following SCI results in neurological recovery of SCI rats *(21, 112)*. Thus, it is possible that infiltrating hMØ in the acute and chronic environment following SCI dictate whether hMØ will participate in a neurodestructive or neuroprotective manner; however, this hypothesis remains to be investigated.

4.1.3 The microglial response to SCI

The mMØ response to SCI was examined and similar to hMØ, I found that they peak in the spinal cord lesion at 7d post-SCI. Additionally, at all times post-SCI, the mMØ numbers in the lesion predominated by 3-fold over that of hMØ and were significantly higher in the SCI mice than in the sham injured and uninjured mice. The source of this microgliosis in response to trauma is still a controversial issue *(75, 79)*. Some studies suggest that microglia proliferate in response to SCI while others suggest that microglia migrate from areas adjacent to the lesion *(75, 147)*. The present study did not examine the source of microgliosis; this issue may be investigated with the use of Bromodeoxyuridine (BrdU), a reagent for detecting proliferating cells *(148)*, in combination with fluorescent antibodies. Microgliosis at the lesion may participate in immune regulation by exhibiting both pro- and anti-inflammatory effector functions thereby contributing to the overall spinal cord microenvironment *(73, 79, 149)*. This in turn may polarize the incoming hMØ to exhibit a beneficial or destructive function *(49, 56)*.

Overall, the results from the first stage of my study provide new insights into the inflammatory response following SCI, including the dynamics of cellular inflammation in the acute (1d, 3d, and 7d) and chronic (14d and 6wks) phases of SCI with attention paid to the differential responses of heterogeneous monocytes and hMØ subsets to SCI.

4.2 PHENOTYPIC ANALYSIS OF LEUKOCYTES FOLLOWING SCI

4.2.1 Phenotyping *lys*-EGFP-*ki* monocytes in the blood

As mentioned in section 4.1.2, three mouse monocyte subsets exist: the 'classical inflammatory', 'non-classical resident', and 'intermediate' monocyte subsets *(48, 52)*. The human counterparts of these monocytes have been identified based on differential expression of CD14 and CD16: 'classical inflammatory' $CD14^{hi}$, $CD16^{-}$; 'non-classical resident' $CD14^{lo}$, $CD16^{+}$; and the 'intermediate' $CD14^{+}$ (as opposed to $CD14^{lo}$) $CD16^{+}$ monocytes; these subsets exhibit homing potential similar to those described for mouse monocyte subsets *(41, 47)*. My results from the first stage of this thesis provide evidence that monocyte/hMØ subsets respond differentially to SCI. Thus, I directed the second stage of my study to further characterize subsets of monocytes in the blood, and hMØ and mMØ in the lesioned spinal cord.

In the present study, blood monocyte subsets in the *lys*-EGFP-*ki* mice were further classified based on differential expression of EGFP, F4/80, Ly6C/G, CD11c, and CD62L. Three $EGFP^{+}$ and three $EGFP^{-}$ monocyte subsets were identified based on inferences made by backgating analysis. The former monocyte populations identified were: i) $EGFP^{+}$, $F4/80^{lo}$, $Ly6C/G^{+}$, $CD11c^{-}$, $CD62L^{+}$, (classical inflammatory); ii) $EGFP^{+}$, $F4/80^{hi}$, $Ly6C/G^{-}$, $CD11c^{-}$, $CD62L^{-}$ (non-classical resident); and

iii) EGFP^{+}, F4/80^{lo}, Ly6C/G^{-}, CD11c^{+}, CD62L^{-} (previously unidentified 'monocyte-like') monocyte subsets. The three EGFP^{-} populations identified were: i) EGFP^{-}, F4/80^{lo}, Ly6C/G^{int}, CD11c^{-}, CD62L^{-} (intermediate); ii) EGFP^{-}, F4/80^{lo}, Ly6C/G^{+}, CD11c^{-}, CD62L^{+}, and iii) EGFP^{-}, F4/80^{hi}, Ly6C/G^{-}, CD11c^{-}, CD62L^{-} monocyte subsets.

The 'classical inflammatory' and 'non-classical resident' monocyte subsets identified in my work are phenotypically consistent with previous descriptions *(41, 48, 52)*. A minor difference is that the present study also showed that the two monocyte subsets have differential F4/80 expression: the 'classical inflammatory' subset being F4/80^{lo} and the 'non-classical resident' subset being F4/80^{hi}. It is possible that because I used a biotin-streptavidin complex for antibody staining, the F4/80 expression was better resolved and thus allowed for identification of the monocyte subsets with higher sensitivity.

The 'intermediate' monocyte subset identified in my work also seems to be consistent with literature *(48, 52)*. As mentioned previously, the identification of this 'intermediate' monocyte supports the theory that Ly6C/G^{+} 'classical inflammatory' monocytes undergo maturation to give rise to Ly6C/G^{-} 'non-classical resident' monocytes in the blood; this transition is mediated by the Ly6C/G^{int} 'intermediate' monocyte *(48, 49, 52)*. However, identification of this 'intermediate' subset in my study was based solely on differential expression of Ly6C/G. Additional studies must be conducted to confirm the nature of this population by examining expression of CCR7 and CCR8, surface markers that are reported to be present on this intermediate monocyte subset *(47, 48, 150)*. Interestingly, my analysis revealed that the 'intermediate' monocyte was EGFP^{-}, indicating a lack of or very little *LysM* activity; the *LysM* promoter is only

active in mature myelomonocytic cells. Thus, it is possible that since this subset is not committed to being a 'classical inflammatory' or a 'non-classical resident' monocyte, it may be 'immature' relative to the two other monocyte subsets. As such, it lacks/has very little EGFP expression that cannot be detected by flow cytometry. This issue may be confirmed by examining the mRNA expression of EGFP in these monocytes. Currently, the exact nature of *LysM* activity with respect to conditions that activate/deactivate its expression is not fully understood. Alternatively, this 'intermediate' monocyte subset may represent myeloid suppressor cells (MSC). MSC are defined as cells that are Ly6C/G$^+$, F4/80$^+$, CD11b$^+$ *(151, 152)*; these criteria are met by the 'intermediate' subset. To confirm the identity of these 'intermediate' monocytes, the functional nature of these cells, such as suppression of T-cell activity *(151, 152)* could be examined.

The other two EGFP$^-$ monocyte subsets identified in my work may correspond to their respective EGFP$^+$ 'classical inflammatory' and 'non-classical resident' monocytes as judged by similar immunophenotypic expression and location on the FSC/SCC plot. Alternatively, the EGFP$^-$ cells may be precursors of their respective monocyte subsets, in which case they would be immature cells and thus would lack/have little EGFP expression. To rule out the latter reason, further phenotyping of monocytic cells in the blood may be performed using markers such as ER-MP12 that specifically stain for immature monocytic cells *(120)*. Additionally, the mRNA expression of EGFP in these monocytes may be examined as was discussed earlier. Overall, the presence of EGFP$^-$ monocytes in the *lys*-EGFP-*ki* mice complicates the interpretations that can be made with respect to the F4/80$^+$, EGFP$^-$ (microglia and mMØ) population in the SCI lesion. As discussed earlier, the premise for identification of hMØ and mMØ in the injured spinal

cord is differential expression of EGFP. It is possible that the $EGFP^-$ monocytes enter the injured lesion and hence would not be distinguishable from microglia and mMØ. Although the numbers of $EGFP^-$ monocytes are relatively small in the blood compared to the other monocyte subsets, its presence in the spinal cord lesion may confound the results that we obtain for microglia and mMØ, an example of which is discussed below.

Previous studies on EAE *(78)* suggest that under CNS inflammatory conditions, mMØ and hMØ can be identified based on CD45 expression; mMØ and hMØ having low and high CD45 expression levels respectively. I investigated whether the same holds true in a SCI mouse model. My results showed that while mMØ and hMØ exhibited low and high CD45.2 MFI respectively, the mMØ and hMØ populations could not be resolved on a pseudocolor dot plot due to the overlap of these two cell types (Figure 14C and E). It is possible that the presence of $EGFP^-$ monocyte-derived hMØs in the SCI lesion confounds the true CD45 expression levels of activated mMØ. To address this issue, *lys*-EFGP-*ki* primary microglial cultures can be activated by LPS and alterations in CD45 expression levels can be examined.

Finally, my study revealed a potentially new 'monocyte-like' subset. This subset was characterized as being $EGFP^+$, $F4/80^{lo}$, $Ly6C/G^-$, $CD11c^+$, and $CD62L^-$. Interest in this population arose from the observation made at 7d post-SCI; at this time point, the 'monocyte-like' subset significantly decreased in the SCI blood compared to the uninjured blood suggesting its involvement in the inflammatory response to SCI. Thus, an attempt was made to classify and verify its potentially novel nature; the following evidence was obtained. Firstly, the 'monocyte-like' subset is monocytic in origin as judged by its expression of F4/80, a pan monocyte/hMØ cell surface marker *(139)*.

Additionally, the subset is a mature myelomoncytic cell as it has active *LysM* promoter activity judged by its EGFP expression. Secondly, this subset is not a premyelocyte or an NK-cell as judged by its lack of CD117 and NK1.1 expression respectively. Thirdly, this subset expresses CD11c, a maker known to be predominantly expressed by DCs *(131-133)*. Further examination of this third aspect revealed that the 'monocyte-like' subset largely lacked CD45R, CD8α, PDCA-1, and Ly6C/G, makers that define pDCs *(131-133)*. However, the 'monocyte-like' subset expressed CD11b, a marker known to be expressed by monocytes/hMØ and cDCs *(131-133, 138)*. Further phenotyping and functional analysis is required to confirm whether or not the 'monocyte-like' populations are true cDC. The 'monocyte-like' subset's involvement in SCI also needs to be investigated. Depletion of this subset in the blood post-SCI suggests that it may be entering the SCI lesion. Concomitant phenotyping of the SCI lesion revealed the presence of an $EGFP^+$, $CD11c^+$, $CCR7^+$ DC in the lesion. However, conclusions regarding the 'monocyte-like' subset being a precursor to DC cannot be made without additional investigations. Sorting of the 'monocyte-like' subset followed by exposure to GM-CSF and IL-4, factors that drive DC formation in culture *(153)*, could be conducted. Additionally, functional studies of these cells in culture such as antigen-presentation and T-cell activation capabilities could be performed to verify the possibility of the 'monocyte-like' subset being a precursor to DCs.

4.2.2 Phenotyping hMØ and mMØ in the *lys*-EGFP-*ki* spinal cord lesion

The present study also examined the phenotypic nature of hMØ and mMØ present in the spinal cord lesion. As mentioned in section 4.1.2, two subsets of hMØs are

observed in the spinal cord lesion. The acute response is defined by the 'classical inflammatory' hMØs and the chronic response by 'non-classical resident' hMØs. I further classified the hMØ subsets at 7d post-SCI, a time at which, maximal numbers of hMØ and mMØ are observed in the lesion. My results suggest that the hMØ subsets in the lesion are phenotypically similar to the monocyte subsets in the blood as judged by differential expression of CD62L, a surface marker that facilitates extravasation to sites of inflammation by binding to carbohydrate moieties *(154)*. It is possible that CD62L also mediates transmigration of hMØ within the lesion by binding to specific ligands in the CNS. Studies have reported the presence of CD62L ligands on oligodendrocytes, neurons, and myelin in the CNS *(154)*.

As mentioned previously, $EGFP^+$, $CD11c^+$, $CCR7^+$ DCs were also observed in the SCI lesion. An in-depth phenotypic analysis of the DCs in the SCI lesion needs to be conducted to identify its exact phenotypic subset and characterize the state of DC maturation and activation. Also, phenotypic analysis could be done to identify presence of DC in the acute and chronic phases of SCI in addition to functional studies, in an effort to examine the biological significance of the presence of DC at the lesion site.

Phenotypic analysis of mMØ also revealed the presence of two subsets: $CD62L^+$ and $CD62L^-$ mMØ. Additionally, results suggested that a fraction of the $CD62L^+$ mMØ may be $CD11c^+$ based on inferences made from backgating analysis. The differential expression of CD62L on mMØ, may possibly give some indication as to their effector function. Grewal et al. *(154)* suggest that CD62L may mediate myelin damage as CD62L deficient mice fail to develop EAE. Additionally, CD62L may facilitate migration of microglia from areas surrounding the lesion to the site of injury. This issue may be

resolved by examining expression of CD62L on mMØ by immunohistochemistry so as to identify the anatomical location of the two subsets with respect to the lesion. Previous studies have identified the presence of $CD11c^+$ microglia in brain inflammation models *(127, 155, 156)*. Some of these studies suggest that $CD11c^+$ microglia may be precursors to DC in CNS inflammation *(155)* while others suggest that expression of CD11c on microglia probably indicates its maturation status *(127)*. $CD11c^+$ microglia exhibit properties of immature antigen-presenting cells with modest amounts of CD40 and MHC expression, and exhibit potent antigen uptake activity when compared to $CD11c^-$ microglia *(127, 156)*. Furthermore, it is also possible that in my study, the $CD11c^+$ microglia are infact blood-derived $EGFP^-$ hMØ; previous brain inflammation studies have reported presence of $CD11c^+$ hMØ *(127)*. To resolve this issue, spinal cord sections of SCI *lys*-EGFP-*ki* mice could be immunohistochemically visualized to identify the anatomical location of $CD11c^+$ hMØ and $CD11c^+$ mMØ. Our laboratory has previously shown that post-SCI, hMØ appear to be centered in the lesion while mMØ are found in the surrounding regions of the lesion (Unpublished data, Leyanna Saville and Gregory Dekaban).

Overall, phenotypic analysis of hMØ and mMØ provide evidence for a complex involvement of the innate immune response to SCI. Simultaneous functional studies such as phagocytic and antigen presentation abilities of hMØ may be performed to further validate hMØ maturation status. Templeton et al. *(127)* report that immature hMØ exhibit greater phagocytic/antigen presenting abilities than mature hMØ. Additionally, similar analysis could be performed for mMØ to elucidate their functional roles to SCI. These

studies will provide insights into the origin, maturation state, and functionality of hMØ and mMØ in the spinal cord following SCI.

4.3 CELL SORTING OF hMØ AND mMØ FOLLOWING SCI

Ultimately, the goal of this project was to define functionality of hMØ and mMØ following SCI. Thus, efforts were made to establish a sorting protocol that gives acceptable purities of sorted populations and allows for downstream applications such as mRNA expression and functional studies.

The sorting protocol established based on testing of different combinations of sorting parameters, permitted hMØ and mMØ in the uninjured and injured spinal cords to be sorted with over 90% purity. However, due to stringent gating strategies used for obtaining high cell purities, the resulting yield of sorted cells was low. The sorting technique may be improved by using CD11b magnetic beads to isolate $CD11b^+$ cells from the spinal cord tissue prior to sorting. CD11b is a surface marker expressed by neutrophils, monocyte, and macrophage (including microglia/mMØ) populations *(78, 138)*. Thus, selection for $CD11b^+$ cells prior to sorting may result in an enriched cell suspension that is minimally contaminated with cell debris and non-relevant cell populations. This may lead to a less stringent gating strategy resulting in higher yields of sorted hMØ and mMØ. Our current results on RNA extraction of sorted cells suggest that it is difficult to extract RNA from the low numbers of sorted cells as it can yield either undetectable levels of RNA or degraded RNA. Thus, a higher yield of hMØ and mMØ may also result in isolation of more intact RNA for gene expression profiling studies.

4.4 SUMMARY

This project investigated the cellular inflammatory response to SCI by specifically examining the neutrophil and monocyte populations in the blood, and infiltrating neutrophils and hMØ, and resident mMØ in the spinal cord lesion following SCI. The results of the present study point to the fact that the above populations participate in the acute and the chronic stages of SCI in distinct patterns.

The identification of heterogeneous monocyte populations raised an interest to examine whether monocyte subsets respond differentially to SCI. My results indicate that the 'classical inflammatory' monocyte and hMØ subsets contribute to the acute inflammatory response while the 'non-classical resident' monocyte and hMØ subsets respond to the chronic stages of SCI inflammation. Additionally, I identified a monocyte subset that to my knowledge has been previously undescribed. I termed this population 'monocyte-like' subset since the population contains both monoctye (F4/80) and DC (CD11c) markers. This 'monocyte-like' subset plays a role in SCI inflammation at least at 7d post-SCI when levels of this population are depleted in the SCI blood. Additionally, I observed the presence of $CD11c^{+}$, $CCR7^{+}$ mature DCs in the spinal cord lesion at 7d post-SCI, although, as previously discussed, we have yet to characterize its phenotypic nature with respect to DC subsets and its functionality. My results provide important and possibly novel insights into the fate of infiltrating monocytes during the acute and chronic stages of CNS inflammation with respect to the SCI model.

In summary, I propose the following possible model for the cellular inflammatory response to SCI. Following SCI in the mouse, the BSCB is compromised, and this facilitates infiltration of hematogenous inflammatory cells into the spinal cord lesion. The

acute stage of SCI is defined by upregulation of neutrophils in the blood and infiltration of massive numbers of neutrophils into the spinal cord lesion at 1-3d post-injury and these levels decrease by 7d. This suggests that the neutrophil response to SCI initiates early on after injury and subsides towards the end of the acute phase of SCI. The acute response to SCI is also defined by upregulation of monocytes in the blood, specifically at 3d post-SCI; the increase in monocyte levels in the blood is contributed by an increase in the 'non-classical resident' monocytes. Simultaneously, infiltration of hMØ into the spinal cord lesion occurs in minimal numbers at 1-3d post-SCI and these numbers maximize towards the end of the acute phase (7d) of SCI. Interestingly, at 1d post-SCI, the 'classical inflammatory' hMØ predominate in the injured lesion and by the end of the acute phase, the hMØ populations show a shift towards the 'non-classical resident' hMØ.

The chronic stage of SCI is defined by a continued elevation of neutrophils in the blood and a resurgence of neutrophil infiltration in low numbers at 14d into the spinal cord lesion that persists to at least 6wks post-SCI. The chronic stage of SCI also involves upregulation of the 'non-classical' monocytes in the blood at 14d and 6wks post-SCI. Simultaneously, in the spinal cord, hMØ remain elevated and shift towards the 'non-classical resident' hMØ phenotype such that at 6wks, this subset of hMØ predominates the spinal cord lesion.

Previous studies by our laboratory with the anti-CD11d mAb treatment showed that improvement in neurological outcome of rodents occurred due to selective blocking of infiltrating neutrophils and early hMØ *(21, 112)*. However, the treatment allowed for the later hMØ influx into the SCI lesion. These results suggested that the beneficial or

harmful effects of hMØ post-SCI may depend on the timing of hMØ influx into the spinal cord lesion. The present study demonstrated differential recruitment of monocyte subsets into the SCI lesion in the acute and chronic phases of SCI. These then differentiate into their respective hMØ subset suggesting that these subsets my exhibit neurodestructive or neurorepair functions. Two possibilities may contribute to the differential presence of hMØ subsets in the lesion during the acute and chronic phases of SCI and are discussed below.

The first possibility is that it is likely only the 'classical inflammatory' monocytes are recruited to the SCI lesion. In the early hours of acute SCI, massive neutrophils, hemorrhage, activated neurons and microglia contribute to a highly toxic environment of the spinal cord *(9, 11, 30, 149, 157)*, and thus the incoming 'classical inflammatory' monocytes respond to the pro-inflammatory signals of the SCI lesion and polarize to the M1 type macrophage *(49, 56)*. The M1 macrophages are known to be highly pro-inflammatory and contribute to tissue damage *(49, 56)*. At the end of the acute stage of SCI, the toxic mechanism contributed by hemorrhage/neutrophils may subside, and thus the incoming 'classical inflammatory' monocytes respond to the more favorable microenvironment and begin to polarize towards the M2 macrophage phenotype. The M2 macrophages are known to participate in tissue repair mechanisms *(49, 56)*. Thus, in the chronic stages of SCI, the shift to M2 polarization continues such that at 6wks, M2 macrophages predominate in the lesioned spinal cord and may possibly participate in repair of the spinal cord. Additionally, microglia and mMØ may also contribute to the microenvironment of the spinal cord; they have the potential to regulate and be regulated by cells of the CNS and by CNS-infiltrating immune cells *(72, 149, 157)*. To my

knowledge, simultaneous studies on macrophage phenotyping and functionality have not been conducted and thus current literature does not indicate a correlation of the 'classical inflammatory' monocytes differentiating to M1 macrophages. Also, whether the phenotype of M2 macrophages is similar to that of the 'non-classical resident' monocyte is not known. Thus, I propose that incoming 'classical inflammatory' monocytes differentiate and mature depending on the cues that it receives in the spinal cord. This maturation process may result in polarization of macrophages, and this polarization determines its neurodestructive and neurorepair functions. Thus future studies need to examine the effector functions of each hMØ subset in an effort to correlate phenotype to maturation and polarization of the hMØ in the spinal cord lesion.

The second possible mechanism that may contribute to the differential recruitment of monocytes into the spinal cord lesion is differential expression of the CD11d/CD18 integrin by the monocyte subsets. Steppich et al. *(158)* have shown that in humans, the monocyte subsets differentially express CD11d adhesion molecule in response to minor stress induction such as exercise. The possibility of the CD11d/CD18 integrin being differentially upregulated in response to trauma such as SCI remains to be investigated. Thus, future studies need to examine expression of CD11d/CD18 integrin on the monocyte subsets in an effort to understand the inflammatory response to SCI. Overall, the results from my study provide new and exciting ventures that can be investigated in the future.

4.5 FUTURE DIRECTIONS

As a continuum from the above proposed mechanism of inflammatory response to SCI, it is first important to carry out mRNA expression studies of the 'classical inflammatory' and 'non-classical resident' monocytes and hMØ as well as mMØ populations post-SCI. I propose examining the spinal cord lesions at 1d (high neutrophil levels, peak 'classical inflammatory' hMØ), 7d (peak hMØ and mMØ levels, a switch to 'non classical resident' hMØ), and 6wks post-SCI (persistent neutrophils and hMØ, peak 'non-classical resident' hMØ). These time points are defined by distinct cellular patterns that may contribute to differential microenvironments of the spinal cord. This in turn would result in a neurodestructive or neuroprotective hMØ effector functions. Specifically, expression of pro-inflammatory versus anti-inflammatory cytokine mRNA expression at various time points post-SCI would allude to possible functional assays that might be next examined.

Functional assays that may be carried out on sorted cell populations include a comparison of the levels of phagocytic activity and ROS production between hMØ and mMØ at the proposed time points. Additionally, markers that define maturation status could be used in order to make inferences as to the immature and mature nature of hMØ and mMØ. The markers include CD40, CD80, CD86, and MHC II. Also, cytokine production studies could be carried out to confirm mRNA expression of particular cytokines that define polarization status/functionality of hMØ subsets. For example expression of pro-inflammatory cytokines such as TNF-, IL-6, and IL-1 may indicate M1 polarization while production of IL-10 may indicate M2 polarization of hMØ. Similar

cytokine studies could also be carried out on mMØ so as to ascribe its functionality in response to SCI.

In light of the results of my study that suggest the presence of DC in response to SCI, additional studies need to be conducted to confirm the phenotype of DC present and establish the infiltration pattern of DC into the injured spinal cord in the acute and chronic stages of SCI. Also, phenotypic analysis of the maturation and activation states of DC with markers such as CD40, CD80, CD86, and MHC II and their cytokine profile may allude to the functional status of DC in the injured spinal cord.

Finally, the above proposed mRNA and functional studies should be carried out in anti-CD11d mAb treated SCI *lys*-EGFP-*ki* mice. These results would allow us to mechanistically understand the anti-inflammatory response associated with the anti-CD11d mAb treatment and develop better therapeutics for SCI.

REFERENCES

1. Fehlings, M. G., and D. C. Baptiste. 2005. Current status of clinical trials for acute spinal cord injury. *Injury.* 36 Suppl 2:B113-22.

2. Siddall, P. J., D. Taylor, and M. J. Cousins. 1995. Pain associated with spinal cord injury. *Curr Opin Neurol.* 8:447-50.

3. Pickett, W., K. Simpson, J. Walker, and R. J. Brison. 2003. Traumatic spinal cord injury in Ontario, Canada. *J Trauma.* 55:1070-6.

4. Pickett, G. E., M. Campos-Benitez, J. L. Keller, and N. Duggal. 2006. Epidemiology of traumatic spinal cord injury in Canada. *Spine.* 31:799-805.

5. Dryden, D. M., L. D. Saunders, P. Jacobs, D. P. Schopflocher, B. H. Rowe, L. A. May, N. Yiannakoulias, L. W. Svenson, and D. C. Voaklander. 2005. Direct health care costs after traumatic spinal cord injury. *J Trauma.* 59:443-9.

6. Ramer, M. S., G. P. Harper, and E. J. Bradbury. 2000. Progress in spinal cord research - a refined strategy for the International Spinal Research Trust. *Spinal Cord.* 38:449-72.

7. Wahlgren, N. G., and N. Ahmed. 2004. Neuroprotection in cerebral ischaemia: facts and fancies--the need for new approaches. *Cerebrovasc Dis.* 17 Suppl 1:153-66.

8. Taoka, Y., and K. Okajima. 1998. Spinal cord injury in the rat. *Prog Neurobiol.* 56:341-58.

9. Demopoulos, H. B., E. S. Flamm, D. D. Pietronigro, and M. L. Seligman. 1980. The free radical pathology and the microcirculation in the major central nervous system disorders. *Acta Physiol Scand Suppl.* 492:91-119.

10. Popovich, P. G., P. Wei, and B. T. Stokes. 1997. Cellular inflammatory response after spinal cord injury in Sprague-Dawley and Lewis rats. *J Comp Neurol.* 377:443-64.

11. Carlson, S. L., M. E. Parrish, J. E. Springer, K. Doty, and L. Dossett. 1998. Acute inflammatory response in spinal cord following impact injury. *Exp Neurol.* 151:77-88.

12. Bethea, J. R., and W. D. Dietrich. 2002. Targeting the host inflammatory response in traumatic spinal cord injury. *Curr Opin Neurol.* 15:355-60.

13. Popovich, P. G., and E. E. Longbrake. 2008. Can the immune system be harnessed to repair the CNS? *Nat Rev Neurosci.* 9:481-93.

14. Donnelly, D. J., and P. G. Popovich. 2008. Inflammation and its role in neuroprotection, axonal regeneration and functional recovery after spinal cord injury. *Exp Neurol.* 209:378-88.

15. Bilgen, M., R. Abbe, and P. A. Narayana. 2001. Dynamic contrast-enhanced MRI of experimental spinal cord injury: in vivo serial studies. *Magn Reson Med.* 45:614-22.

16. Yakovlev, A. G., and A. I. Faden. 1994. Sequential expression of c-fos protooncogene, TNF-alpha, and dynorphin genes in spinal cord following experimental traumatic injury. *Mol Chem Neuropathol.* 23:179-90.

17. Wang, C. X., B. Nuttin, H. Heremans, R. Dom, and J. Gybels. 1996. Production of tumor necrosis factor in spinal cord following traumatic injury in rats. *J Neuroimmunol.* 69:151-6.

18. Taoka, Y., and K. Okajima. 2000. Role of leukocytes in spinal cord injury in rats. *J Neurotrauma.* 17:219-29.

19. Ley, K., D. C. Bullard, M. L. Arbones, R. Bosse, D. Vestweber, T. F. Tedder, and A. L. Beaudet. 1995. Sequential contribution of L- and P-selectin to leukocyte rolling in vivo. *J Exp Med.* 181:669-75.

20. Vaddi, K., and R. C. Newton. 1994. Regulation of monocyte integrin expression by beta-family chemokines. *J Immunol.* 153:4721-32.

21. Mabon, P. J., L. C. Weaver, and G. A. Dekaban. 2000. Inhibition of monocyte/macrophage migration to a spinal cord injury site by an antibody to the integrin alphaD: a potential new anti-inflammatory treatment. *Exp Neurol.* 166:52-64.

22. Argenbright, L. W., L. G. Letts, and R. Rothlein. 1991. Monoclonal antibodies to the leukocyte membrane CD18 glycoprotein complex and to intercellular adhesion molecule-1 inhibit leukocyte-endothelial adhesion in rabbits. *J Leukoc Biol.* 49:253-7.

23. Lee, S. J., and E. N. Benveniste. 1999. Adhesion molecule expression and regulation on cells of the central nervous system. *J Neuroimmunol.* 98:77-88.

24. Guth, L., Z. Zhang, and O. Steward. 1999. The unique histopathological responses of the injured spinal cord. Implications for neuroprotective therapy. *Ann N Y Acad Sci.* 890:366-84.

25. Mawhinney, L. A., S. Thawer, K. Chan, F. C. Simedrea, and G. A. Dekaban. 2007. The lys-EGFP-ki transgenic mouse as a model to study the cellular inflammatory responses following spinal cord injury. . *Journal of Neurotrauma.* 24:1229-88 (Abstract).

26. Fleming, J. C., M. D. Norenberg, D. A. Ramsay, G. A. Dekaban, A. E. Marcillo, A. D. Saenz, M. Pasquale-Styles, W. D. Dietrich, and L. C. Weaver. 2006. The cellular inflammatory response in human spinal cords after injury. *Brain.* 129:3249-69.

27. Sampson, A. P. 2000. The role of eosinophils and neutrophils in inflammation. *Clin Exp Allergy.* 30 Suppl 1:22-7.

28. Faurschou, M., and N. Borregaard. 2003. Neutrophil granules and secretory vesicles in inflammation. *Microbes Infect.* 5:1317-27.

29. Burg, N. D., and M. H. Pillinger. 2001. The neutrophil: function and regulation in innate and humoral immunity. *Clin Immunol.* 99:7-17.

30. Taoka, Y., K. Okajima, M. Uchiba, K. Murakami, S. Kushimoto, M. Johno, M. Naruo, H. Okabe, and K. Takatsuki. 1997. Role of neutrophils in spinal cord injury in the rat. *Neuroscience.* 79:1177-82.

31. Zhou, J., S. A. Stohlman, D. R. Hinton, and N. W. Marten. 2003. Neutrophils promote mononuclear cell infiltration during viral-induced encephalitis. *J Immunol.* 170:3331-6.

32. Sadrzadeh, S. M., D. K. Anderson, S. S. Panter, P. E. Hallaway, and J. W. Eaton. 1987. Hemoglobin potentiates central nervous system damage. *J Clin Invest.* 79:662-4.

33. Bullock, R., and H. Fujisawa. 1992. The role of glutamate antagonists for the treatment of CNS injury. *J Neurotrauma.* 9 Suppl 2:S443-62.

34. Mautes, A. E., M. R. Weinzierl, F. Donovan, and L. J. Noble. 2000. Vascular events after spinal cord injury: contribution to secondary pathogenesis. *Phys Ther.* 80:673-87.

35. Popovich, P. G., B. T. Stokes, and C. C. Whitacre. 1996. Concept of autoimmunity following spinal cord injury: possible roles for T lymphocytes in the traumatized central nervous system. *J Neurosci Res.* 45:349-63.

36. Sroga, J. M., T. B. Jones, K. A. Kigerl, V. M. McGaughy, and P. G. Popovich. 2003. Rats and mice exhibit distinct inflammatory reactions after spinal cord injury. *J Comp Neurol.* 462:223-40.

37. Hauben, E., and M. Schwartz. 2003. Therapeutic vaccination for spinal cord injury: helping the body to cure itself. *Trends Pharmacol Sci.* 24:7-12.

38. Jones, T. B., R. P. Hart, and P. G. Popovich. 2005. Molecular control of physiological and pathological T-cell recruitment after mouse spinal cord injury. *J Neurosci.* 25:6576-83.

39. Crutcher, K. A., H. E. Gendelman, J. Kipnis, J. R. Perez-Polo, V. H. Perry, P. G. Popovich, and L. C. Weaver. 2006. Debate: "is increasing neuroinflammation beneficial for neural repair?" *J Neuroimmune Pharmacol.* 1:195-211.

40. Deshpande, P., I. L. King, and B. M. Segal. 2007. Cutting edge: CNS CD11c+ cells from mice with encephalomyelitis polarize Th17 cells and support CD25+CD4+ T cell-mediated immunosuppression, suggesting dual roles in the disease process. *J Immunol.* 178:6695-9.

41. Geissmann, F., S. Jung, and D. R. Littman. 2003. Blood monocytes consist of two principal subsets with distinct migratory properties. *Immunity.* 19:71-82.

42. Hume, D. A., I. L. Ross, S. R. Himes, R. T. Sasmono, C. A. Wells, and T. Ravasi. 2002. The mononuclear phagocyte system revisited. *J Leukoc Biol.* 72:621-7.

43. Lawson, L. J., V. H. Perry, and S. Gordon. 1992. Turnover of resident microglia in the normal adult mouse brain. *Neuroscience.* 48:405-15.

44. Merad, M., M. G. Manz, H. Karsunky, A. Wagers, W. Peters, I. Charo, I. L. Weissman, J. G. Cyster, and E. G. Engleman. 2002. Langerhans cells renew in the skin throughout life under steady-state conditions. *Nat Immunol.* 3:1135-41.

45. Yamamoto, T., M. Naito, H. Moriyama, H. Umezu, H. Matsuo, H. Kiwada, and M. Arakawa. 1996. Repopulation of murine Kupffer cells after intravenous administration of liposome-encapsulated dichloromethylene diphosphonate. *Am J Pathol.* 149:1271-86.

46. Bruno, L., T. Seidl, and A. Lanzavecchia. 2001. Mouse pre-immunocytes as non-proliferating multipotent precursors of macrophages, interferon-producing cells, CD8alpha(+) and CD8alpha(-) dendritic cells. *Eur J Immunol.* 31:3403-12.

47. Randolph, G. J., C. Jakubzick, and C. Qu. 2008. Antigen presentation by monocytes and monocyte-derived cells. *Curr Opin Immunol.* 20:52-60.

48. Tacke, F., and G. J. Randolph. 2006. Migratory fate and differentiation of blood monocyte subsets. *Immunobiology.* 211:609-18.

49. Gordon, S., and P. R. Taylor. 2005. Monocyte and macrophage heterogeneity. *Nat Rev Immunol.* 5:953-64.

50. Auffray, C., D. Fogg, M. Garfa, G. Elain, O. Join-Lambert, S. Kayal, S. Sarnacki, A. Cumano, G. Lauvau, and F. Geissmann. 2007. Monitoring of blood vessels and tissues by a population of monocytes with patrolling behavior. *Science.* 317:666-70.

51. Tacke, F., D. Alvarez, T. J. Kaplan, C. Jakubzick, R. Spanbroek, J. Llodra, A. Garin, J. Liu, M. Mack, N. van Rooijen, S. A. Lira, A. J. Habenicht, and G. J. Randolph. 2007. Monocyte subsets differentially employ CCR2, CCR5, and CX3CR1 to accumulate within atherosclerotic plaques. *J Clin Invest.* 117:185-94.

52. Sunderkotter, C., T. Nikolic, M. J. Dillon, N. Van Rooijen, M. Stehling, D. A. Drevets, and P. J. Leenen. 2004. Subpopulations of mouse blood monocytes differ in maturation stage and inflammatory response. *J Immunol.* 172:4410-7.

53. Adams, D. O., and T. A. Hamilton. 1984. The cell biology of macrophage activation. *Annu Rev Immunol.* 2:283-318.

54. Mantovani, A., A. Sica, S. Sozzani, P. Allavena, A. Vecchi, and M. Locati. 2004. The chemokine system in diverse forms of macrophage activation and polarization. *Trends Immunol.* 25:677-86.

55. Mosser, D. M. 2003. The many faces of macrophage activation. *J Leukoc Biol.* 73:209-12.

56. Gordon, S. 2003. Alternative activation of macrophages. *Nat Rev Immunol.* 3:23-35.

57. Popovich, P. G., and W. F. Hickey. 2001. Bone marrow chimeric rats reveal the unique distribution of resident and recruited macrophages in the contused rat spinal cord. *J Neuropathol Exp Neurol.* 60:676-85.

58. Rapalino, O., O. Lazarov-Spiegler, E. Agranov, G. J. Velan, E. Yoles, M. Fraidakis, A. Solomon, R. Gepstein, A. Katz, M. Belkin, M. Hadani, and M. Schwartz. 1998. Implantation of stimulated homologous macrophages results in partial recovery of paraplegic rats. *Nat Med.* 4:814-21.

59. Hirata, K., and M. Kawabuchi. 2002. Myelin phagocytosis by macrophages and nonmacrophages during Wallerian degeneration. *Microsc Res Tech.* 57:541-7.

60. Vivers, S., I. Dransfield, and S. P. Hart. 2002. Role of macrophage CD44 in the disposal of inflammatory cell corpses. *Clin Sci (Lond).* 103:441-9.

61. Leskovar, A., L. J. Moriarty, J. J. Turek, I. A. Schoenlein, and R. B. Borgens. 2000. The macrophage in acute neural injury: changes in cell numbers over time and levels of cytokine production in mammalian central and peripheral nervous systems. *J Exp Biol.* 203:1783-95.

62. Heasman, S. J., K. M. Giles, C. Ward, A. G. Rossi, C. Haslett, and I. Dransfield. 2003. Glucocorticoid-mediated regulation of granulocyte apoptosis and macrophage phagocytosis of apoptotic cells: implications for the resolution of inflammation. *J Endocrinol.* 178:29-36.

63. Klusman, I., and M. E. Schwab. 1997. Effects of pro-inflammatory cytokines in experimental spinal cord injury. *Brain Res.* 762:173-84.

64. Thomas, W. E. 1999. Brain macrophages: on the role of pericytes and perivascular cells. *Brain Res Brain Res Rev.* 31:42-57.

65. Hickey, W. F., and H. Kimura. 1988. Perivascular microglial cells of the CNS are bone marrow-derived and present antigen in vivo. *Science.* 239:290-2.

66. Jordan, F. L., and W. E. Thomas. 1988. Brain macrophages: questions of origin and interrelationship. *Brain Res.* 472:165-78.

67. Hickey, W. F., K. Vass, and H. Lassmann. 1992. Bone marrow-derived elements in the central nervous system: an immunohistochemical and ultrastructural survey of rat chimeras. *J Neuropathol Exp Neurol.* 51:246-56.

68. Polfliet, M. M., P. J. Zwijnenburg, A. M. van Furth, T. van der Poll, E. A. Dopp, C. Renardel de Lavalette, E. M. van Kesteren-Hendrikx, N. van Rooijen, C. D. Dijkstra, and T. K. van den Berg. 2001. Meningeal and perivascular macrophages of the central nervous system play a protective role during bacterial meningitis. *J Immunol.* 167:4644-50.

69. Polfliet, M. M., F. van de Veerdonk, E. A. Dopp, E. M. van Kesteren-Hendrikx, N. van Rooijen, C. D. Dijkstra, and T. K. van den Berg. 2002. The role of perivascular and meningeal macrophages in experimental allergic encephalomyelitis. *J Neuroimmunol.* 122:1-8.

70. Hanisch, U. K., and H. Kettenmann. 2007. Microglia: active sensor and versatile effector cells in the normal and pathologic brain. *Nat Neurosci.* 10:1387-94.

71. Barron, K. D. 1995. The microglial cell. A historical review. *J Neurol Sci.* 134 Suppl:57-68.

72. Gehrmann, J., Y. Matsumoto, and G. W. Kreutzberg. 1995. Microglia: intrinsic immuneffector cell of the brain. *Brain Res Brain Res Rev.* 20:269-87.

73. Streit, W. J., M. B. Graeber, and G. W. Kreutzberg. 1988. Functional plasticity of microglia: a review. *Glia.* 1:301-7.

74. Davoust, N., C. Vuaillat, G. Androdias, and S. Nataf. 2008. From bone marrow to microglia: barriers and avenues. *Trends Immunol.*

75. Mildner, A., H. Schmidt, M. Nitsche, D. Merkler, U. K. Hanisch, M. Mack, M. Heikenwalder, W. Bruck, J. Priller, and M. Prinz. 2007. Microglia in the adult brain arise from Ly-6ChiCCR2+ monocytes only under defined host conditions. *Nat Neurosci.* 10:1544-53.

76. Priller, J., A. Flugel, T. Wehner, M. Boentert, C. A. Haas, M. Prinz, F. Fernandez-Klett, K. Prass, I. Bechmann, B. A. de Boer, M. Frotscher, G. W. Kreutzberg, D. A. Persons, and U. Dirnagl. 2001. Targeting gene-modified hematopoietic cells to the central nervous system: use of green fluorescent protein uncovers microglial engraftment. *Nat Med.* 7:1356-61.

77. Wehner, T., M. Bontert, I. Eyupoglu, K. Prass, M. Prinz, F. F. Klett, M. Heinze, I. Bechmann, R. Nitsch, F. Kirchhoff, H. Kettenmann, U. Dirnagl, and J. Priller. 2003. Bone marrow-derived cells expressing green fluorescent protein under the control of the glial fibrillary acidic protein promoter do not differentiate into astrocytes in vitro and in vivo. *J Neurosci.* 23:5004-11.

78. Guillemin, G. J., and B. J. Brew. 2004. Microglia, macrophages, perivascular macrophages, and pericytes: a review of function and identification. *J Leukoc Biol.* 75:388-97.

79. Kreutzberg, G. W. 1996. Microglia: a sensor for pathological events in the CNS. *Trends Neurosci.* 19:312-8.

80. Vela, J. M., A. Yanez, B. Gonzalez, and B. Castellano. 2002. Time course of proliferation and elimination of microglia/macrophages in different neurodegenerative conditions. *J Neurotrauma.* 19:1503-20.

81. Lee, Y. B., A. Nagai, and S. U. Kim. 2002. Cytokines, chemokines, and cytokine receptors in human microglia. *J Neurosci Res.* 69:94-103.

82. Ling, E. A., D. Penney, and C. P. Leblond. 1980. Use of carbon labeling to demonstrate the role of blood monocytes as precursors of the 'ameboid cells' present in the corpus callosum of postnatal rats. *J Comp Neurol.* 193:631-57.

83. Carson, M. J., C. R. Reilly, J. G. Sutcliffe, and D. Lo. 1998. Mature microglia resemble immature antigen-presenting cells. *Glia.* 22:72-85.

84. Stoll, G., and S. Jander. 1999. The role of microglia and macrophages in the pathophysiology of the CNS. *Prog Neurobiol.* 58:233-47.

85. Smith, M. E. 2001. Phagocytic properties of microglia in vitro: implications for a role in multiple sclerosis and EAE. *Microsc Res Tech.* 54:81-94.

86. Smith, M. E. 1993. Phagocytosis of myelin by microglia in vitro. *J Neurosci Res.* 35:480-7.

87. Franzen, R., J. Schoenen, P. Leprince, E. Joosten, G. Moonen, and D. Martin. 1998. Effects of macrophage transplantation in the injured adult rat spinal cord: a combined immunocytochemical and biochemical study. *J Neurosci Res.* 51:316-27.

88. Bomstein, Y., J. B. Marder, K. Vitner, I. Smirnov, G. Lisaey, O. Butovsky, V. Fulga, and E. Yoles. 2003. Features of skin-coincubated macrophages that promote recovery from spinal cord injury. *J Neuroimmunol.* 142:10-6.

89. Rabchevsky, A. G., and W. J. Streit. 1997. Grafting of cultured microglial cells into the lesioned spinal cord of adult rats enhances neurite outgrowth. *J Neurosci Res.* 47:34-48.

90. Mantovani, A., F. Bussolino, and M. Introna. 1997. Cytokine regulation of endothelial cell function: from molecular level to the bedside. *Immunol Today.* 18:231-40.

91. Blight, A. R. 1994. Effects of silica on the outcome from experimental spinal cord injury: implication of macrophages in secondary tissue damage. *Neuroscience.* 60:263-73.

92. Popovich, P. G., Z. Guan, P. Wei, I. Huitinga, N. van Rooijen, and B. T. Stokes. 1999. Depletion of hematogenous macrophages promotes partial hindlimb recovery and neuroanatomical repair after experimental spinal cord injury. *Exp Neurol.* 158:351-65.

93. Bethea, J. R., H. Nagashima, M. C. Acosta, C. Briceno, F. Gomez, A. E. Marcillo, K. Loor, J. Green, and W. D. Dietrich. 1999. Systemically administered interleukin-10 reduces tumor necrosis factor-alpha production and significantly improves functional recovery following traumatic spinal cord injury in rats. *J Neurotrauma.* 16:851-63.

94. Farooque, M., J. Isaksson, and Y. Olsson. 1999. Improved recovery after spinal cord trauma in ICAM-1 and P-selectin knockout mice. *Neuroreport.* 10:131-4.

95. Farooque, M., J. Isaksson, and Y. Olsson. 2001. White matter preservation after spinal cord injury in ICAM-1/P-selectin-deficient mice. *Acta Neuropathol.* 102:132-40.

96. Rosenberg, J. C., and K. Lysz. 1980. Suppression of the immune response by steroids. Comparative potency of hydrocortisone, methylprednisolone, and dexamethasone. *Transplantation.* 29:425-8.

97. Bracken, M. B. 2001. Methylprednisolone and acute spinal cord injury: an update of the randomized evidence. *Spine.* 26:S47-54.

98. Weaver, L. C., D. Gris, L. R. Saville, M. A. Oatway, Y. Chen, D. R. Marsh, E. F. Hamilton, and G. A. Dekaban. 2005. Methylprednisolone causes minimal improvement after spinal cord injury in rats, contrasting with benefits of an anti-integrin treatment. *J Neurotrauma.* 22:1375-87.

99. Rabchevsky, A. G., I. Fugaccia, P. G. Sullivan, D. A. Blades, and S. W. Scheff. 2002. Efficacy of methylprednisolone therapy for the injured rat spinal cord. *J Neurosci Res.* 68:7-18.

100. Hugenholtz, H. 2003. Methylprednisolone for acute spinal cord injury: not a standard of care. *Cmaj.* 168:1145-6.

101. Hurlbert, R. J., and M. G. Hamilton. 2008. Methylprednisolone for acute spinal cord injury: 5-year practice reversal. *Can J Neurol Sci.* 35:41-5.

102. Schwartz, M. 2003. Macrophages and microglia in central nervous system injury: are they helpful or harmful? *J Cereb Blood Flow Metab.* 23:385-94.

103. Brocke, S., C. Piercy, L. Steinman, I. L. Weissman, and T. Veromaa. 1999. Antibodies to CD44 and integrin alpha4, but not L-selectin, prevent central nervous system inflammation and experimental encephalomyelitis by blocking secondary leukocyte recruitment. *Proc Natl Acad Sci U S A.* 96:6896-901.

104. Springer, T. A. 1990. Adhesion receptors of the immune system. *Nature.* 346:425-34.

105. van der Flier, A., and A. Sonnenberg. 2001. Function and interactions of integrins. *Cell Tissue Res.* 305:285-98.

106. Hemler, M. E., C. Huang, and L. Schwarz. 1987. The VLA protein family. Characterization of five distinct cell surface heterodimers each with a common 130,000 molecular weight beta subunit. *J Biol Chem.* 262:3300-9.

107. Takada, Y., X. Ye, and S. Simon. 2007. The integrins. *Genome Biol.* 8:215.

108. Grayson, M. H., M. Van der Vieren, S. A. Sterbinsky, W. Michael Gallatin, P. A. Hoffman, D. E. Staunton, and B. S. Bochner. 1998. alphadbeta2 integrin is expressed on human eosinophils and functions as an alternative ligand for vascular cell adhesion molecule 1 (VCAM-1). *J Exp Med.* 188:2187-91.

109. Saville, L. R., C. H. Pospisil, L. A. Mawhinney, F. Bao, F. C. Simedrea, A. A. Peters, P. J. O'Connell, L. C. Weaver, and G. A. Dekaban. 2004. A monoclonal antibody to CD11d reduces the inflammatory infiltrate into the injured spinal cord: a potential neuroprotective treatment. *J Neuroimmunol.* 156:42-57.

110. Danilenko, D. M., P. V. Rossitto, M. Van der Vieren, H. Le Trong, S. P. McDonough, V. K. Affolter, and P. F. Moore. 1995. A novel canine leukointegrin, alpha d beta 2, is expressed by specific macrophage subpopulations in tissue and a minor CD8+ lymphocyte subpopulation in peripheral blood. *J Immunol.* 155:35-44.

111. Van der Vieren, M., H. Le Trong, C. L. Wood, P. F. Moore, T. St John, D. E. Staunton, and W. M. Gallatin. 1995. A novel leukointegrin, alpha d beta 2, binds preferentially to ICAM-3. *Immunity.* 3:683-90.

112. Gris, D., D. R. Marsh, M. A. Oatway, Y. Chen, E. F. Hamilton, G. A. Dekaban, and L. C. Weaver. 2004. Transient blockade of the CD11d/CD18 integrin reduces secondary damage after spinal cord injury, improving sensory, autonomic, and motor function. *J Neurosci.* 24:4043-51.

113. Bao, F., Y. Chen, G. A. Dekaban, and L. C. Weaver. 2004. Early anti-inflammatory treatment reduces lipid peroxidation and protein nitration after spinal cord injury in rats. *J Neurochem.* 88:1335-44.

114. Bao, F., Y. Chen, G. A. Dekaban, and L. C. Weaver. 2004. An anti-CD11d integrin antibody reduces cyclooxygenase-2 expression and protein and DNA oxidation after spinal cord injury in rats. *J Neurochem.* 90:1194-204.

115. Oatway, M. A., Y. Chen, J. C. Bruce, G. A. Dekaban, and L. C. Weaver. 2005. Anti-CD11d integrin antibody treatment restores normal serotonergic projections to the dorsal, intermediate, and ventral horns of the injured spinal cord. *J Neurosci.* 25:637-47.

116. Ulvestad, E., K. Williams, S. Mork, J. Antel, and H. Nyland. 1994. Phenotypic differences between human monocytes/macrophages and microglial cells studied in situ and in vitro. *J Neuropathol Exp Neurol.* 53:492-501.

117. Zhang, G. X., J. Li, E. Ventura, and A. Rostami. 2002. Parenchymal microglia of naive adult C57BL/6J mice express high levels of B7.1, B7.2, and MHC class II. *Exp Mol Pathol.* 73:35-45.

118. Sedgwick, J. D., S. Schwender, H. Imrich, R. Dorries, G. W. Butcher, and V. ter Meulen. 1991. Isolation and direct characterization of resident microglial cells from the normal and inflamed central nervous system. *Proc Natl Acad Sci U S A.* 88:7438-42.

119. Ponomarev, E. D., L. P. Shriver, K. Maresz, and B. N. Dittel. 2005. Microglial cell activation and proliferation precedes the onset of CNS autoimmunity. *J Neurosci Res.* 81:374-89.

120. Faust, N., F. Varas, L. M. Kelly, S. Heck, and T. Graf. 2000. Insertion of enhanced green fluorescent protein into the lysozyme gene creates mice with green fluorescent granulocytes and macrophages. *Blood.* 96:719-26.

121. Ganz, T., V. Gabayan, H. I. Liao, L. Liu, A. Oren, T. Graf, and A. M. Cole. 2003. Increased inflammation in lysozyme M-deficient mice in response to Micrococcus luteus and its peptidoglycan. *Blood.* 101:2388-92.

122. Clarke, S., and S. Gordon. 1998. Myeloid-specific gene expression. *J Leukoc Biol.* 63:153-68.

123. Keshav, S., P. Chung, G. Milon, and S. Gordon. 1991. Lysozyme is an inducible marker of macrophage activation in murine tissues as demonstrated by in situ hybridization. *J Exp Med.* 174:1049-58.

124. Cross, M., I. Mangelsdorf, A. Wedel, and R. Renkawitz. 1988. Mouse lysozyme M gene: isolation, characterization, and expression studies. *Proc Natl Acad Sci U S A.* 85:6232-6.

125. Clausen, B. E., C. Burkhardt, W. Reith, R. Renkawitz, and I. Forster. 1999. Conditional gene targeting in macrophages and granulocytes using LysMcre mice. *Transgenic Res.* 8:265-77.

126. Givan, A. L. 2001. *Flow Cytometry : First Principles*. Chichester : Wiley pp. 81-113, New York.

127. Templeton, S. P., T. S. Kim, K. O'Malley, and S. Perlman. 2008. Maturation and localization of macrophages and microglia during infection with a neurotropic murine coronavirus. *Brain Pathol.* 18:40-51.

128. Ponomarev, E. D., M. Novikova, K. Maresz, L. P. Shriver, and B. N. Dittel. 2005. Development of a culture system that supports adult microglial cell proliferation and maintenance in the resting state. *J Immunol Methods.* 300:32-46.

129. Schell, J. B., C. A. Crane, M. F. Smith, Jr., and M. R. Roberts. 2007. Differential ex vivo nitric oxide production by acutely isolated neonatal and adult microglia. *J Neuroimmunol.* 189:75-87.

130. Joshi, M., and M. G. Fehlings. 2002. Development and characterization of a novel, graded model of clip compressive spinal cord injury in the mouse: Part 1. Clip design, behavioral outcomes, and histopathology. *J Neurotrauma.* 19:175-90.

131. Wu, L., and A. Dakic. 2004. Development of dendritic cell system. *Cell Mol Immunol.* 1:112-8.

132. Wu, L., and Y. J. Liu. 2007. Development of dendritic-cell lineages. *Immunity.* 26:741-50.

133. Randolph, G. J., J. Ochando, and S. Partida-Sanchez. 2008. Migration of dendritic cell subsets and their precursors. *Annu Rev Immunol.* 26:293-316.

134. Koo, G. C., and J. R. Peppard. 1984. Establishment of monoclonal anti-Nk-1.1 antibody. *Hybridoma.* 3:301-3.

135. Wang, Y., O. Berezovska, and S. Fedoroff. 1999. Expression of colony stimulating factor-1 receptor (CSF-1R) by CNS neurons in mice. *J Neurosci Res.* 57:616-32.

136. Maurer, M., B. Echtenacher, L. Hultner, G. Kollias, D. N. Mannel, K. E. Langley, and S. J. Galli. 1998. The c-kit ligand, stem cell factor, can enhance innate immunity through effects on mast cells. *J Exp Med.* 188:2343-8.

137. Donovan, J. A., and G. A. Koretzky. 1993. CD45 and the immune response. *J Am Soc Nephrol.* 4:976-85.

138. Lagasse, E., and I. L. Weissman. 1996. Flow cytometric identification of murine neutrophils and monocytes. *J Immunol Methods.* 197:139-50.

139. Austyn, J. M., and S. Gordon. 1981. F4/80, a monoclonal antibody directed specifically against the mouse macrophage. *Eur J Immunol.* 11:805-15.

140. Morris, L., C. F. Graham, and S. Gordon. 1991. Macrophages in haemopoietic and other tissues of the developing mouse detected by the monoclonal antibody F4/80. *Development.* 112:517-26.

141. Kigerl, K. A., V. M. McGaughy, and P. G. Popovich. 2006. Comparative analysis of lesion development and intraspinal inflammation in four strains of mice following spinal contusion injury. *J Comp Neurol.* 494:578-94.

142. Neumann, H. 2001. Control of glial immune function by neurons. *Glia.* 36:191-9.

143. Gris, D., D. R. Marsh, G. A. Dekaban, and L. C. Weaver. 2005. Comparison of effects of methylprednisolone and anti-CD11d antibody treatments on autonomic dysreflexia after spinal cord injury. *Exp Neurol.* 194:541-9.

144. Vallieres, N., J. L. Berard, S. David, and S. Lacroix. 2006. Systemic injections of lipopolysaccharide accelerates myelin phagocytosis during Wallerian degeneration in the injured mouse spinal cord. *Glia.* 53:103-13.

145. Bou-Abdallah, F., N. D. Chasteen, and M. P. Lesser. 2006. Quenching of superoxide radicals by green fluorescent protein. *Biochim Biophys Acta.* 1760:1690-5.

146. Drevets, D. A., M. J. Dillon, J. S. Schawang, N. Van Rooijen, J. Ehrchen, C. Sunderkotter, and P. J. Leenen. 2004. The Ly-6Chigh monocyte subpopulation transports Listeria monocytogenes into the brain during systemic infection of mice. *J Immunol.* 172:4418-24.

147. Streit, W. J., S. A. Walter, and N. A. Pennell. 1999. Reactive microgliosis. *Prog Neurobiol.* 57:563-81.

148. Kukley, M., M. Kiladze, R. Tognatta, M. Hans, D. Swandulla, J. Schramm, and D. Dietrich. 2008. Glial cells are born with synapses. *Faseb J.* 22(8): 2957-69.

149. Carson, M. J., T. V. Bilousova, S. S. Puntambekar, B. Melchior, J. M. Doose, and I. M. Ethell. 2007. A rose by any other name? The potential consequences of microglial heterogeneity during CNS health and disease. *Neurotherapeutics.* 4:571-9.

150. Qu, C., E. W. Edwards, F. Tacke, V. Angeli, J. Llodra, G. Sanchez-Schmitz, A. Garin, N. S. Haque, W. Peters, N. van Rooijen, C. Sanchez-Torres, J. Bromberg, I. F. Charo, S. Jung, S. A. Lira, and G. J. Randolph. 2004. Role of CCR8 and other chemokine pathways in the migration of monocyte-derived dendritic cells to lymph nodes. *J Exp Med.* 200:1231-41.

151. Wakim, L. M., J. Waithman, N. van Rooijen, W. R. Heath, and F. R. Carbone. 2008. Dendritic cell-induced memory T cell activation in nonlymphoid tissues. *Science.* 319:198-202.

152. Mazzoni, A., V. Bronte, A. Visintin, J. H. Spitzer, E. Apolloni, P. Serafini, P. Zanovello, and D. M. Segal. 2002. Myeloid suppressor lines inhibit T cell responses by an NO-dependent mechanism. *J Immunol.* 168:689-95.

153. Inaba, K., M. Inaba, N. Romani, H. Aya, M. Deguchi, S. Ikehara, S. Muramatsu, and R. M. Steinman. 1992. Generation of large numbers of dendritic cells from mouse bone marrow cultures supplemented with granulocyte/macrophage colony-stimulating factor. *J Exp Med.* 176:1693-702.

154. Grewal, I. S., H. G. Foellmer, K. D. Grewal, H. Wang, W. P. Lee, D. Tumas, C. A. Janeway, Jr., and R. A. Flavell. 2001. CD62L is required on effector cells for local interactions in the CNS to cause myelin damage in experimental allergic encephalomyelitis. *Immunity.* 14:291-302.

155. Fischer, H. G., and G. Reichmann. 2001. Brain dendritic cells and macrophages/microglia in central nervous system inflammation. *J Immunol.* 166:2717-26.

156. Reichmann, G., M. Schroeter, S. Jander, and H. G. Fischer. 2002. Dendritic cells and dendritic-like microglia in focal cortical ischemia of the mouse brain. *J Neuroimmunol.* 129:125-32.

157. Carson, M. J., and D. D. Lo. 2007. Perspective is everything: an irreverent discussion of CNS-immune system interactions as viewed from different scientific traditions. *Brain Behav Immun.* 21:367-73.

158. Steppich, B., F. Dayyani, R. Gruber, R. Lorenz, M. Mack, and H. W. Ziegler-Heitbrock. 2000. Selective mobilization of CD14(+)CD16(+) monocytes by exercise. *Am J Physiol Cell Physiol.* 279:C578-86.

APPENDIX

Appendix 1. Proof of Ethics Approval. A copy of the document that shows the ethical approval from the University Council on Animal Care for using the *Lys*-EGFP-*ki* and C57BL/6 mice for experimental SCI studies.

Western

December 13, 2007

This is the Original Approval for this protocol
A Full Protocol submission will be required in 2011

Dear Dr. Dekaban:

Your Animal Use Protocol form entitled:
Experimental Spinal Cord Injury
Funding Agency CIHR - Grant #RMN-63187

has been approved by the University Council on Animal Care. This approval is valid from **December 13, 2007** to **December 31, 2008.** The protocol number for this project is **2007-104-12.**

1. This number must be indicated when ordering animals for this project.
2. Animals for other projects may not be ordered under this number.
3. If no number appears please contact this office when grant approval is received.
   If the application for funding is not successful and you wish to proceed with the project, request that an internal scientific peer review be performed by the Animal Use Subcommittee office.
4. Purchases of animals other than through this system must be cleared through the ACVS office. Health certificates will be required.

ANIMALS APPROVED FOR 1 YR.

Species	Strain	Other Detail	Pain Level	Animal # Total for 1 Year
Mouse	Cd11 d ko	20-28 gm M/F	D	100
Mouse	C57Bl/6	20-28 gm M/F	D	100
Mouse	lys-EGFP-ki	20-28 gm M/F	D	100
Rat	Wistar	200-250 gm F	D	35

STANDARD OPERATING PROCEDURES
Procedures in this protocol should be carried out according to the following SOPs. Please contact the Animal Use Subcommittee office (661-2111 ext. 86770) in case of difficulties or if you require copies.
SOP's are also available at http://www.uwo.ca/animal/acvs
310 Holding Period Post-Admission
320 Euthanasia
321 Criteria for Early Euthanasia/Rodents
330 Post-Operative Care/Rodent
343 Surgical Prep/Rodent/Recovery Surgery

REQUIREMENTS/COMMENTS
Please ensure that individual(s) performing procedures on live animals, as described in this protocol, are familiar with the contents of this document.

c.c. Approved Protocol - G. Dekaban, M. Pickering
Approval Letter - M. Pickering

Appendix 2. Determination of purities of sorted cells from the spinal cord and blood of *lys*-EGFP-*ki* mouse. Aliquots of sorted cells were examined to determine whether they met the initial sorting criteria. Sorted microglia in the uninjured spinal cords (A). Sorted mMØ (B) and hMØ (C) in the spinal cord lesion at 7d post-SCI. Sorted 'non-classical resident' (D) and 'classical inflammatory' (E) monocytes in the uninjured blood. The color representations correspond as follows; blue: microglia and mMØ (A-C), green: hMØ (A-C), pink: 'non-classical resident' monocyte (D) and light blue: 'classical inflammatory' monocyte (E). N=3, n=4-5.

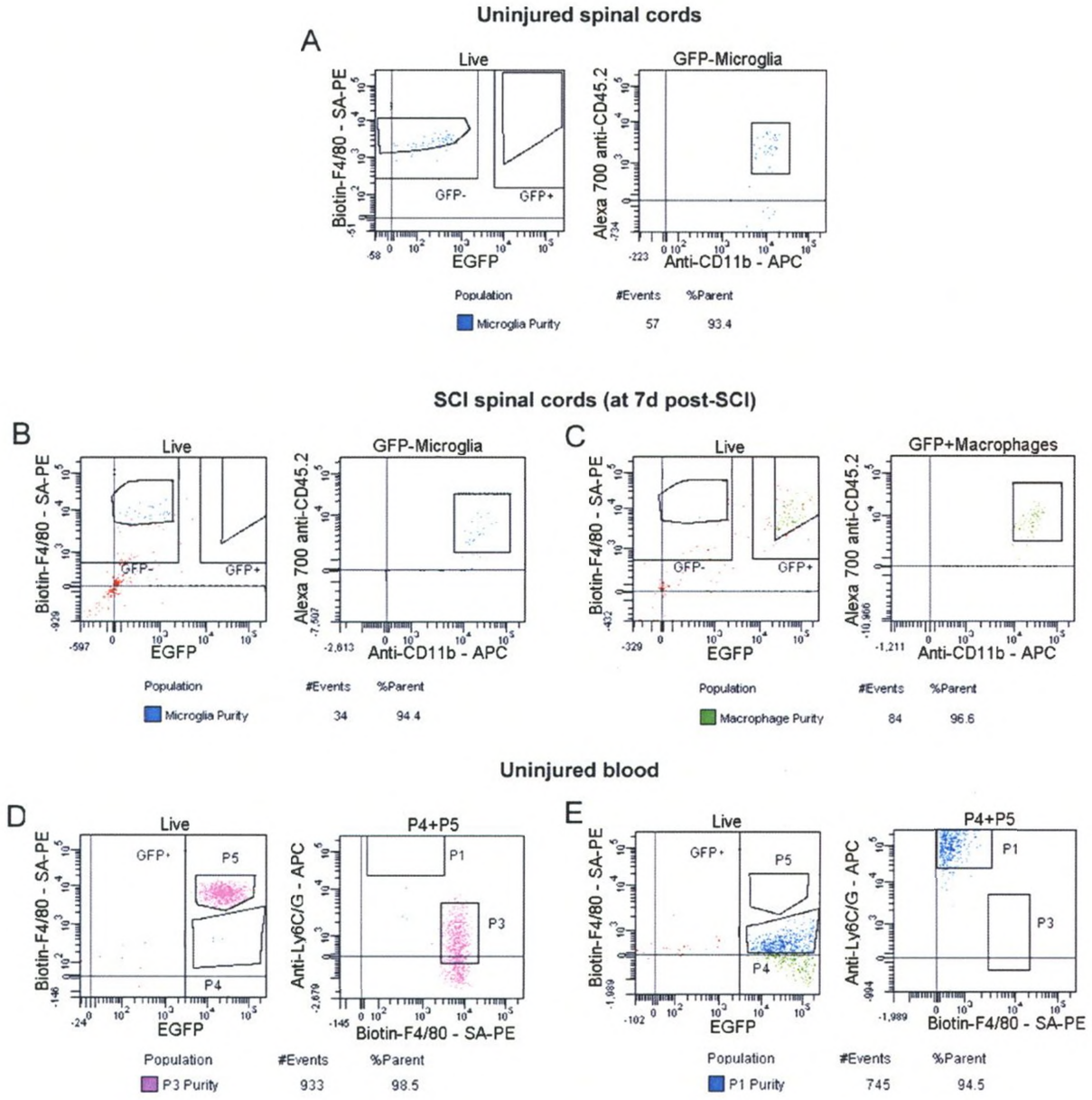
Uninjured spinal cords
A
Live
GFP-Microglia
Biotin-F4/80 - SA-PE
GFP-
GFP+
EGFP
Alexa 700 anti-CD45.2
Anti-CD11b - APC
Population
#Events
%Parent
Microglia Purity
57
93.4
SCI spinal cords (at 7d post-SCI)
B
Live
GFP-Microglia
Biotin-F4/80 - SA-PE
GFP-
GFP+
EGFP
Alexa 700 anti-CD45.2
Anti-CD11b - APC
Population
#Events
%Parent
Microglia Purity
34
94.4
C
Live
GFP+Macrophages
Biotin-F4/80 - SA-PE
GFP-
GFP+
EGFP
Alexa 700 anti-CD45.2
Anti-CD11b - APC
Population
#Events
%Parent
Macrophage Purity
84
96.6
Uninjured blood
D
Live
P4+P5
Biotin-F4/80 - SA-PE
GFP+
P5
P4
EGFP
Anti-Ly6C/G - APC
P1
P3
Biotin-F4/80 - SA-PE
Population
#Events
%Parent
P3 Purity
933
98.5
E
Live
P4+P5
Biotin-F4/80 - SA-PE
GFP+
P5
P4
EGFP
Anti-Ly6C/G - APC
P1
P3
Biotin-F4/80 - SA-PE
Population
#Events
%Parent
P1 Purity
745
94.5